Formation of functional SiO:CH thin films by plasma enhanced chemical vapor deposition

Yongsup Yun

Formation of functional SiO:CH thin films by plasma enhanced chemical vapor deposition

A Doctoral Dissertation by
Yongsup Yun

2007

Submitted to Graduate School of Engineering,
Department of Materials, Physics and Energy Engineering,
Nagoya University,
In partial fulfillment of the requirements for the degree of
DOCTOR OF ENGINEERING

Contents

Chapter 1. Introduction

1.1. SiO_2 thin films

Silicon dioxide (SiO_2) films, also known as silica films, are a major material with many applications particularly in the optical instrument, semiconductor and food industry, which are produced mostly by chemical vapor deposition (CVD) [1-3]. It is an excellent electrical insulator with very low thermal expansion and good resistance to thermal shock. Moreover, SiO_2 films are resistant to oxidation and not attacked by most chemical reagents at room temperature. Its characteristics and properties are summarized in Table 1.1 [1]. Because of these properties, SiO_2 films can be used in the following application fields:

1. passivation layers, surface dielectric, and doping barriers in semiconductor devices,
2. intermetallic dielectrics,
3. diffusion sources,
4. etch barriers,
5. oxidation protection of stainless steel in nuclear reactors,
6. preparation of optical fibers,
7. passivation layers in energy-saving architectural glass (E-glass),
8. barrier layer for SnO_2 films for glass coating.

In these films, the organic functional groups of the reactants had been regarded as problematic impurities. However, SiO_2 films with organic constituents have been found to show interesting properties, which are not realized in pure SiO_2. Various kinds of organosilicon molecules have been utilized in plasma enhanced chemical vapor deposition

Table 1.1. Summary of characteristics of SiO_2.

Content	Value
Molecular Weight	60.09 g/mol
Color	Transparent (near-ultraviolet − infrared region)
X-ray Density	2.20 g/cm^3
Crystal structure	Hexagonal
Melting Point	1610 ℃ (molten SiO_2 has high viscosity)
Thermal Conductivity (W/m•℃)	12
Thermal Expansion (10^{-6}/℃)	0.5 (0 - 150℃ range)
Electrical Resistivity	10^{21} μΩcm
Dielectric Constant	3.9 to 4.3 at 1000 cps (depending on process conditions)
Refractive index	1.46
Vickers Hardness	Up to 9 GPa
Note: Test temperature is 20℃ unless otherwise stated	

(PECVD) in order to improve the properties of SiO_2 films. Novel functional films prepared by the PECVD, such as SiOF films for their dielectric properties, SiON films for their mechanical properties and SiO:CH films for their ultra water repellent as well as dielectric properties, have been intensively investigated [4-9].

1.2. SiO:CH thin films

SiO:CH films, referred to as carbon- or hydrocarbon-doped SiO_2 films, have attracted particular attention as a low-dielectric constant insulating layer material of ultra large-scale integrated circuit (ULSI) [10-11]. The feature size in ULSI production continuously scales down to achieve high-speed and high device performance. With a decrease in feature size, resistance–capacitance (RC) delay becomes a major limitation for the device performance. RC delay can be reduced by using copper instead of aluminum for approximately 35% resistance reduction, or by using inter-metal dielectric with dielectric constant k lower than that of SiO_2 (≈ 4). Replacement of SiO_2 by air ($k = 1$), and aluminum by copper with the same geometry can reduce RC delay by 75% [12].

Sol-gel deposition process was the only method realized so far for preparation of ultra low-k ($k < 2.2$) dielectrics. However, The ultra low-k SiO:CH films prepared by PECVD have been reported recently due to a compatibility with existing silicon processing technology. An introduction of porosity into the SiO:CH films has been researched for decreasing its dielectric constant.

1.2.1. SiO:CH ultra water-repellent (UWR) thin films

In another applications of the SiO:CH films, many researchers investigate the functional SiO:CH films, such as light emitting material, and ultra water-repellent (UWR) films, which

show a water contact angle greater than 150°. In particular, Takai laboratory has proposed UWR films prepared at room temperature by PECVD [9,13-19]. This PECVD method is useful to give the water-repellency to plastic, glass, semiconductor, metal, and paper substrates due to a low temperature process. Y. Wu, et al. reported the hard SiO:CH thin films with ultra water-repellency and high optical transparency [20]. These films were prepared by the microwave PECVD using trimethylmethoxysilane (TMMOS) and CO_2 gas, and show 2.48 GPa of hardness as well as relatively good mechanical durability (the contact angle is maintained at 132° after 3000 times cycle of a rubbing test). Moreover, they have studied the cell motility with an ultra hydrophobic / ultra hydrophilic patterning on SiO:CH films recently. However, these films have not been used in practical applications, mainly due to a poor mechanical durability.

1.3. UWR surfaces

1.3.1. UWR surfaces in nature

During the past decades, researchers have paid attention to the study of hydrophobic materials that can be found in nature [21-24]. The primary example studied showing this behavior is hydrophobic leaves. Many kinds of leaf surfaces of plants have been studied to see the effect of roughness and water repellency [25]. One of the most famous examples is lotus leaves (Figure 1.1). Lotus leaves have micro- and nano-structures in the surface together with wax crystals, leading to ultra water-repellency. Water droplets on the lotus surface are almost spherical and roll off easily, which is usually referred to as the “lotus effect”. Hydrophobic lotus leaves repel water via multiple mechanisms. First, the surface of lotus leaves is usually covered with wax crystals which are mixture of large hydrocarbon molecules, measuring

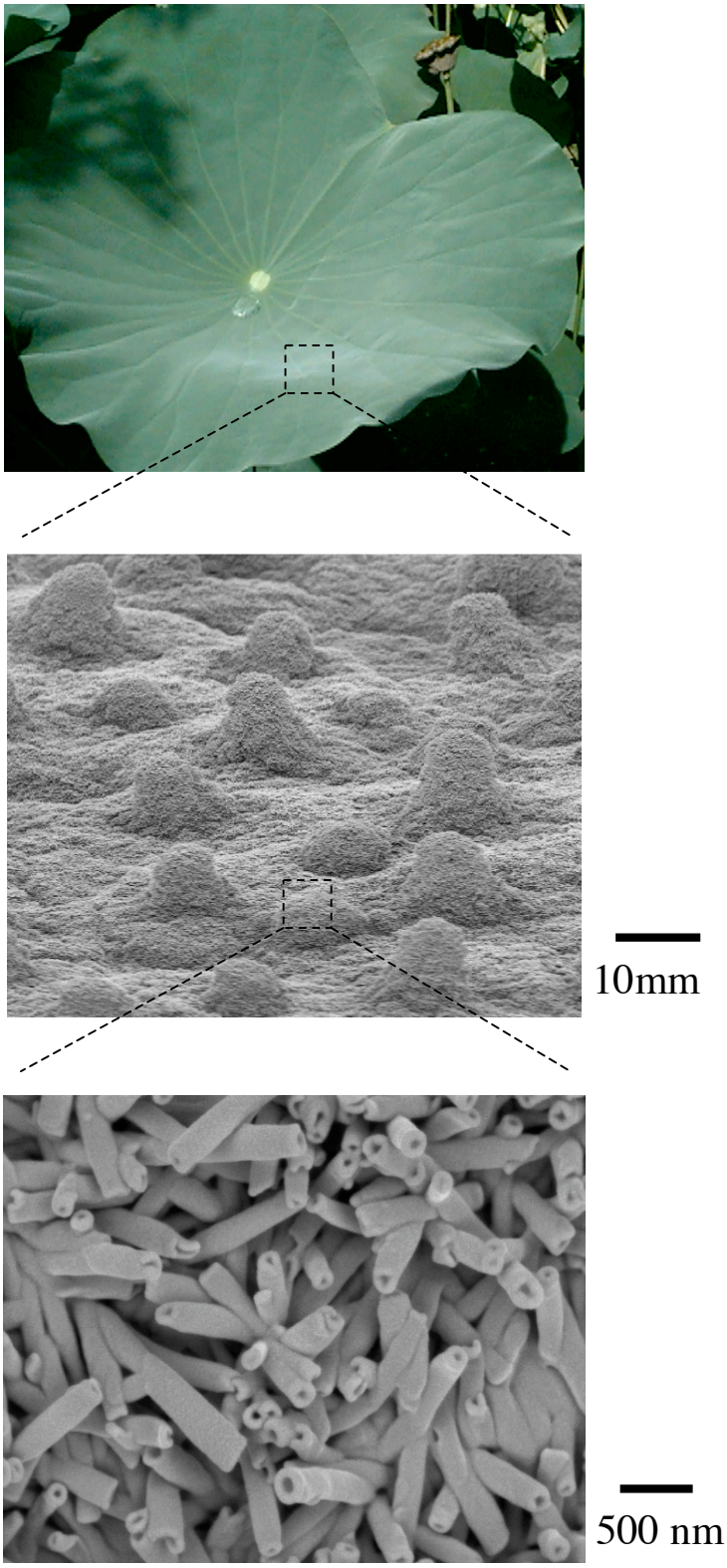

Figure 1.1. Ultra water-repellent lotus leaf.

about 1 nm in diameter, that are very hydrophobic alone. Second, the surface of the leaves is very rough due to papillose epidermal cells that create papillae or bumps on the surface of the leaf. The combination of the thin wax film and the large bumps on the surface of the leaves provides the ability for the leaves to be ultra hydrophobic.

In addition to the leaves of plants, many insects [26-28], such as the water strider, butterfly and the cicada also show ultra water-repellency. Water striders are remarkable in that their non-wetting legs that enable them to stand effortlessly on water. The maximal supporting force of a single leg is 1.52×10^{-3} N, which is about 15 times the weight of the insect. The leg is composed of numerous needle-shaped setae with diameters on the micro-scale and that each micro-seta is composed of many elaborate nano-scale grooves. Such a hierarchical surface structure together with the hydrophobic, secreted wax is considered to be the origin of the ultra water-repellency of the water strider's legs.

Butterflies and cicadae can keep themselves uncontaminated by removing dust particles, and dew or water droplets easily from their wings. Such properties also originate from the special microstructures on their wings. The cicada wing is composed of aligned nano-columns with diameters of about 70 nm and a column-to-column distance of about 90 nm. These surface microstructures bestow the wing with its self-cleaning property.

1.3.2. Artificial UWR surfaces

Inspired by UWR living organisms in nature, such as lotus leaves and water-strider legs, artificial UWR surfaces have attracted great interest in both fundamental research and industrial fields due to an expansion of requirements in the following practical applications [29-36]:

1. prevention of adhesion of raindrops or snowflakes onto windows and antennas,
2. traffic indicators with self-cleaning surface,
3. reduction of frictional drag on ship hulls,
4. metal refining,
5. stain-resistant textiles, and
6. cell motility.

On the basis of these aspects, various approaches have been proposed for the preparation of UWR surfaces via the construction of an appropriate surface-geometry structure. In particular, many significant techniques have been developed to produce UWR surfaces, including the sol–gel method [37], microwave plasma enhanced chemical vapor deposition (MPECVD) [13-20], plasma polymerization and modification [37], physical vapor deposition (PVD) [38], chemical vapor deposition (CVD) [39], phase separation [40], mixing powders of silica or PTFE [41], dispersion plating [42], molding [43], template-based extrusion method [44], laser etching [45], spray-and-dry method [46], electrochemical deposition [47] and hot filament chemical vapor deposition process [48]. Typical fabrication method of UWR films was summarized in Table 1.2 [49]. All these methods have a common feature that UWR surfaces are constructed by combining suitable roughness with low surface energy materials, since enhancement of the water repellency involves in two factors: one is to the chemical functional groups that can lower the surface energy, which is generally referred to as chemical factor. This modification leads to an increase in the contact angle of a water-droplet, with a maximum value of ~120° reported for smooth CF_3- terminated surfaces [50]. The other factor is to make surface roughness so as to increase the specific surface area resulting in an increase in nominal surface energy, which is known as geometrical factor. For the formation of UWR

Table 1.2. Typical fabrication method of ultra water-repellent films.

Process		Substrate	Treatment temperature (℃)	Raw material	Trans-parency
Wet process	Sol-gel method	Metal(Cu, Al, etc.) and glass	Below 400	Organosilicon compounds and organozirconium compounds	Good
	Chemical absorption method	Metal(Cu, Al, etc.), glass, and dental material	Room temperature ~ 150	Organosilicon compounds and graphite fluoride	Good
	Distributed plating	Metal (Cu, Al, etc.)	45	cationic surfactant and Ni distribution electrolyte	Not good
Dry process	Low temperature plasma treatment	Plastic, rubber, wood, and ceramic	Room temperature	Carbon fluoride, silicon fluoride, nitrogen fluoride, and methane	Similar with a substrate
	Plasma polymerization	Plastic, glass, and ceramic	Room temperature	Carbon fluoride and organofluoric compounds	Good
	Plasma CVD	Plastic, glass, ceramic, metal, and semiconductor	Room temperature	Organosilicon compounds	Good
	Sputtering method	Plastic and glass	Room temperature	Teflon and organofluoric compounds	Good
Composite process	Chemical absorption and plasma treatment	PET film	Room temperature	Organosilicon compoung and oxygen	Good

films, modification of surface chemistry must be always combined with surface roughness. Classical theories on the relationship between surface wettability and surface roughness will be briefly reviewed in the next section.

1.4. Surface energy and wettability

The wetting behavior of solid surfaces against water droplets is a very important phenomenon in academic as well as in industrial fields [29-35], which depends on both the chemical composition and the geometric micro-structure of the solid surface as described in the previous section. When a water droplet contacts a substrate, it will either remain as a droplet or spread out on the surface. These properties are normally characterized by contact angle (CA). As shown in Table 1.3 [49], when the water contact angle (WCA) is larger than 150°, it is called ultra water-repellency (ultra hydrophobicity) [51]. On the other hand, when the WCA is almost 0°, it is called ultra hydrophilicity [52]. Regarding the wettability of surface, it has been studied since Young's paper in 1805 and accumulated in many aspects [53-55].

1.4.1. Young's equation [29, 49, 56-57]

For a liquid droplet on a flat film, the wettability is determined by the surface free energy of a solid substrate, which is commonly given by the Young's equation 1.1,

$$\cos\theta = (\gamma_S - \gamma_{SL}) / \gamma_L , \qquad (1.1)$$

where θ is the CA in the Young's model, and γ_S, γ_L, and γ_{SL} are the different surface free energy (solid, liquid, and solid/liquid) involved in the system (Figure 1.2).

Table 1.3. Wettability of solid surface by water droplet.

Appearance of water droplet	Water contact angle(˚)	Classification
	~ 0	Ultra hydrophilicity
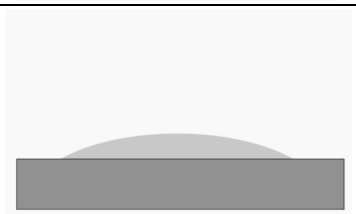	< 10	Hydrophilicity
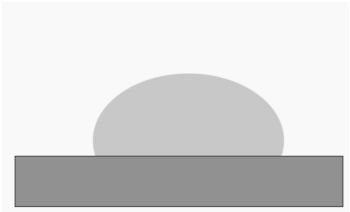	> 80	Water-repellency
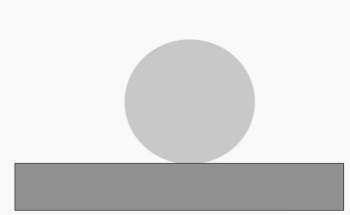	> 150	Ultra water-repellency

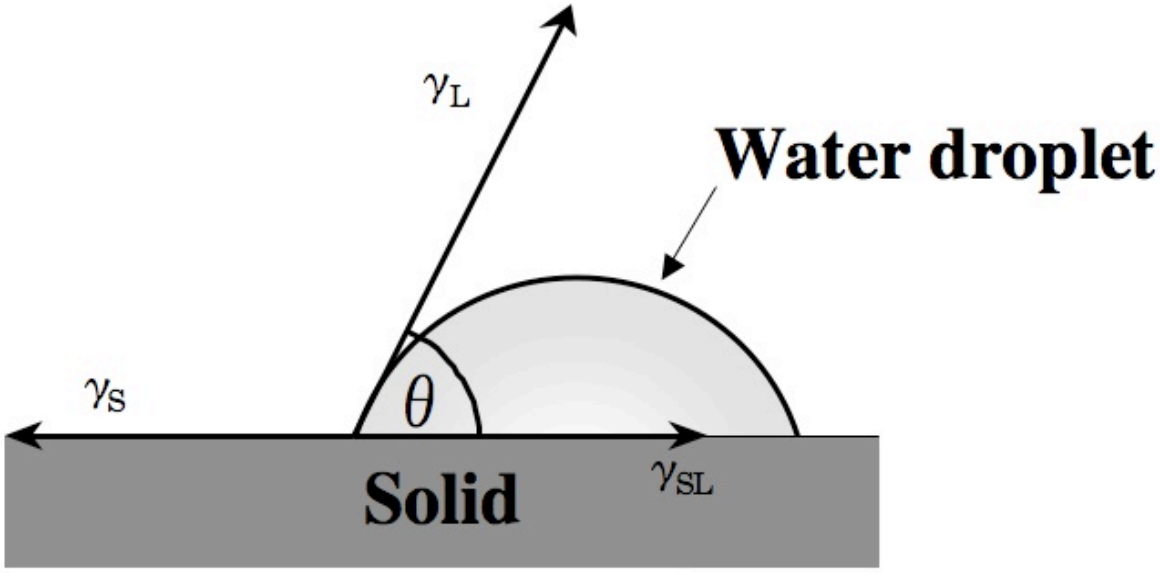

Figure 1.2. Water droplet on a flat surface (Young's model).

1.4.2. Wenzel's theory [29, 56-57]

When the solid surface is not flat, CA has been known to depend on surface roughness. Models have been proposed in the past to determine how roughness affects water repellency. Wenzel developed the first model, which is based on the consideration net energy decrease during spreading of a droplet on a rough surface.

In the Wenzel case, as illustrated in Figure 1.3, the liquid completely fills the grooves of the rough surface where they contact, described by Equation 1.2,

$$\cos\theta_W = (r\gamma_S - r\gamma_{SL}) / \gamma_L , \qquad (1.2)$$

where θ_W is the apparent CA in the Wenzel model and r is the surface roughness factor. The roughness factor is defined as the ratio of the total surface area of the rough surface to the footprint (or projected) surface area. Combining Equation 2 with Equation 1 yields Equation 1.3,

$$\cos\theta_W = r\cos\theta . \qquad (1.3)$$

From Equation 1.3, it can be predicts that if the CA of a liquid on a smooth surface is less than 90°, the apparent angle on a rough surface will be smaller. While the CA is greater than 90°, the angle on a rough surface will be larger.

1.4.3. Cassie's theory [29, 56-57]

Cassie and Baxter extended Wenzel's theory, which was originally developed for the homogeneous solid-liquid interface, to the composite interface. For this case, there are two

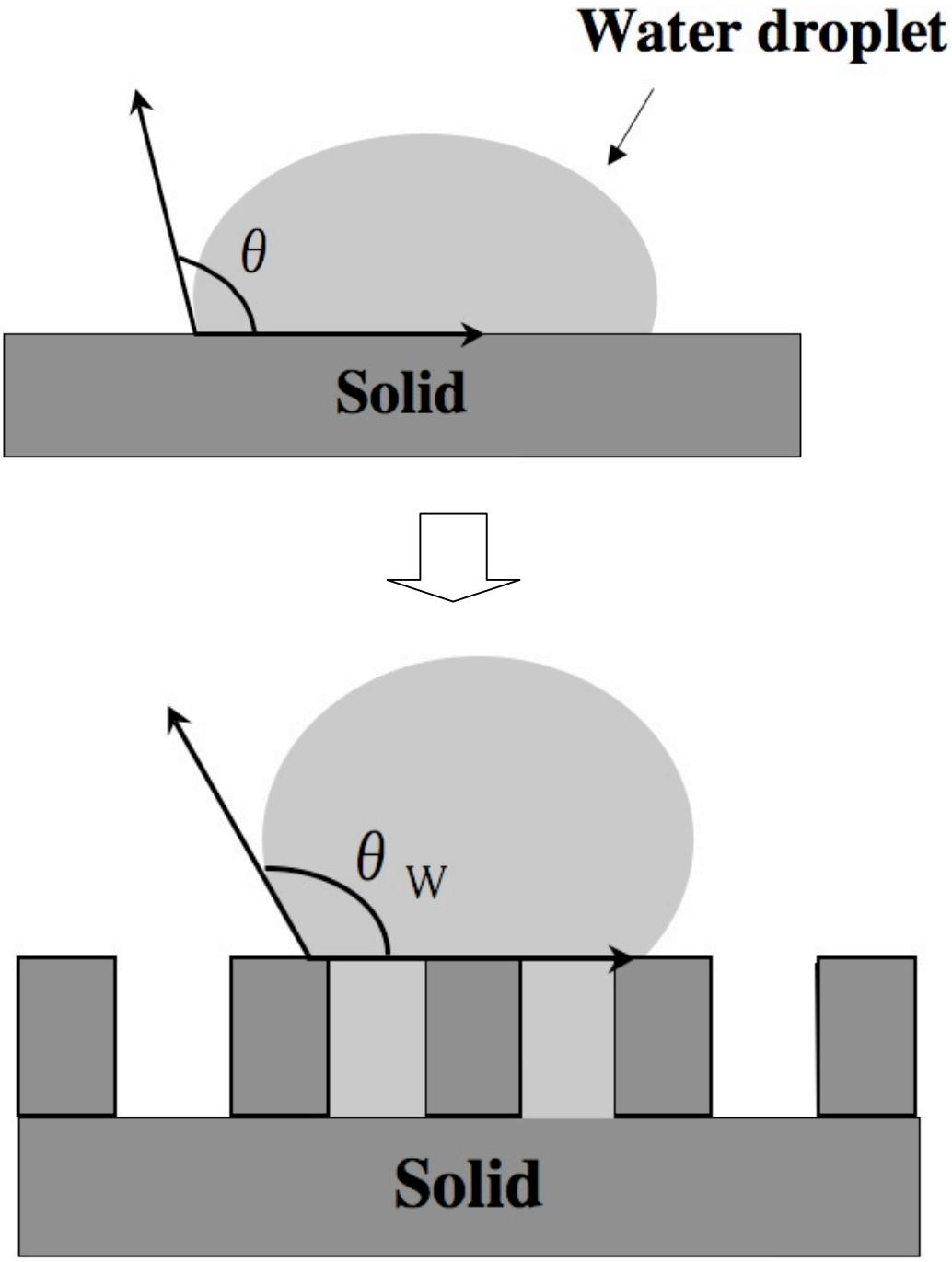

Figure 1.3. Effect of surface roughness on the wettability (Wenzel's model).

sets of interfaces: a liquid–air interface with the ambient environment surrounding the droplet and a flat composite interface under the droplet involving solid–liquid, liquid–air, and solid–air interfaces.

In the Cassie theory, air pockets are trapped underneath the liquid, which gives a composite surface (Figure 1.4). Defining the apparent CA in the Cassie model, θ_C can be correlated to the chemical heterogeneity of a rough surface by Equation 1.4,

$$\cos\theta_C = f_S \cos\theta_S + f_A \cos\theta_A, \quad (1.4)$$

where f_S and f_A are the area fractions of the solid and air on the surface, respectively. Since $f_S + f_A = 1$, $\theta_S = \theta$, and $\theta_A = 180°$, Equation 1.4 can be written as Equation 1.5,

$$\cos\theta_C = -1 + f_S (\cos\theta + 1). \quad (1.5)$$

From Equations 1.5, it can be found that for the material of original CA> 90°, the surface roughness will increase the apparent CA. This is unlike the Wenzel case, because even when the intrinsic CA of a liquid on a smooth surface is less than 90°, the contact angle can still be enhanced as a result of the as-trapped UWR air pockets.

1.4.4. Transition between Cassie's and Wenzel's states

According to Equations 1.3 and 1.5, for a surface with the same roughness, there should exist two distinct apparent CAs. It has also been reported that the solid/liquid contact mode will change from the Cassie to the Wenzel state when the spherical liquid droplet is pressed

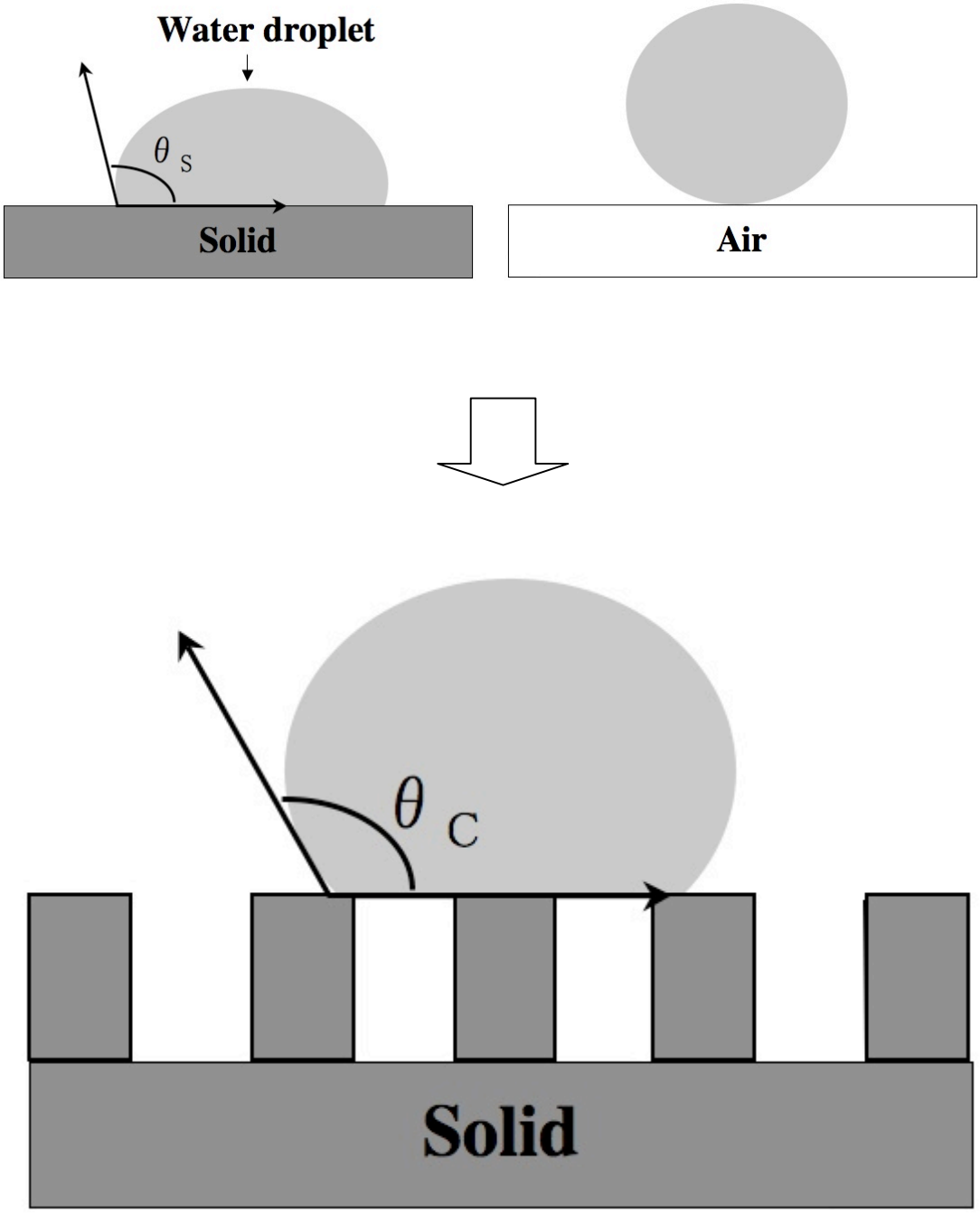

Figure 1.4. Effect of composite surface on the wettability (Cassie's model).

physically [58-60]. This indicates that in addition to coexisting, a transition between these two ultra water-repellent states can also occur [61-64] (Figure 1.5). When the wetting behavior changes from the Cassie model to the Wenzel model, the liquid droplet will fill the grooves of the rough substrate with a decrease in the apparent CA, and Equations 1.5 and 1.3 should be obeyed before and after the transition, respectively. Equating these two results, the threshold value θ_{T1} between the two modes can be obtained as Equation 1.7 [65],

$$\cos\theta_{T1} = (f_S - 1)/(r - f_S) , \quad (1.7)$$

where the subscript T1 denotes that θ_{T1} is a threshold value between the Wenzel and Cassie models. If the Young's CA is lower than the threshold value given by Equation 1.7, the as-trapped air pockets are metastable and the Wenzel model will be obtained. For the apparent CA of a liquid droplet to agree with the Cassie model, the solid substrate must be water-repellent enough or θ_{T1} must be as small as possible, because only when $\theta > \theta_{T1}$ are the as-trapped vapor pockets sTable

1.5. Objective and outline of this thesis

As mentioned in the previous sections, many functional SiO:CH films, which include UWR thin films, have been proposed using PECVD method. In particular, Takai laboratory has been succeeded in fabricating the transparent and highly-durable UWR thin films by using radio frequency plasma-enhanced chemical vapor deposition (RF PECVD) and MPECVD using organosilicon molecules [13-20]. In these papers, they found that the UWR feature originates in both the hydrophobic hydrocarbon functional groups which terminate the whole SiO:CH films and an appropriate surface roughness provided by SiO:CH nano-clusters. For step

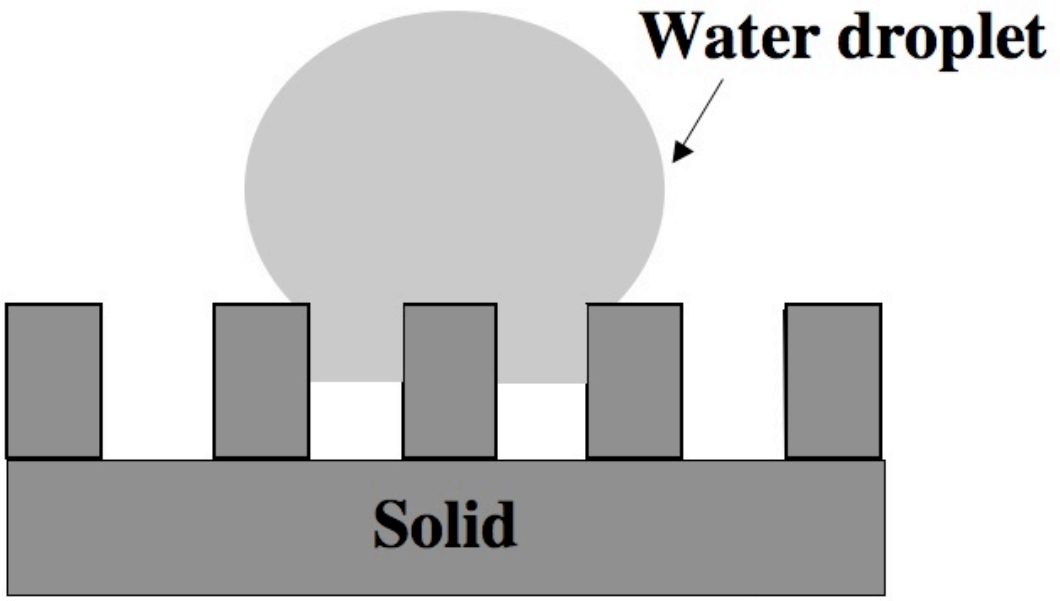

Figure 1.5. Intermediate state between the Wenzel and the Cassie models.

toward the practical use of these UWR thin films, it is necessary to improve the film properties, such as the hardness, adhesion, chemical durability and optical characteristic. In order to realize these improvements, it is indispensable to clarify the formation mechanism of the UWR thin films, which consist of both the SiO:CH nano-clusters for providing surface roughness and the SiO:CH films as a binding material among the nano-clusters, and then the deposition process should be controlled and monitored. That is to say, the followings must be understood: (1) the behavior of the reactant organosilicon molecules, *e.g.* dissociation and recombination in the plasma phase, (2) the deposition mechanisms of the SiO:CH films on the substrate surface, and (3) the formation and the deposition of the SiO:CH nano-clusters.

Therefore, the aim of this thesis is to attain three objectives as follows:

1. Analysis of the behavior of organosilicon molecules at electron impact, which is known as one of the most fundamental phenomena in plasma,
2. Fabrication of SiO:CH thin films and clarification of roles of deposition conditions, the films were fabricated at low pressure to extract simply the deposition phenomenon of the SiO:CH films, and dependences on RF power and Ar gas mixture ratio were investigated since these two conditions have the largest influence on wettability of the SiO:CH films,
3. Fabrication of UWR thin films and observation of their formation process, in particular, the formation mechanism of the SiO:CH nano-clusters must be investigated.

Chapter 1 includes general information of SiO:CH films, UWR thin films, and applications of those films. In Chapter 2, electron impact dissociation behavior of organosilicon molecules was analyzed using a quadrupole mass spectrometry (QMS) and a semi empirical molecular orbital method (MOPAC-PM3). In Chapter 3, SiO:CH thin films were fabricated by RF

PECVD. Moreover, RF power and Ar gas dependence in the film formation was investigated by Fourier-transform infrared spectrometer (FT-IR), X-ray photoelectron spectrometer (XPS), water contact angle, and optical emission spectroscopy (OES). Chapter 4 gives a fabrication of UWR thin films, and consideration about the formation process of UWR thin films. Lastly, Chapter 5 summarizes all the chapters.

References

[1] H. O. Pierson, Handnook of Chemical Vapour Deposition William Andrew Publishing, New York (1999) 2nd ed., 302.

[2] Y. T. Kim, D. S. Kim and D. H. Yoon, Thin Solid Films, 475 (2005) 271.

[3] K. Teshima, H. Sugimura, Y. Inoue and O. Takai, A. Takano, Langmuir, 19 (2003) 8331.

[4] S. C. Deshmukh and E. S. Aydil, J. Vac. Sci. Technol. B, 14 (1996) 738.

[5] H. Chatham, Surf. Coat. Technol., 78 (1996) 1.

[6] T. Homma, Mater. Sci. Eng. R, 23 (1998) 243.

[7] K. E. Mattsson, J. Appl. Phys., 77 (1995) 6616.

[8] M. N. P. Carreno, M. I. Alayo, I. Pereyra and A.T. Lopes, Sens. Actuators A, 100 (2002) 295.

[9] Y. Wu, H. Sugimura, Y. Inoue and O. Takai, Thin Solid Films, 435 (2003) 161.

[10] T. B. Casserly and K. K. Gleason, Plasma Process. Polym., 2 (2005) 669.

[11] V. Rouessac, L. Favennec, B. Remiat, V. Jousseaume, G. Passemard and J. Durand, Microelec. Eng., 82 (2005) 333.

[12] D. Shamiyan, M. R. Baklanov, S. Vanhaelemeersch and K. Maex, J. Vac. Sci. Technol. B, 20 (2002) 1923.

[13] O. Takai, A. Hozumi and N. Sugimoto, J. Non-Cryst. Solids, 218 (1997) 280.

[14] A. Hozumi and O. Takai, Thin Solid Films, 334, (1998) 54.

[15] Y. Wu, M. Kuroda, H. Sugimura, Y. Inoue and O. Takai, Surf. Coating Tech., 174-175 (2003) 867.

[16] Y. Yun, T. Yoshida, N. Shimazu, N. Nanba, Y. Inoue, N. Saito and O. Takai, J. Surf. Fin. Soc. Jpn, 58 (2007) 307 [in Japanese].

[17] Y. Wu, Y. Inoue, H. Sugimura, O. Takai, H. Kato, S. Murai and H. Oda, Thin Solid Films, 407 (2002) 45.

[18] A. Hozumi and O. Takai, Thin Solid Films, 303 (1997) 222.

[19] K. Teshima, H. Sugimura, Y. Inoue and O. Takai, A. Takano, Applied Surface Science, 244 (2005) 619.

[20] Y. Wu, M. Bekke, Y. Inoue, H. Sugimura, H. Kitaguchi, C. Liu and O. Takai, Thin Solid Films, 457 (2002) 122.

[21] A. R. Parker, C. R. Lawrence, Nature, 414 (2001) 33.

[22] S. Herminghaus, Europhys. Lett., 52 (2000) 165.

[23] C. Neinhuis and W. Barthlott, Ann. Bot., 79 (1997) 667.

[24] P. Ball, Nature, 400 (1999) 507.

[25] W. Barthlott and C. Neinhuis, Planta 202 (1997) 1.

[26] X. F. Gao and L. Jiang, Nature, 432 (2004) 36.

[27] T. Wagner, C. Neinhuis and W. Barthlott, Acta Zool., 77 (1996) 213.

[28] W. Lee, M. K. Jin, W. C. Yoo and J. K. Lee, Langmuir, 20 (2004) 7665.

[29] X. Feng and L. Jiang, Adv. Mater., 18 (2006) 3063.

[30] A. B. D. Cassie and S. Baxter, Trans. Faraday Soc., 40 (1944) 546.

[31] R. Blossey, Nat. Mater., 2 (2003) 301.

[32] A. Nakajima, K. Hashimoto and T. Watanabe, Monatsh. Chem., 132 (2001) 31.

[33] Y. Liu, L. Mu, B. H. Liu and J. L. Kong, Chem. Eur. J., 11 (2005) 2622.

[34] I. P. Parkin and R. G. Palgrave, J. Mater. Chem., 15 (2005) 1689.

[35] T. L. Sun, L. Feng, X. F. Gao and L. Jiang, Acc. Chem. Res., 38 (2005) 644.

[36] K. Tadanage, N. Katata and T. Minami, J. Am. Ceram. Soc., 80 (1997) 1040.

[37] M. Kogoma, H. Kasai, K. Takahashi and T. Moriwaki, Appl. Phys., 20 (1987) 147.

[38] R.H. Hopkins, Appl. Opt., 14 (1975) 2831.

[39] H. Atsushi, U. Kazuya, S. Hiroyuki and T. Osamu, Langmuir, 15 (1999) 7600.

[40] A. Nakajima, K. Abe, K. Hashimoto and T. Watanabe, Thin Solid Films, 376 (2000) 140.

[41] A. Nakajima, K. Hashimoto and T. Watanabe, Monatsh. Chem., 132 (2001) 31.

[42] N. Watanabe and Y. Tei, Chemistry, 46 (1991) 477.

[43] J. Bico, C. Marzolin and D. Que´re´, Europhys. Lett., 47 (1999) 220.

[44] L. Feng, Y. Song, J. Zhai, B. J. Xu, L. Jiang and D. Zhu, Angew. Chem., Int. Ed., 42 (2003) 800.

[45] M. Thieme, R. Frenzel, S. Schmidt, F. Simon, A. Henning, H. Worch, K. Lunkwitz and D. Scharnweber, Adv. Eng. Mater., 3 (2001) 691.

[46] L. Feng, Z. Zhang, Z. Mai, Y. Ma, B. Liu, J. Xu and D. Zhu, Angew. Chem., Int. Ed., 43 (2004) 2012.

[47] X. Zhang, F. Shi, X. Yu, H. Liu, Y. Fu, Z. Wang, L. Jiang and X. Li, J. Am. Chem. Soc., 126 (2004) 3064.

[48] K.K.S. Lau, J. Bico, K.B.K. Tea and M. Chhowalla, Nano Lett., 3 (2003) 1701.

[49] A. Kinbara, Engineering of Thin Films, Maruzen, Tokyo, (2004) 2nd ed. 267 [in Japanese].

[50] T. Nishino, M. Meguro, K. Nakamae, M. Matsushita and Y. Ueda, Langmuir, 15 (1999) 4321.

[51] D. Öner and T. J. McCarthy, Langmuir, 16 (2000) 7777.

[52] R. Wang, K. Hashimoto, A. Fujishima, M. Chikuni, E. Kojima, A. Kitamura, M. Shimohigoshi and T. Watanabe, Adv. Mater., 10 (1998) 135.

[53] H. M. Shang, Y. Wang, S. J. Limmer, T. P. Chou, K. Takahashi and G. Z. Cao, Thin Solid Films, 472 (2005) 37.

[54] X. Lu, C. Zhang and Y. Han, Macromol. Rapid Commun., 25 (2004) 1606.

[55] W. Li and A. Amirfazli, J. Colloid Interface Sci., 292 (2005) 195.

[56] N. Fuzimoto, Technology of wetting, hydrophobic and hydrophilic, and their control, Techical Information Institute, Tokyo (2007) 8 [in Japanese].

[57] Z. Burton and B. Bhushan, Ultramicroscopy, 106 (2006) 709.

[58] J. Bico, C. Marzolin and D. Quéré, Europhys. Lett., 47 (1999) 220.

[59] A. Lafuma and D. Quéré, Nat. Mater., 2 (2003) 457.

[60] C. Ishino, K. Okumura and D. Quéré, Europhys. Lett., 68 (2004) 419.

[61] A. Marmur, Langmuir, 20 (2004) 3517.

[62] A. Dupuis and J. M. Yeomans, Langmuir, 21 (2005) 2624.

[63] N. A. Patankar, Langmuir, 19 (2003) 1249.

[64] N. A. Patankar, Langmuir, 20 (2004) 7097.

[65] J. Bico, C. Tordeux and D. Quéré, Colloids Surf. A, 206 (2002) 41.

Chapter 2. Electron impact dissociation behavior of organosilicon molecules

2.1. Introduction

As mentioned in Chapter 1, various kinds of organosilicon molecules have been utilized in PECVD processes in order to improve the properties of SiO_2 films [1-3], and novel functional films have been proposed by PECVD, such as SiOF films for its dielectric properties, SiON for its mechanical properties and SiO:CH films for its dielectric properties as well as ultra water repellency, have been intensively investigated [4-7]. In order to improve the properties of those films, it is necessary to clarify the reaction in the PECVD processes, and the deposition process should be controlled and monitored effectively. However, the reaction mechanisms of the organosilicon molecules in plasma have not been clarified due to its complexity.

To understand the reactions in the plasma, it is necessary to investigate the electron impact dissociation of the monomers, which is one of the most fundamental processes in plasma. In this section, I discuss the dissociative ionization of the organosilicon molecules with methyl groups by electron impact phenomenon, on the basis of the fragment patterns and molecular-orbital calculation of the bond dissociation energies. However, there is a possibility that the dissociative ionization and neutral dissociation shows quite different behavior, i.e., X^+ ionic radical production occurs but X radical production does not occur. Hence I describe only the dissociative ionization behavior in this work.

2.2. Experimental procedure

Electron impact dissociation phenomenon was investigated by using a quadrupole mass

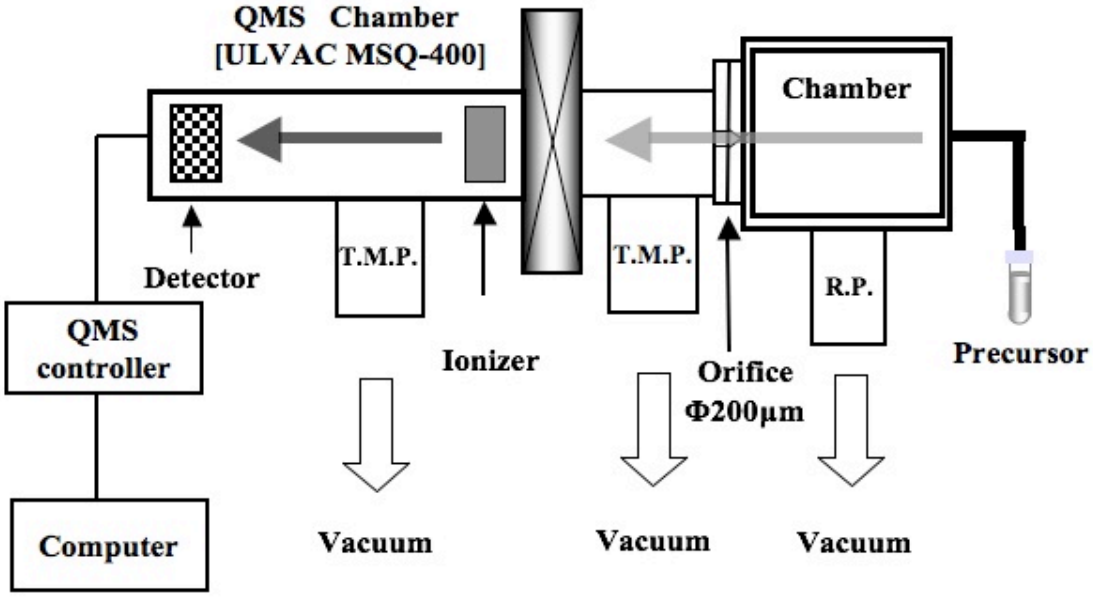

Figure 2.1. Schematic diagram of QMS system.

spectrometer (QMS : MSQ-400, ULVAC Japan). As shown in Figure 2.1, the experimental system consists of the QMS unit, a chamber for reactant introduction and a vacuum system. The vacuum system is made up of a rotary pump (R.P., ULVAC, G-50D) and a turbo molecular pump (T.M.P., Leybold, TUROVA35). Pressure of the QMS unit was maintained at under 1.5×10^{-4} Pa. The organosilicon reactants used in this work were trimethylmethoxysilane [TMMOS; $(CH_3)_3SiOCH_3$] and hexamethyldisiloxane [HMDSO; $(CH)_3SiOSi(CH)_3$]. After pumping the chamber below 0.1 Pa, the reactant gas was fed into the chamber through a needle valve upto 5 Pa. The gas molecules in the chamber were sampled into the QMS unit through an orifice of 0.2 mm in diameter. The pressure in the QMS unit became $\sim 5.5 \times 10^{-3}$ Pa at the reactant pressure in the chamber of 5 Pa. Electron impact ionization was carried out at 10 ~ 40 eV of electron energy. Bond dissociation energies for the molecules were estimated by a semi-empirical molecular orbital (MO) calculations with PM3 Hamiltonian [8]. Each bond dissociation energy was calculated by difference of heat of formation between the reactants and the productants.

2.3. Results and discussion

2.3.1. Bond dissociation energy of organosilicon molecules

To investigate the electron impact dissociation behavior, the calculated bond dissociation energies were listed in Table 2.1. The bond dissociation energies obtained by the MO calculation with AM1 Hamiltonian were also shown there for the comparison [9]. Although the bonding energies of Si-O and C-H were estimated smaller in our results than the reference, a general tendency can be found that Si-C bonding is significantly weak compared to the other chemical bondings in the reactants. Si-O and O-C bonding in TMMOS are stronger than C-H bonding. In the HMDSO, on the other hand, the order in the bond dissociation energies is

Table 2.1. Bond dissociation energy of neighboring atoms of reactants and reference citation. Values of the reactant bond dissociation energy were obtained by the molecular orbital calculation of MOPAC.

	Bond dissociation energy (eV)				
	Reference	TMMOS		HMDSO	
$Si-CH_3$	3.44	$Si-CH_3$	2.95	$Si-CH_3$	2.82
				$Si-CH_3$	2.74
Si-O	4.96	$Si-OCH_3$	4.13	Si-OSi	4.48
O-C	3.95	$SiO-CH_3$	4.17	-	-
C-H	4.50	SiC-H	3.98	SiC-H	3.70
		SiOC-H	4.09		

similar with that of the TMMOS, except that Si-O bonding in the HMDSO (siloxane bonding) is much stronger than that in TMMOS. These results indicate that methyl group in TMMOS and HMDSO are possible to be dissociated preferentially by the electron impact. Regarding Si-O in the reactants, the Si-O bonding of TMMOS is capable to dissociate easier than that of HMDSO.

2.3.2. Fragment patterns of organosilicon molecules

Figure 2.2 shows the QMS fragment patterns for the reactants at various electron energies. Each peak was identified as m/e = 15 (CH_3^+), 31 (OCH_3^+), 43 ($SiCH_3^+$), 59 ($SiOCH_3^+$), 89 ($SiO(CH_3)_3^+$), 73 ($Si(CH_3)_3^+$) and 147 ($Si_2O(CH_3)_5^+$), respectively. The results are given for the dominant isotope 28 Si (92.3 %). Comparing with the peak intensities and the isotope abundance ratio of Si, the much less abundant isotopes ^{29}Si (4.7 %) and ^{30}Si (3.0 %) emerged as two additional peaks at m/e 60 - 61 and 90 - 91 in TMMOS, m/e = 60 - 61 and 148 - 149 in HMDSO, respectively. In the fragment patterns of TMMOS (Figure 2.2 (a)), the fragment peak at m/e = 89 appeared primarily with 13 eV of electron energy, and m/e = 15, 31 and 59 emerged slightly. Over 20 eV of electron energy, intensity of the peak at m/e = 59 exceeded that of m/e = 89. This is attributed to an increase in the electron energy to dissociate the methyl group in the reactant. Meanwhile, intensity of methyl group (m/e = 15) shows smaller value in comparison to that of the other species in all range of energy explored in this work. It suggests that in the electron impact dissociation of TMMOS, the dissociated methyl group exists with neutral state in the plasma. About the TMMOS reactant of m/e = 104 ($SiO(CH_3)_4^+$), it was observed weakly. The TMMOS reactant ionizes preferentially with dissociation of methyl groups in the electron-impact circumstances. In the HMDSO (Figure 2.2 (b)), fragment patterns were similar with that of the TMMOS, which consisted of ions dissociated

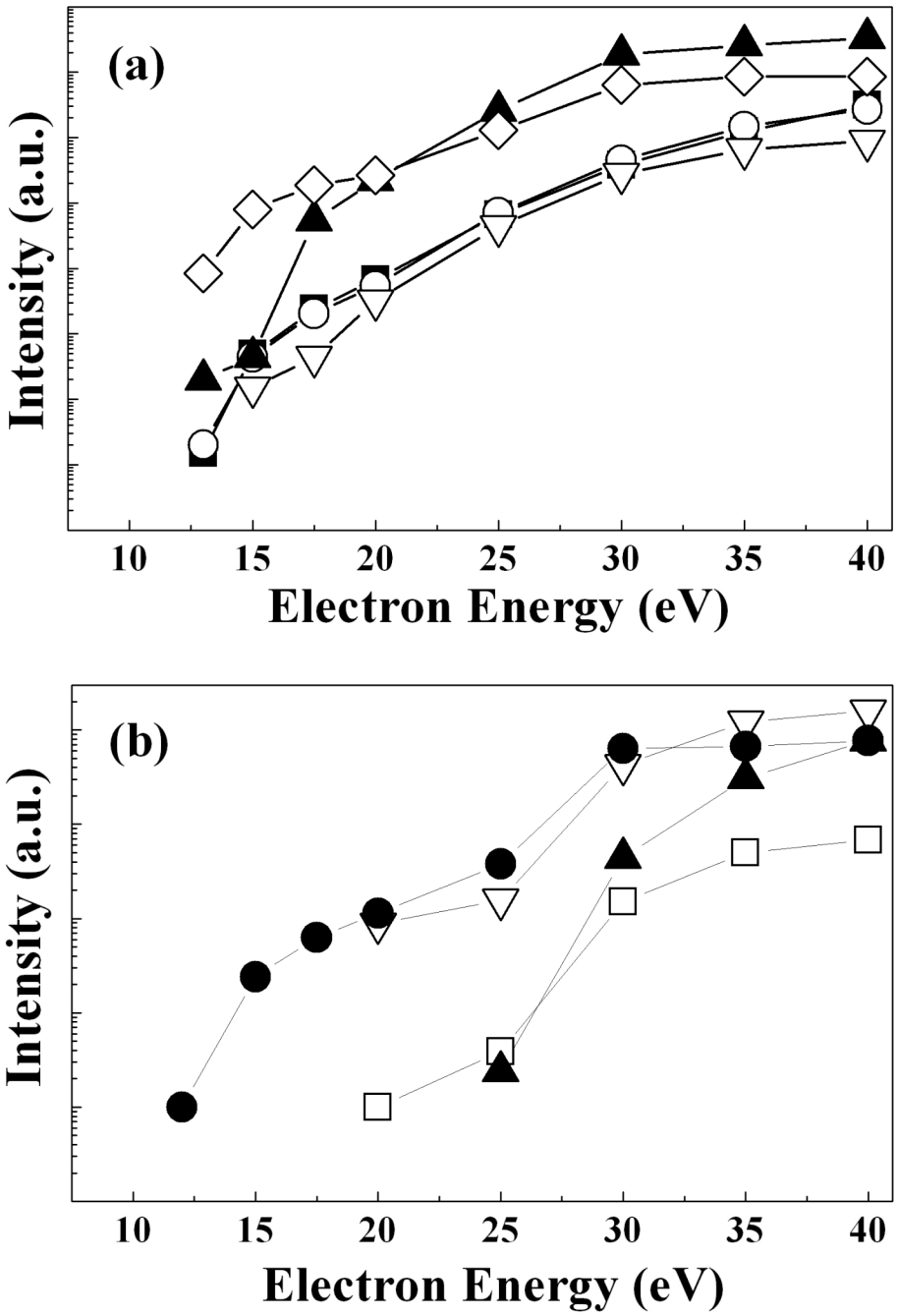

Figure 2.2. QMS fragment patterns in TMMOS (a) and HMDSO (b) at various electron energies. Closed squares (■), open circles (○), open squares (□), closed triangles (▲), open triangles (▽), open diamonds (◇) and closed circles (●) indicate m/e = 15, 31, 43, 59, 73, 89 and 147, respectively.

methyl groups by electron impact, *e.g*. methyl group in the HMDSO dissociated at first under 12 eV of electron energy. However, dissociated ions from the HMDSO appeared under higher electron energy than that from TMMOS. At 20 eV, m/e = 73 ($Si(CH_3)_3^+$) and 43 ($SiCH_3^+$) emerged, and then m/e = 59 ($SiOCH_3^+$) appeared at 25 eV. From the fragment patterns of the reactants, the HMDSO is hard to dissociate comparing with the TMMOS due to a strong Si-O bonding energy.

2.3.3. Molecular orbital calculation of organosilicon molecules

Figure 2.3 shows the highest occupied molecular orbitals (HOMO) of the reactants calculated by MOPAC-PM3. Chemical reaction is often governed by electron transfer from the HOMO to the lowest unoccupied molecular orbitals (LUMO) in molecules. The HOMO-LUMO energies gap is important to predict the reactions. While in the electron impact dissociation, HOMO plays an important role due to low ionization energy. That is, the electron in HOMO is more likely to collide elastically or inelastically with an external electron, and it leads to ionize itself or dissociation reaction [10]. From the HOMO orbital of TMMOS (Figure 2.3 (a)), the electrons were localized on two methyl groups in Si-C bonding, oxygen atom and C-H bonding. It suggests that the electrons on those chemical bonds are easily emitted by electron impacts. Moreover, this electron impact affects the dissociation reaction of molecule. For the dissociation reactions, however, it is necessary further investigations, *e.g*. exited state MO calculations with high-accuracy. From the former fragment pattern of reactants, the intensity of m/e = 89 saturated slightly at 20 eV, and that of m/e = 59 exceeded over 20 eV. To produce the ions which have a mass of m/e = 59 by the electron impact in TMMOS, 3 methyl groups must be removed from the TMMOS. The methyl groups which have not HOMO orbital (Figure 2.3 (a)) are hard to interact with

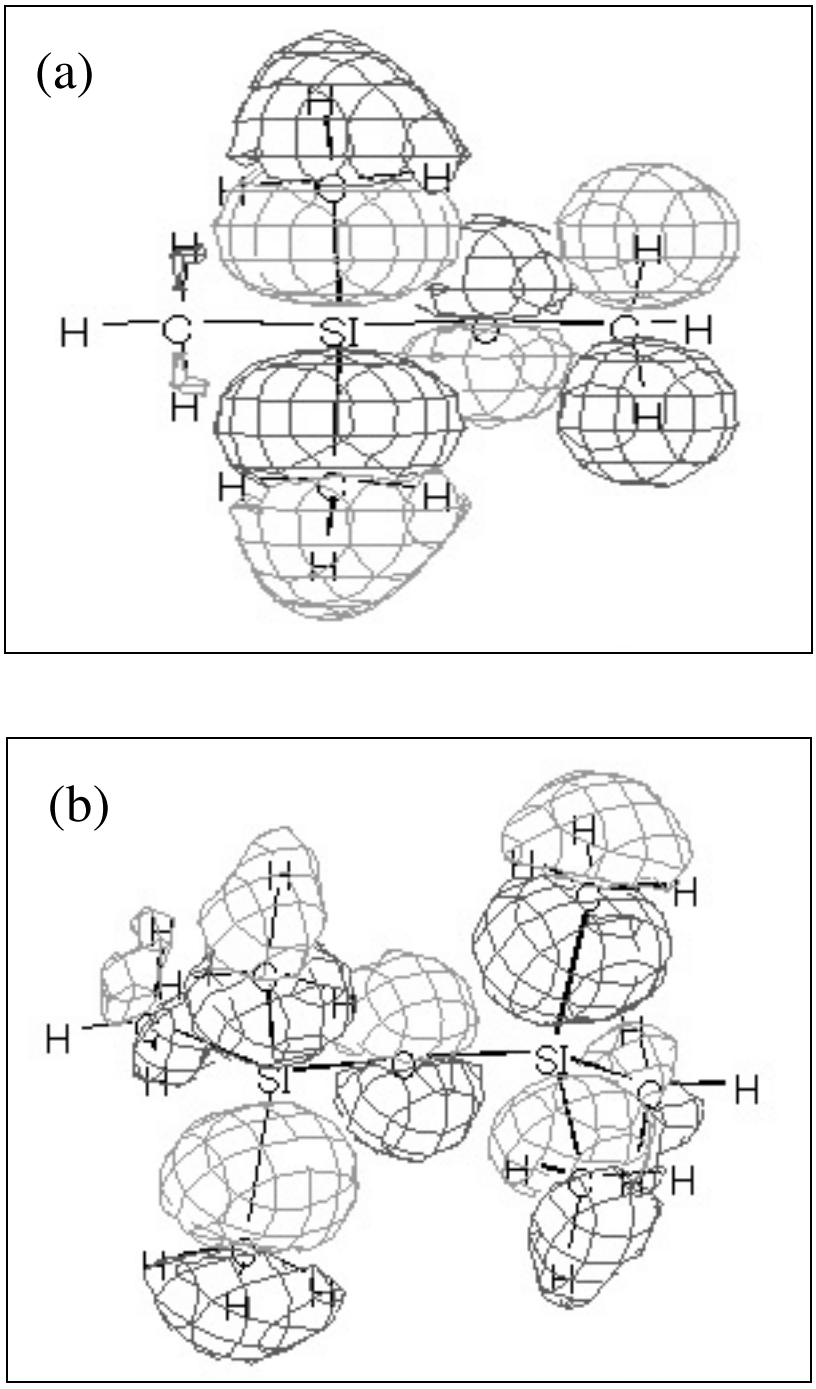

Figure 2.3. Highest occupied molecular orbitals of TMMOS (a) and HMDSO (b) calculated by MOPAC.

colliding electrons because of its geometrical configuration of electron clouds. Therefore, the mass peak of $SiOCH_3^+$ (m/e = 59) is lower than $SiO(CH_3)_3^+$ (m/e = 89) for lower energy of electron impact as shown in Figure 2.2 (a). The degree ofinteraction between colliding electrons and the electron clouds in the molecules can be enhanced when increasing energy of colliding electrons. This could be an explanation of increase of $SiOCH_3^+$ (m/e = 59). From the 28th orbital (HOMO) of HMDSO (Figure 2.3 (b)), the orbital presents symmetrically centered at oxygen atom, and consists in methyl groups and oxygen atom. In the orbital of methyl groups, two orbitals are distributed to one methyl group independently and spread over last of two methyl groups. Regarding the fragment pattern of HMDSO, it is concerned in the geometrical configuration of electron clouds, *i.e*. the combined methyl groups with one orbital is possible to dissociate together by the electron impact.

2.4. Summary

From the calculation of bond dissociation energy of the organosilicon molecules, methyl groups bonded directly to silicon atom was found as weakest. Regarding the fragment patterns of the reactants investigated by QMS, the HMDSO was hard to dissociate comparing with the TMMOS due to the strong Si-O bonding force, and it affected the dissociation in the plasma. From the above considerations, dissociation reactions by electron impact could be partly identified.

References

[1] H. O. Pierson, Handnook of Chemical Vapour Deposition William Andrew Publishing, New York (1999) 2nd ed., 302.

[2] J. C. Alonso and A. Ortiz: Vacuum 43 (8) (1992) 843.

[3] Shashank C. Deshmukh and Eray S. Aydil, J. Vac. Sci. Technol. B 14 (1996) 738.

[4] T. Homma, Mater. Sci. Eng., R23 (1998) 243.

[5] K. E. Mattsson, J. Appl. Phys., 77 (1995) 6616.

[6] M. N. P. Carreno, M. I. Alayo, I. Pereyra and A. T. Lopes, Sensors Actuators A 100 (2002) 295.

[7] Y. Wu, H. Sugimura, Y. Inoue and O. Takai, Thin Solid Films 435 (2003) 161.

[8] N. Senda and Idemitsu, Technical Report, 49 (2006) 106.

[9] H. Sugitani, T. Kikuchi, Y. Sugimoto and T. Saitou, Appl. Organomet. Chem., 5 (1991) 309.

[10] M. Hirota, Application of molecular orbital theory to organic chemistry 3rd ed., Shokabo, Tokyo (2004) 76.

[11] Y. Yun, T. Yoshida, N. Shimazu, Y. Inoue, N. Saito and O. Takai, Solid State Phenomena 124-126 (2007) 347.

Chapter 3. Formation of SiO:CH thin films by RF PECVD process

In the previous chapter, the electron-impact dissociation phenomenon of the organosilicon molecules (TMMOS and HMDSO) were discussed based both on the experimental results obtained by using a quadrupole mass spectrometer as a simple simulation for the dissociation process of the organosilicon molecules in plasma phase, and on the bond dissociation energy estimated from MOPAC calculation. A preferred dissociation was found in methyl groups bonded directly with silicon atoms. The PECVD processes must proceed with the deposition of the gas species originated in both the dissociation and the subsequent recombination reactions each other until they reach an equilibrium in plasma. In this chapter, the actual deposition processes are investigated by using two types of widely-used RF PECVD, inductively-coupled and capacitively-coupled PECVD systems.

3.1. Formation of SiO:CH thin films by the inductively coupled PECVD

3.1.1. Introduction

In recent years, innovative functional SiO:CH films have been prepared by PECVD using organosilicon molecules have been intensively investigated [1-5]. As an application of these films, Takai laboratory has been succeeded in fabricating the UWR films by remote-type MPECVD [6-7], and S. Nunomura, et al. proposed nano-cluster composite porous SiO:CH films having dielectric constants of 1.7 - 3.5 [8]. According to these reports, it is important to investigate the formation process of the SiO:CH thin films on substrates in order to fabricate those high performance films. In this section, the SiO:CH films are prepared by an inductively-coupled RF PECVD system with the remote-type configuration same as the

MPECVD system used in the deposition of UWR films [6-7]. For preparation of the UWR and the low-k films, the total pressure was kept at relatively high values, 80 Pa [6] and 133 Pa [8], respectively, expecting formation of the nanoclusters. In this chapter, however, the total pressure was kept at 10 Pa, being low enough for deposition of flat SiO:CH films without nano-clustering, in order to simplify the reaction circumstances. I discuss formation process of the SiO:CH films through a comparative analysis between the dissociation reaction and chemical bonding states, on the basis of the consideration of the electron impact dissociation behavior in Chapter 2.

3.1.2. Experimenal procedure

This work was carried out with a RF PECVD system. As shown Figure 3.1, the PECVD system consists of a deposition chamber and a quartz discharge tube whose length and diameter was 200 and 55mm, respectively. A 13.56 MHz generator (ENI, OEM-12A) supplied the RF power into the copper coil through a matching network in order to activate the discharge. The reactants used in this work were trimetylmethoxysilane [TMMOS; $(CH_3)_3SiOCH_3$] and hexamethyldisiloxane [HMDSO; $(CH)_3SiOSi(CH)_3$]. Si (100) substrates were located at 150 mm below from the center of the plasma to avoid the direct thermal damage by the plasma. The reactant was introduced into the chamber upto the total pressure of 10 Pa at the flow rate of 10 sccm. The films were prepared under various RF power in the range of 10~100 W. Plasma diagnostics was performed by optical plasma emission spectroscopy (OES). Optical emission spectra were obtained through a quartz-glass window positioned top of the quartz discharge tube. A fiber optic cable transmitted collected light to a monochromator (Chromex, 500-IS) attached with a CCD detector (Princeton Instrument, CCD-1100PF/UV). Wavelength resolution of this OES system was 0.15 nm. After deposition,

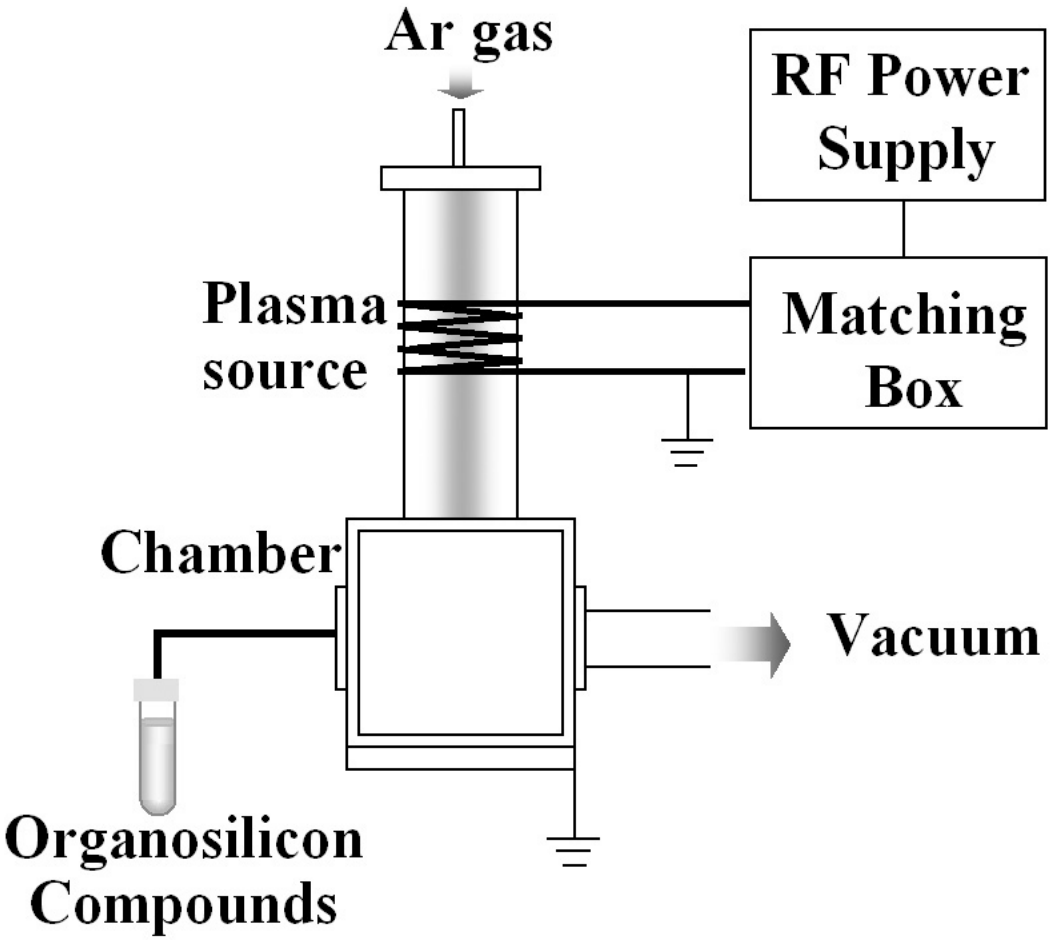

Figure 3.1. Schematic diagram of the PECVD system.

the chemical bonding states were characterized by a Fourier-transform infrared spectrometer (FT-IR ; Digilab, FTS-7000).

3.1.3. Results and Discussion

3.1.3.1. Optical emission spectroscopy of plasma

Figure 3.2 shows the optical emission spectra in a region of 420 ~ 490 nm for organosilicon plasma ((A) TMMOS, (B) HMDSO) recorded during deposition of the SiO:CH films. In TMMOS plasma, emissions from atomic H, CO, CH (4300 Å system, $A^2\Delta$-$X^2\Pi$) radicals and H_2 molecules were detected. The strongest intensity peak in this wavelength region was atomic state of H_β which locates at 486.1 nm. As the CO emission, the Ångström system bands ($B^1\Sigma$-$A^1\Pi$) and the triplet bands ($d^3\Delta$-$a^3\Pi$) were observed between 440 and 480 nm wavelengths. Each emission intensity increased with the RF power. Although the optical emission intensity was almost below the detection limit at the RF power of 10 W, the H_β line and the CO bands come into view firstly with an increase in the RF power. In HMDSO plasma, on the other hand, the CO bands were not detected at all. The strongest intensity peak was also atomic state of H_β. In the region of 430 ~ 490 nm, emission lines from H_2 can be prominently observed.

In organosilicon plasma, the hydrogen atoms are generated from the $-CH_3$ groups of the precursors or the CH_x radicals dissociated from precursors (here generically describe both as $-CH_x$) in collisions with electrons;

$$-CH_x + e \rightarrow -CH_{x-1} + H + e. \qquad (3.1)$$

One of the origins of H_2 molecules is believed to be three body recombination of H atoms, which come primarily via dissociation of the $-CH_3$ groups in TMMOS. In organosilicon plasma, the hydrogen atoms can be emitted from the $-CH_3$ groups of TMMOS or the CH_x

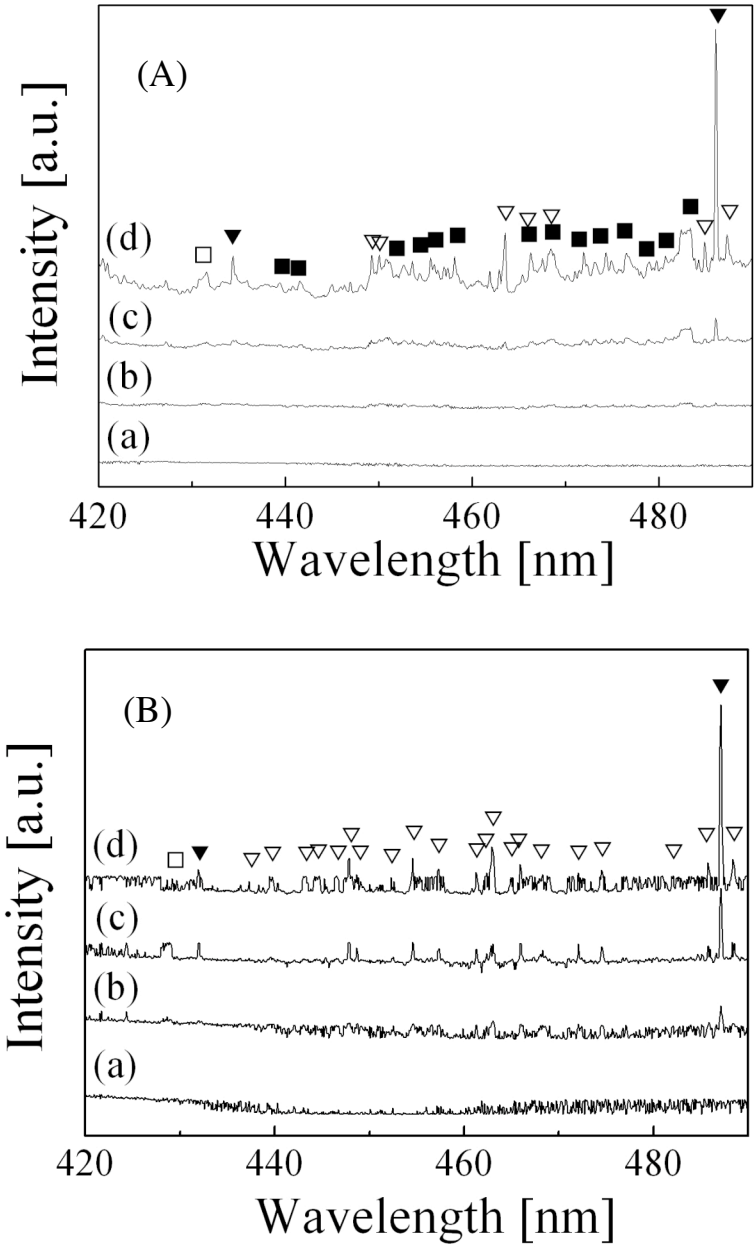

Figure 3.2. Optical emission spectra of inductively coupled organosilicon plasma, during deposition of hydrocarbon-doped silicon oxide films at the reactant of (A) TMMOS, (B) HMDSO ((a): 10W, (b): 30W, (c): 50W, (d): 100W). The closed triangles(▼), open triangles (▽), closed square (■) and open square(□) indicate the lines and bands from atomic H, H_2, CO and CH molecules, respectively.

radicals dissociated from in collisions with electrons;

$$\text{TMMOS} + e \rightarrow \text{H emission}, \quad (3.2)$$

$$\text{-CH}_x + e \rightarrow \text{H emission}, \quad (3.3)$$

$$\text{C}_x\text{H}_m \text{ stable molecules or radicals} + e \rightarrow \text{H emission}, \quad (3.4)$$

$$H + H + M \rightarrow H_2 \text{ emission} + M, \quad (3.5)$$

$$\text{C}_x\text{H}_m \text{ stable molecules or radicals} + e \rightarrow H_2 \text{ emission}. \quad (3.6)$$

Needless to say, the counterreaction, re-dissociation of H_2 also occurs and are purported to be under equilibrium. Hydrogen abstraction reactions are also expected to be another origin of H_2 molecules,

$$\text{-CH}_x + H \rightarrow \text{-CH}_{x-1} + H_2 \text{ emission}. \quad (3.7)$$

The CH radicals can arise from this reaction if x=2, and those can be emitted through

$$\text{TMMOS} + e \rightarrow \text{CH emission}, \quad (3.8)$$

$$\text{TMMOS like radicals} \rightarrow \text{CH emission}, \quad (3.9)$$

$$\text{C}_x\text{H}_m \text{ stable molecules} + e \rightarrow \text{CH emission}, \quad (3.10)$$

$$\text{C}_x\text{H}_n \text{ radicals} + e \rightarrow \text{CH emission}. \quad (3.11)$$

Under the low power regime, Equation 3.8 should be predominant and hence all the emission intensities as well as the deposition rate are proportional to the RF power. Under a RF power regime of 40-100 W the contribution of Equation 3.9 – 3.11 becomes appreciable, because the emission intensities increases with the RF power whereas the deposition rate is constant. Concerning to the emissions of CO, it is completely different from the absence of CO bands between TMMOS and HMDSO plasma. That is, emissions from CO bands were clearly seen in TMMOS plasma. In HMDSO plasma, on the other hand, they were not detected. The origin of the O atoms in the CO molecules must be the O of methoxy groups and siloxane bondings in TMMOS and HMDSO, respectively, while the C atoms must be from the $–CH_3$ groups.

These molecules consist of Si, C, H, and O atoms with the ratio of 1 : 4 : 12 : 1 and 2 : 6 : 18 : 1, respectively. The composition of O atoms in HMDSO plasma (3.7 at%) is surely lower than that in TMMOS plasma (5.6 at%) in the ideal gas approximation. However, the complete absence of the CO optical emission in the HMDSO plasma means the qualitative difference between these two reactants, that is, the O atoms in siloxane bondings are hardly expelled into the plasma, while those in methoxy groups can be released. Even though there are many suggestions about the generation route of CO molecules in TMMOS plasma, it is difficult to clarify in this paper due to the insufficiency of data. At least, it is easily understood that the O atoms in methoxy groups released once into the plasma as the form of CO can behave as a kind of oxidizing agent, because the absolute oxygen composition in the TMMOS plasma is quite low compared to the other gas species, H atoms, H_2 molecules, hydrocarbons etc., which have reducing characteristics.

From the above consideration on the plasma reactions, it can be concluded that, in TMMOS plasma, the oxygen atoms of methoxy groups can be dissociated in the plasma. Siloxane bondings in HMDSO, on the other hand, hardly expel oxygen atoms. This tendency must result in remaining of the siloxane bondings of the raw molecules in the deposited films.

3.1.3.2. Chemical bonding states of SiO:CH thin films

The FT-IR spectra of the films deposited from TMMOS (I) and HMDSO (II) are shown in Figure 3.3. Each absorption band was identified as O-H stretching (A), C-H stretching (B), CH_3 stretching (C), Si-H stretching (D), Si-CH_3 stretching (E), Si-CH_3 symmetric deformation (F), Si-O-CH_3 asymmetric stretching (G), polymer-like Si-O-Si, Si-CH_2-Si, Si-O-CH_2-Si, Si-CH_2-CH_2-Si, etc. (expressed hereafter as poly Si-X-Si) asymmetric stretching (H), Si-CH_3 rocking (I), poly Si-X-Si deformation (J) and Si-O-Si asymmetric stretching (K) [10-11].

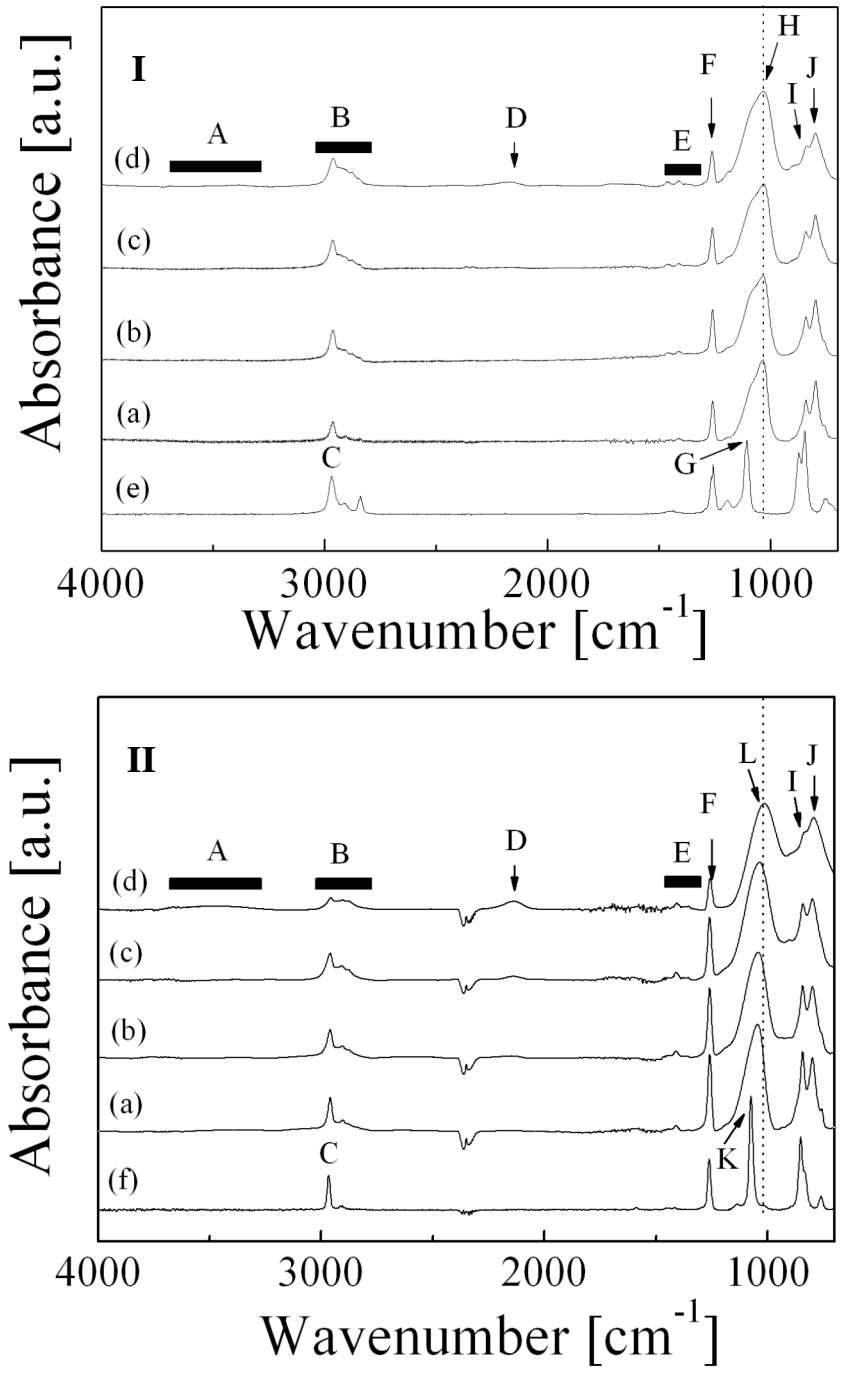

Figure 3.3. FT-IR absorption spectra for the reactants and films of TMMOS(**I**), HMDSO(**II**) ((a): 10W, (b): 30W, (c): 50W, (d): 100W, (e): TMMOS precursor, (f): HMDSO precursor). The alphabet notations are defined in the text.

Though the band (L) has probably same origin as the band (H), different notation was given since the band shape is different. The strongest intensity of absorption bands were poly Si-X-Si (H, L). In the FT-IR spectra for the TMMOS films (Figure 3.3-I), the absorption intensities of these bands were found to grow with an increase in the RF power (note that the intensities of the spectra were normalized in the figure). The band B (C-H) becomes broader with an increase in the rf power. Comparing the appearances of the absorption bands with that in the spectrum for the reactant (e), the absorption bands B (C-H) and H (poly Si-X-Si) become obviously broader. This broadening is due to the diverseness of the chemical bonding states. Specifically, the band (C), with a sharp head at 2969 cm^{-1}, a small shoulder at 2910 cm^{-1}, and another head at 2839 cm^{-1}, is ascribable to exactly the C-H bonds of TMMOS, mainly in three Si-$\underline{C\text{-}H_3}$ groups and partly in a Si-O$\underline{C\text{-}H_3}$, here the underline means the origin of the absorption band. The broadening of the band (C) means the C-H bonding in the sample becomes to have various types of C-H bonds, in more precise description, various types of chemical environment of C atoms which have at least one C-H bond. For example, longer alkyl chains, double bond around the relevant C atoms, aromatic rings, polymer-like networks, etc. These chemical bonds did not exist in the reactant molecule TMMOS, but generated as a result of dissociation and recombination of the raw material in plasma phase, and subsequent impingement and chemisorption on the substrates. Taking into account the newly-appeared bands A (O-H), D (Si-H) and J (poly Si-X-Si), these results show that the deposited films can be described as poly Si-X-Si and/or -CH_2- networks with -OH, -CH_3 and -H terminations. In the FT-IR spectrum for the HMDSO films (Figure 3.3-II), the basic chemical bonding states seem to be not far from those of the TMMOS films (Figure 3.3-I), since the positions and the fundamental shapes of the absorption bands B, D, E, F, I and J are similar to the spectra in Figure 3.3-I. However, the RF power dependence of the absorption band L in the films

deposited from HMDSO precursor was found to be different from the band H. The band H has a shoulder at higher wavenumber and the peak position at 1040 cm^{-1} does not depend on the RF power, while the band L has no obvious shoulder and shifts from 1046 cm^{-1} to 1016 cm^{-1} with the RF power. Taking into account the two facts that the position of the shoulder in the band H coincides with the band G (Si-O-CH_3 asymmetric vibration) and that the band L seems to shift from the band K (Si-O-Si asymmetric vibration), it can be speculated that the band H originates mainly in the polymer-like bonding states (poly Si-X-Si) generated in the recombination of the fragments of the TMMOS molecules, while the band L is ascribable mainly to the siloxane bond in HMDSO molecules. The shoulder in the band H means the weak trace of the methoxy group in TMMOS, and the shift of the band L is caused by the diverseness of the bonding states of Si atoms which constructs the siloxane bonds. The difference between the behaviors of these two chemical bonds may come from terminative and networking characteristics of the methoxy group and the siloxane, respectively, as well as the bonding strength of them discussed in Chapter 2.

3.1.4. Summary

SiO:CH films on Si (100) substrates were prepared by RF PECVD. From the result of the OES, existence of atomic H, CO, CH radicals and H_2 molecules were proved in TMMOS plasma, which can describe the oxygen atoms of methoxy groups in TMMOS can be dissociated easily in plasma, and behave as a kind of oxidizing agent. Meanwhile, in HMDSO plasma, H, CH radicals and H_2 molecules were observed, which can be supposed that siloxane bondings in HMDSO hardly expel oxygen atoms. The films deposited from TMMOS and HMDSO are supposed to be formed by poly Si-X-Si through plasma polymerization reaction of partly-dissociated reactant molecules and termination of the dangling bonds in the

polymer-like networks by the small fragments of the reactants such as methyl radicals and hydrogen atoms. The chemical bonding states such as methoxy group in TMMOS and siloxane in HMDSO remain partly in the deposited films. This is corresponding to the result of OES, which is that emission spectra of CO bands were observed only in TMMOS plasma.

References

[1] J. C. Alonso and A. Ortiz: Vacuum 43 (8) (1992), 843.

[2] Shashank C. Deshmukh and Eray S. Aydil, J. Vac. Sci. Technol. B 14(2) (1996) 738.

[3] Amit Khandelwal, Hiro Niimi, Gerald Lucovsky and H. Henry Lamb, J. Vac. Sci. Technol. A 20(6) (2002) 1989.

[4] H. Chatham, Surf. Coat. Technol. 78 (1996) 1.

[5] T. Homma, Mater. Sci. Eng., R23 (1998) 243.

[6] Y. Wu, H. Sugimura, Y. Inoue and O. Takai, Thin Solid Films 435 (2003) 161.

[7] Y. Yun, T. Yoshida, N. Shimazu, N. Nanba, Y. Inoue, N. Saito and O. Takai, J. Surf. Fin. Soc. Jpn, 58 (2007) 307 [in Japanese].

[8] S. Nunomura, K. Koga, M. Shiratani and Y. Watanabe, Jpn. J. Appl. Phys. 44 (2005) L1509.

[9] A Granier, M Vervoloet, K Aumaille and C Vallee: Plasma Sources Sci. Technol. 12 (2003) 89.

[10] K. Teshima, H. Sugimura, Y. Inoue, O. Takai and A. Takano: Chemical Vapor Deposition 10 (2004) 295.

[11] G.Socrates: Infrared Characteristic Group Frequencies 2nd ed., Wiley, Chichester, UK (1994) P. 188.

3.2. Formation of SiO:CH thin films by the capacitively coupled PECVD

3.2.1. Introduction

From the previous consideration in Section 3.1, I discussed the correlation between the dissociation reaction in inductively coupled organosilicon plasma and film formation on the substrate. In this section, SiO:CH films were prepared with a capacitively coupled RF PECVD method with an organosilicon reactant. On the basis of the deposition rate, chemical composition, chemical bonding states of the films and optical emission spectroscopy from the plasma, I discuss the formation mechanism through an investigation of the RF power and Ar gas flow rate dependence.

3.2.2. Experimental procedure

This work was carried out with a capacitively coupled RF PECVD system. As shown in Figure 3.4, the PECVD system consists of a deposition chamber with a height and diameter of 200 and 300 mm, respectively, a power supply system, a vacuum system, and gas supply lines. The chamber was connected to the vacuum system and the gas supply line of the organosilicon reactant as well as Ar gas. The vacuum system is made up of a rotary pump (R.P., Alcatel, Pascal 2015SD) and a turbo molecular pump (T.M.P., Mitubishi, PT-300). The diameter and distance between stainless steel parallel plate electrodes, were 200 and 50 mm, respectively. A 13.56 MHz generator (Astec Co., Ltd., R-300) supplied the RF power into the lower electrode through a matching network in order to activate the discharge. The upper electrode was connected to ground, and circulated 50℃ water to keep the electrode temperature constant by a water circulation system (EYELA, HS-1). N-type Si (100) substrates were located on the upper electrode in order to avoid ion impact by negative self bias voltage as well as attachment of dusty particles produced in the chamber. The reactant

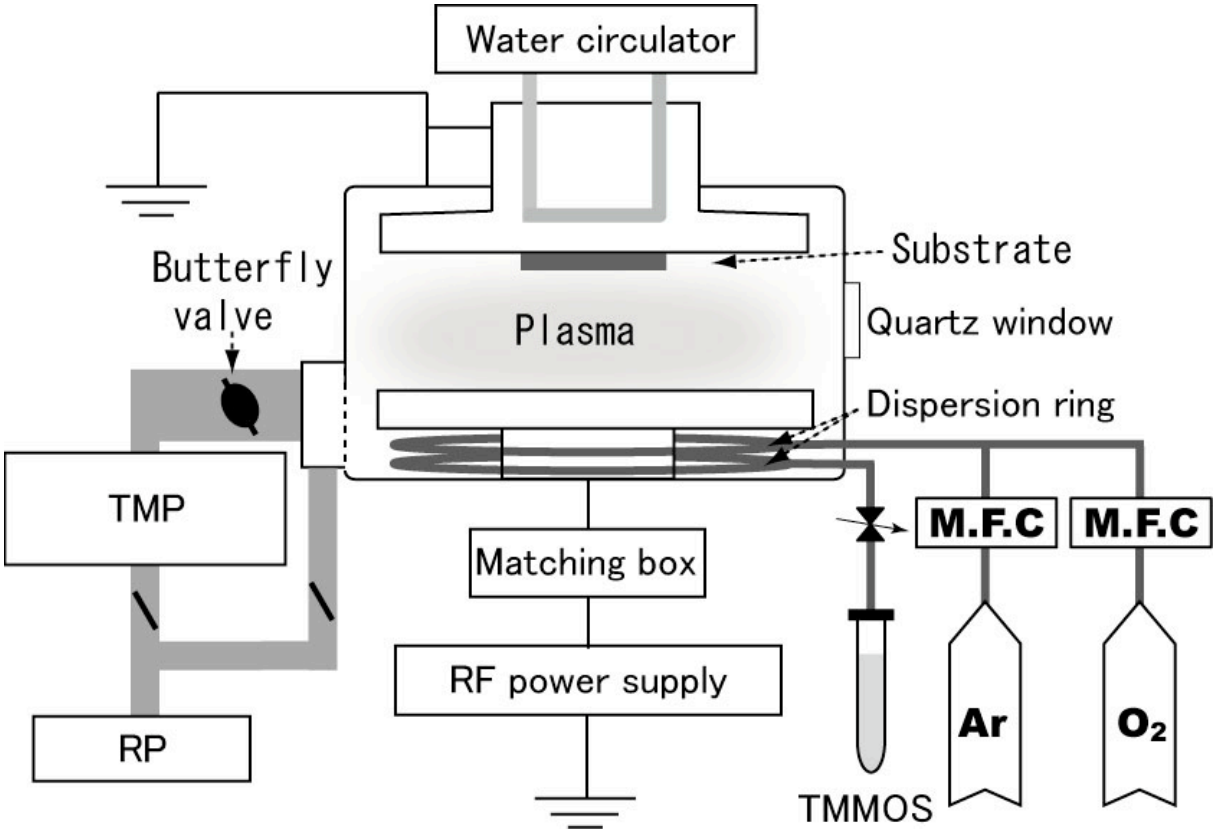

Figure 3.4. Schematic diagram of the capacitively coupled RF PECVD system.

used in this work was trimethylmethoxysilane [TMMOS; $(CH_3)_3SiOCH_3$]. The TMMOS reactant was supplied through the dispersion ring under the lower electrode. As shown in Table 3.1, the films were prepared under varying RF power in the range of 10 ~ 100 W. The flow rate of TMMOS reactant was supplied in the range of 20 ~ 70 sccm. The chamber pressure was maintained at 10 Pa. Deposition time was fixed at 30 minutes. After deposition, film thickness was measured by a surface profilometer (Mitutoyo, SV-600). The deposition rate of the films was calculated from the film thickness divided by deposition time. Water repellency of the films was measured by a static water-contact-angle meter (Kyowa Interface Science, CA-D and Kuluss, DSA10-Mk2) with water droplets of 1 mm in diameter. Chemical composition was determined by an X-ray photoelectron spectrometer (XPS, Shimazu-Kratos, AXIS) with Mg Kα radiation. The chemical bonding states were characterized by a Fourier-transform infrared spectrometer (FT-IR, Digilab, FTS-7000). Plasma diagnostics was performed by optical emission spectroscopy (OES, Chromex, 500-IS). Optical emission spectra were obtained through a quartz-glass window positioned between the parallel plate electrodes.

3.2.3 Results and discussion

3.2.3.1 RF power dependence in plasma

Figure 3.5 shows the effect of RF power on deposition rate of the SiO:CH films deposited under various TMMOS flow rates. As a density of the films was not altered under these deposition conditions, the deposition rate of the films can be used as a quantity of the reaction rate for the formation of the films. The deposition rate increased with RF power in all deposition conditions, though not linearly. At the TMMOS flow rate of 20 sccm, the deposition rate was increased until 40 W of the RF power, above which the deposition rate

Table 3.1. Deposition conditions of the films prepared by capacitively coupled RF PECVD on Si(100) substrate.

Parameter	Condition
RF power (W)	10, 20, 40, 70, 100
TMMOS flow rate (sccm)	20 (40, 70)
Ar flow rate (sccm)	0, 0.4, 2.2, 20, 50
Ar flow ratio (%)	0, 2, 10, 50, 71.4
Chamber pressure (Pa)	10
Deposition time (min)	30

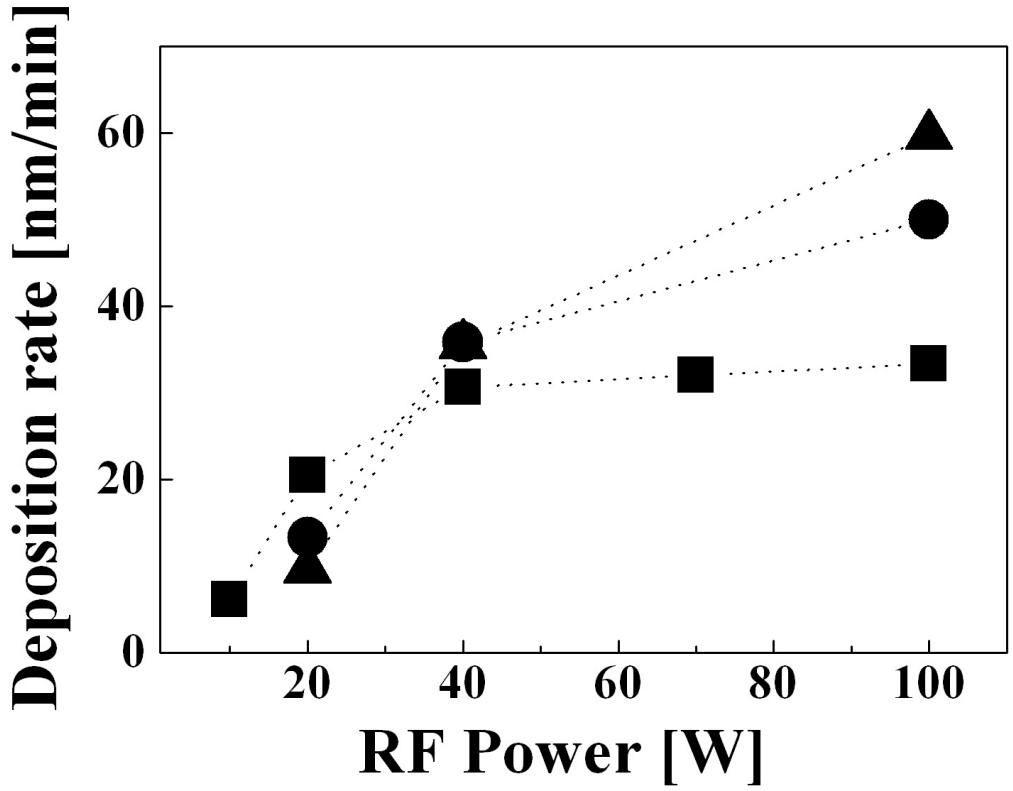

Figure 3.5. Effect of RF power on deposition rate of the films deposited at various TMMOS flow rates. Squares(■), circles(●) and triangles(▲) show 20, 40 and 70 sccm of TMMOS flow rate, respectively.

was saturated. Other flow rate conditions show a similar tendency. In the region of 40 - 100 W of the RF power, the deposition rate increased with the TMMOS flow rate, *i.e.* the reactant flow rate influenced the deposition rate. These results suggest the presence of two regimes of film growth, one being a reaction-controlled regime (hereinafter referred to as "R-regime"), and the other an reactant flow rate-controlled regime (as "F-regime"). In the R-regime, the RF power controls the growth rate under all the deposition conditions. It is considered that the increase in the RF power is reflected in the plasma as an elevation of electron density, and it leads to the formation of reaction precursors owing to the dissociation of organosilicon molecules. In the F-regime, the deposition rate was saturated against the RF power, and the deposition rate increased with the gas flow rate under 100 W of the RF power. These results suggest that the gas flow rate affect the film deposition rather than the RF power under these conditions. The limited quantity of the molecules in the plasma saturates the dissociation and subsequent recombination reaction. This restricted formation of chemical networks in the film, leading to the saturation of film growth.

In this section, chemical composition, chemical bonding states and dissociation reaction in plasma were analyzed at the condition of 20 sccm of flow rate. The FT-IR spectra of the films are shown in Figure 3.6. Absorption bands were identified as O-H stretching (A), C-H stretching (B), Si-H stretching (C), C=O stretching (D), Si-CH_3 stretching (E), Si-CH_3 symmetric deformation (F), poly Si-X-Si asymmetric stretching (G), Si-$(CH_3)_3$ rocking (H), and poly Si-X-Si (I) [1-3], here the expression poly Si-X-Si is defined in Subsection 3.1.3.2. Comparing the appearance of the absorption bands with those in the spectrum for the reactant, the absorption bands B (C-H) and G (Si-X-Si) became broader. The levels of Si-CH_3 symmetric stretching (2960 cm^{-1}) and Si-CH_3 (1260 cm^{-1}) symmetric deformation decreased, while the intensities of the C=O band (D) and O-H band (A) increased with RF power. These

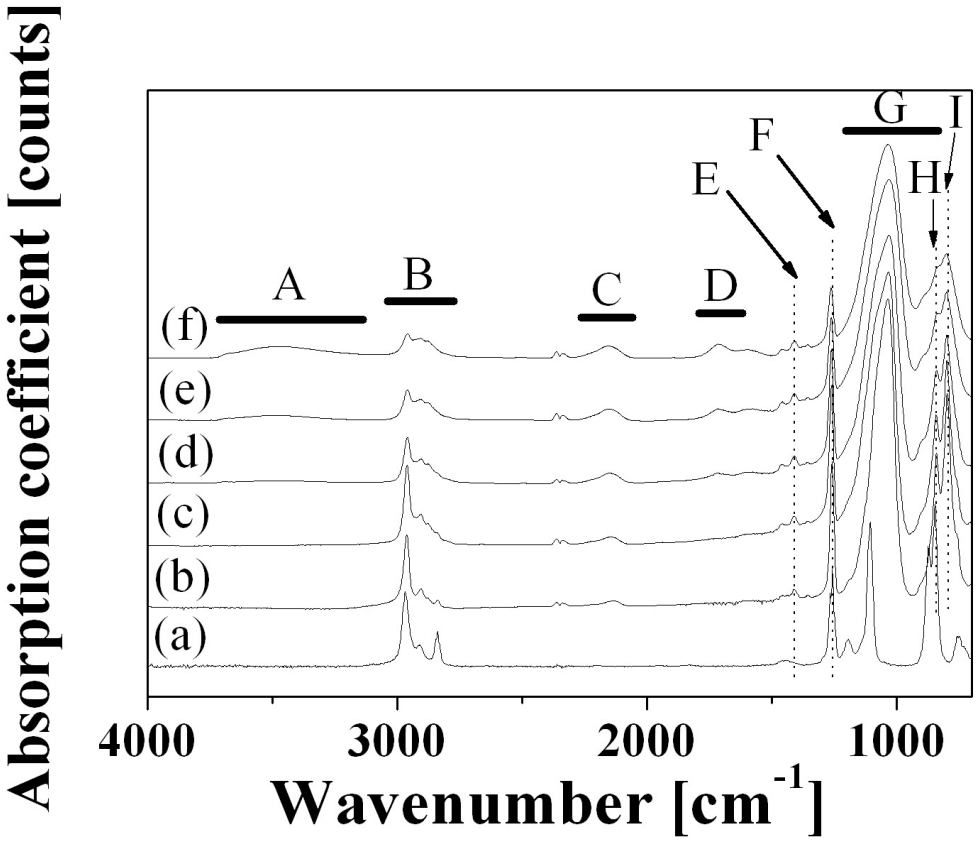

Figure 3.6. FT-IR absorption spectra of the films deposited at 20 sccm of TMMOS flow rate ((a): TMMOS reactant, (b): 10W, (c): 20W, (d): 40W, (e): 70W and (f): 100W). Alphabetic notations are defined in the text.

results show that the film consists of the polymer-like Si-X-Si networks with -OH, -CH_3 and -H terminations. Regarding the bands D and A, it is possible to identify the former as C=O and the latter as O-H groups in carboxylic groups. However, this idea remains a matter of further discussion, and additional study is necessary to confirm. Meanwhile, the basic chemical bonding states of the networks are similar to those of the reactant molecule at 20 W of the RF power, because positions and the fundamental shapes of the absorption bands B, F, and G are similar to those of the reactant molecule except for the broadening of these bands, which is due to the diversity of the chemical bonding states of the relevant atoms. Therefore, the films are considered to form through recombination reactions of partly-dissociated reactant molecules and the termination of dangling bonds in polymer-like networks with small fragments of reactant molecules such as methyl radicals and hydrogen atoms.

Figure 3.7 shows the effect of RF power on chemical composition of the films measured by XPS. Under all the deposition conditions, the films consist of Si, O, and C in the composition of Si : O : C ~ 1 : 1 : 3, where the carbon composition is lower than that of the reactant, Si : O : C = 1 : 1 : 4. The atomic ratio of carbon increased slightly, while that of silicon and oxygen decreased gradually with the RF power. This suggests that carbon networks in the films increased with the RF power, which corresponds to the tendency confirmed in the C-H absorption band observed by FT-IR spectra.

Figure 3.8 shows the full width at half maximum (FWHM) of the XPS spectra of the films. The FWHM of the films increased primarily in the R-regime. Meanwhile, it was saturated in the F-regime except for the FWHM of silicon. In the case of silicon, the FWHM was saturated slightly in the 40 W of the RF power, and increased again.

In the R-regime, the RF power activates the dissociation and recombination of the reactant in the plasma, and was found to form various types of bonding networks in the films, as well as

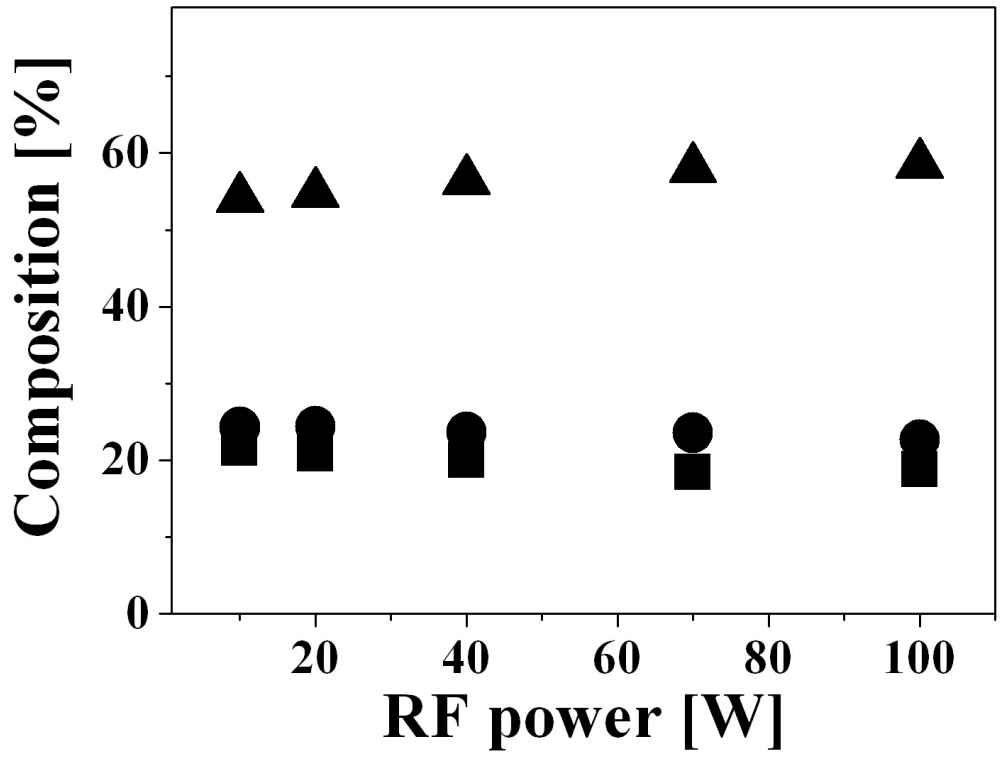

Figure 3.7. Effect of RF power on chemical composition of the films measured by XPS. Squares(■), circles(●) and triangles(▲) indicate silicon, oxygen and carbon, respectively.

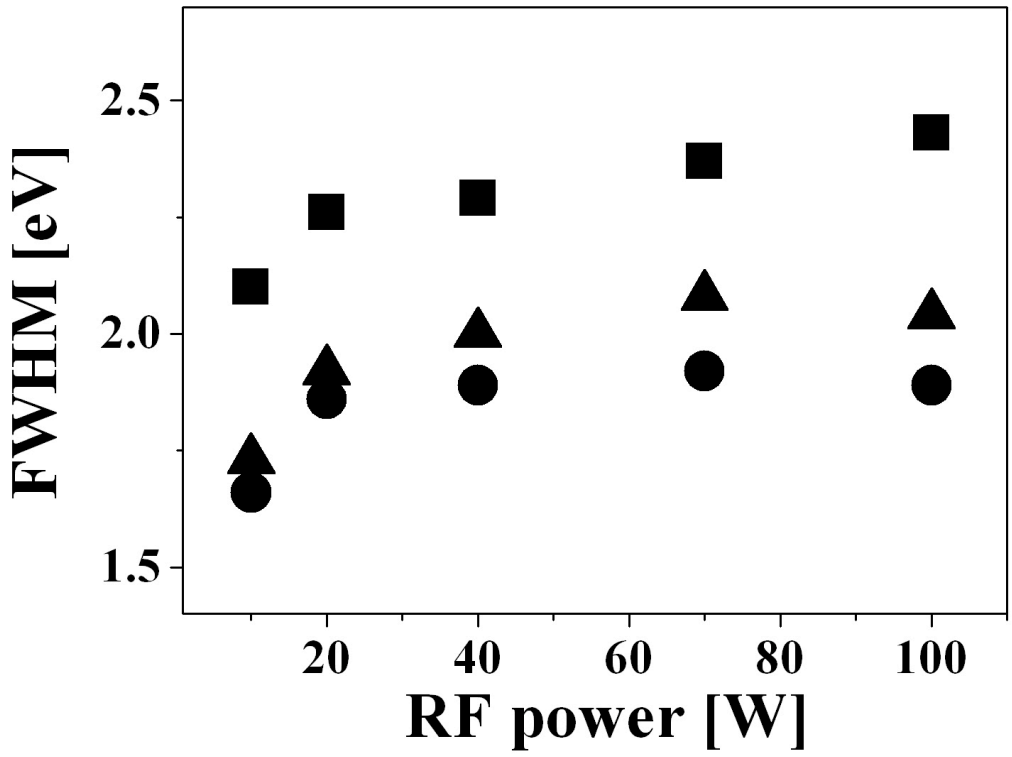

Figure 3.8. Full width at half maximum in XPS spectra of the films at 20 sccm of TMMOS flow rate. Squares(■), circles(●) and triangles(▲) demonstrate silicon, oxygen and carbon, respectively.

broaden the XPS signatures. In the F-regime, the limited quantity of the molecules led to the saturation of the reaction in the plasma, which restricted the formation of chemical networks in the films. In the case of silicon, which is the main constituent in the bonding networks, the increase in carbon ratio and the variety in the carbon networks aided in the diversification of silicon networks in the films.

Figure 3.9 indicates the water contact angle of the films deposited at 20 sccm of the TMMOS flow rate. The water contact angle of the films was distributed between 89 - 100°, which decreased with the RF power. In particular, the water contact angle decreased more rapidly in the R-regime than in the F-regime. These correlate with the previous results regarding the chemical bonding states of the films. The hydrophobic CH_3 terminations decreased with RF power, while the hydrophilic OH increased. A discussion regarding the difference of reduction rate in water contact angle between the two regimes will be connected with the following results on plasma diagnostics, which is inseparably connected with the reaction in plasma, and with the following OES results.

Figure 3.10 shows the optical emission spectra in the range of 410 ~ 490 nm for TMMOS plasma recorded during the deposition of films. In these spectra, emissions from H, H_2, CO, and CH (4300 Å system, $A^2\Delta$-$X^2\Pi$) were detected. About the CO emission, The Ångström system band ($B^1\Sigma^-A^1\Pi$) were observed at ~ 420 - 480 nm of wavelengths. In the range of ~ 460 - 470 nm, overlapping lines from H_2 molecules can be seen. Origins of atomic H, CO and H_2 molecules in organosilicon plasma were mentioned in previous Subsection 3.1.3.1. Concerning the CO molecules, the generation mechanism in TMMOS plasma can be considered as follows. In the gas phase, CO molecules can be physically created from TMMOS through the electron impact dissociation of Si-O and three C-H bonds in methoxy groups. O atoms, which are expelled from TMMOS molecules by electron impact, may

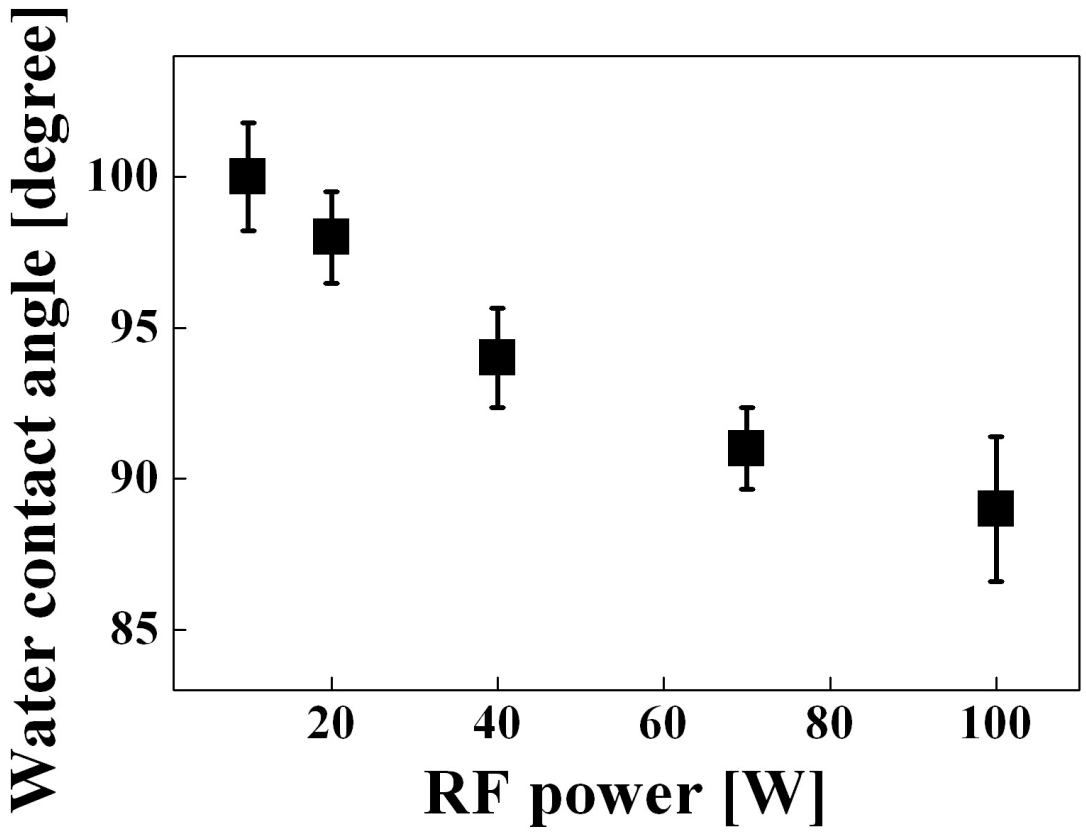

Figure 3.9. Water contact angle of the films deposited at 20 sccm of TMMOS flow rate.

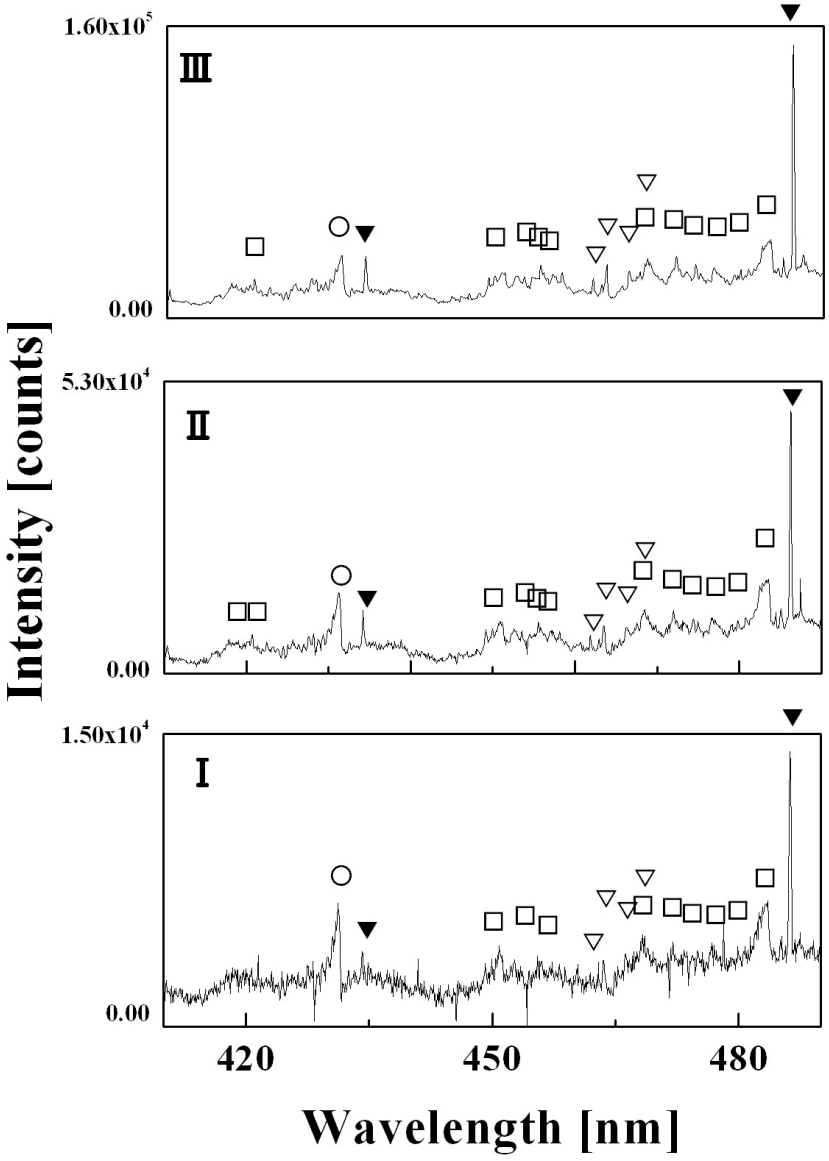

Figure 3.10. Optical emission spectra of capacitively coupled organosilicon plasma, during deposition of the films at the rf power of (Ⅰ): 20W, (Ⅱ): 40W, (Ⅲ): 100W. Closed triangles(▼), open triangles (▽), open circle (○) and open squares (□) indicate the lines and bands from H, H_2, CH and CO, respectively.

chemically generate CO species through oxidization reactions with CH_x species. Surface reactions must be also considered as a step in CO generation. The oxygen atoms expelled in the plasma have the ability to oxidize surface hydrocarbon terminations. Granier, *et al*. suggested that the CO molecules in TEOS plasma are likely to originate in desorption from the growing film surface on the reactor walls induced by energetic ion bombardment from the plasma [4].

3.2.3.2. Ar gas flow rate dependence in plasma

Figure 3.11 shows the effect of Ar gas flow ratio on deposition rate of the SiO:CH films deposited on Si(100) substrates under varying the mixing ratio of Ar gas, with the TMMOS flow rate and the RF power were kept constant at 20 sccm and 100 W, respectively. The deposition rate of the films decreased with Ar gas flow rate, which can be explained as follows. Since the TMMOS gas was introduced at same flow rate, the absolute amount of the reactant molecules is constant in the chamber. Meanwhile, in order to maintain the chamber pressure under an identical condition of 10 Pa, the exhaust speed was increased with the Ar gas flow rate. Therefore it led to a decrease of the residence time to dissociate and recombine the TMMOS reactant in plasma. That is to say, the deposition condition in the R-region (the TMMOS flow rate at 20 sccm with the RF power at 100 W) changed into the F-region due to the mixture of Ar gas. In this view point, the deposition rate must be reduced by half at the Ar mixing ratio of 50 %. From the experimental data in Figure 3.11, the deposition rate at the Ar mixing ratio of 50 % is slightly smaller than a half value of that at 0 %. This result suggests that another factor to decrease the deposition rate must exist, such as Ar ion bombardment phenomenon.

The FT-IR spectra of the films are shown in Figure 3.12. Absorption bands were identified

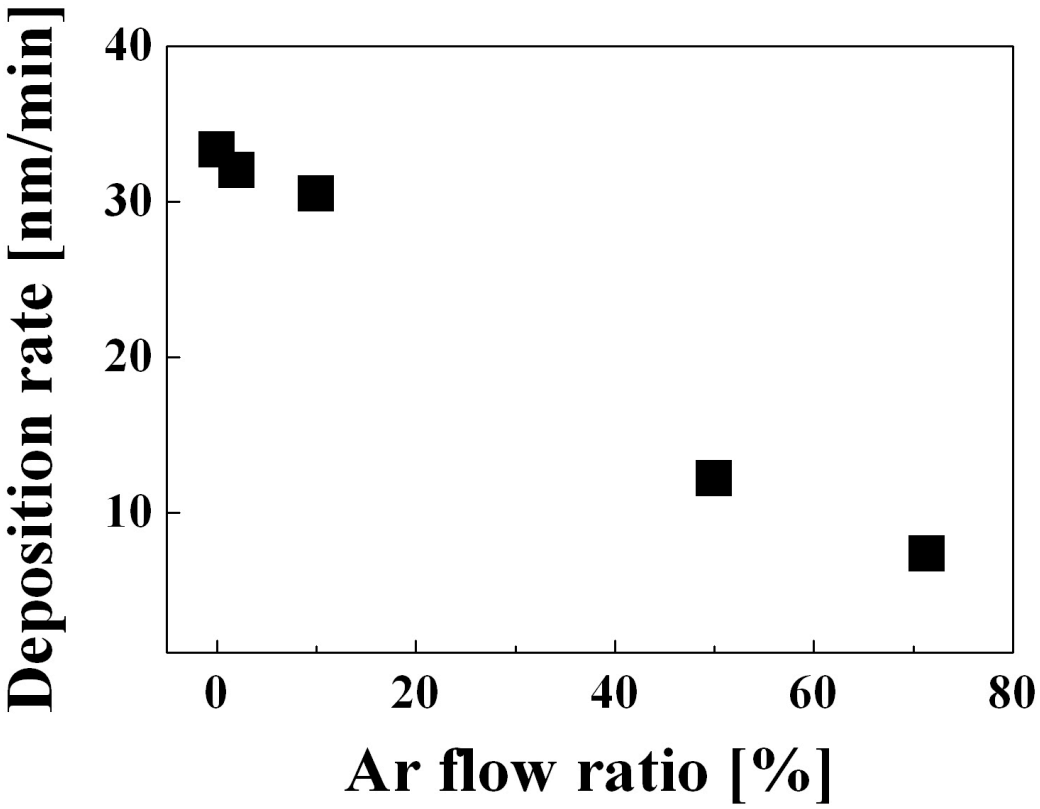

Figure 3.11. Effect of Ar flow ratio on deposition rate of the films deposited under 100 W of RF power and various Ar gas flow ratio.

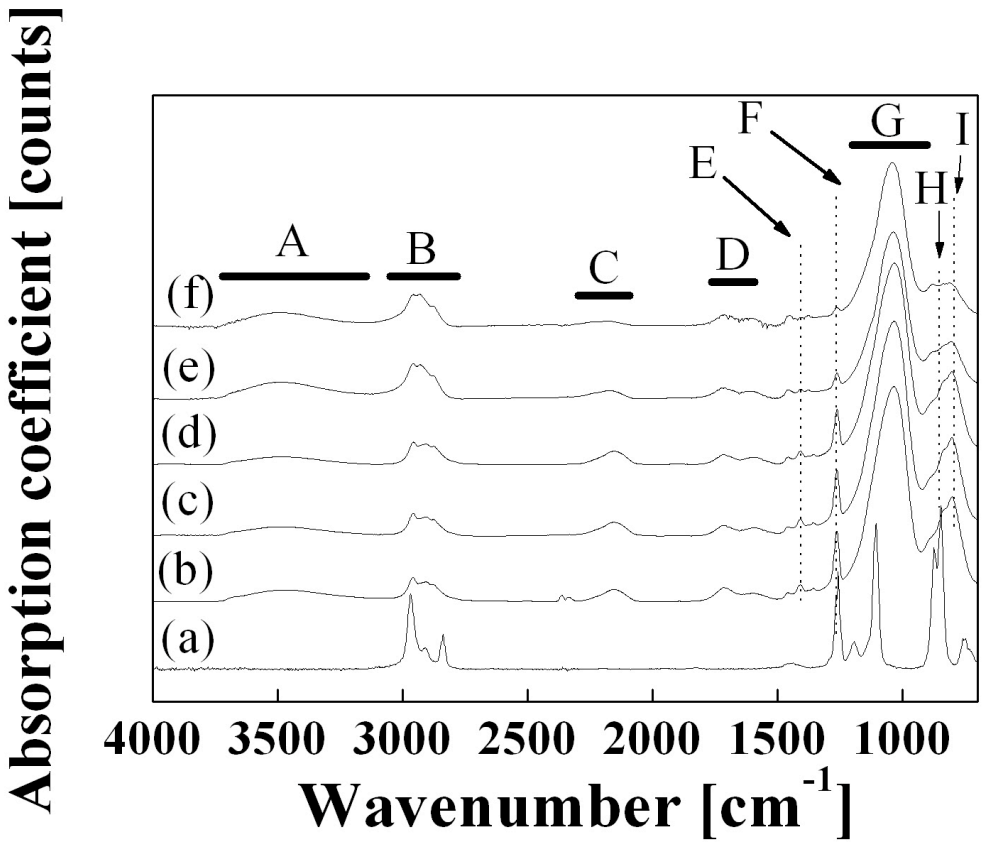

Figure 3.12. FT-IR absorption spectra of the films deposited at100 W of RF power (TMMOS reactant (a), Ar flow ratio of 0 % (b), 2 % (c), 10 % (d), 50 % (e) and 71.4 % (f), respectively). Alphabetic notations are defined in the text.

as O-H stretching (A), C-H stretching (B), Si-H stretching (C), C=O stretching (D), Si-CH_3 stretching (E), Si-CH_3 symmetric deformation (F), poly Si-X-Si asymmetric stretching (G), Si-$(CH_3)_3$ rocking (H), and poly Si-X-Si deformation (I) [1-3]. Comparing the appearance of the absorption bands with those in the spectrum for the reactant, the bands B (C-H), C (Si-H), F (Si-CH_3), G (poly Si-X-Si), H (Si-$(CH_3)_3$), and I (poly Si-X-Si) decreased with Ar gas flow ratio, while the band A (O-H) increased. The absorption bands B (C-H) and G (poly Si-X-Si) became broader. These results show that the film consists of Si-X-Si networks with -OH, -CH_3 and -H terminations. Meanwhile, in spite of the drastic decrease in the intensity of the band F with the Ar gas flow ratio, the band B increased the intensity, and broadened. This is caused by an increase of amorphous-carbon (a-C:H) like networks in the films due to the Ar ion bombardment. Moreover, instead of decreasing the -CH_3 and -H terminations, the films are formed a termination of the dangling bonds or -OH terminations with Ar gas flow ratio. Further investigation is necessary to clarify a mechanism to terminate the -OH network with the Ar gas flow ratio.

Figure 3.13 shows the relationship between Ar gas flow ratio and chemical composition of the films. In the deposition condition without mixing Ar gas, the films consist of Si, O, and C in the composition of Si : O : C = 1 : 1 : 3. The atomic ratio of carbon increased obviously with mixing Ar, while that of silicon and oxygen decreased. In order to investigate a diversity of chemical network in the films, the FWHM in XPS spectra is shown in Figure 3.14. The FWHM values for silicon and oxygen seem to be independent of the Ar mixing ratio, while that for carbon decreased slightly with the Ar mixing ratio. From the XPS results, it can be said that carbon content in the film surface increased with the Ar mixing ratio, and diverseness of carbon bonding states decreased. These results correspond to the results of FT-IR, which show that -CH_x terminations in the films switch to a-C:H-like networks with

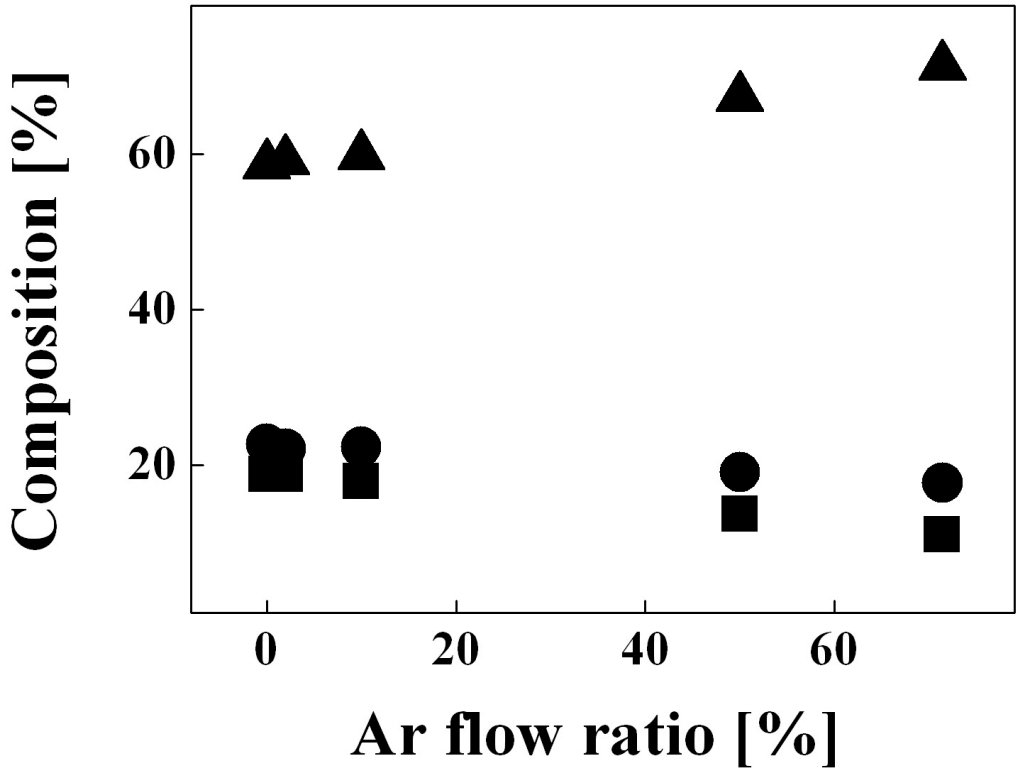

Figure 3.13. Effect of Ar gas flow ratio on chemical composition of the films measured by XPS. Squares(■), circles(●) and triangles(▲) indicate silicon, oxygen and carbon, respectively.

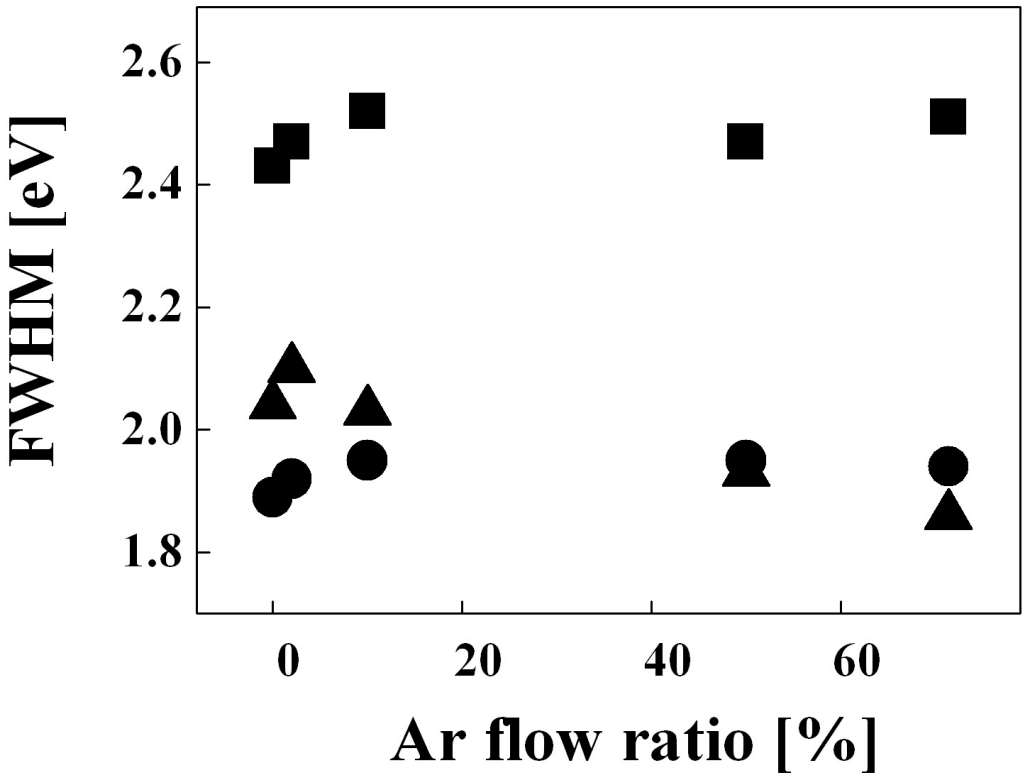

Figure 3.14. Full width at half maximum in XPS spectra of the films deposited at 100 W of RF power. Squares(■), circles(●) and triangles(▲) demonstrate silicon, oxygen and carbon, respectively.

mixing Ar gas. The conversion of the $–CH_x$ termination into the a-C:H-like networks must be observed in various film properties. An example can be found in the water contact angle of the film surfaces. The water contact angle of the films decreased monotonically with increasing the Ar mixing ratio except for the slight increase at a small amount of Ar mixing (2 %) as shown in Figure 3.15. Since the contact angles have been reported for the flat surface covered with high density $-CH_3$ terminations [8] and a-C:H surface [9] as ~108° and ~94°, respectively, the decrease in water contact angle of the films is a natural consequence of the evolution of the chemical bonding states involved in the hydrocarbon constituents. The lower angles in the case of the films prepared in this study than the reference values above is due to the fact that the functional groups on the film surfaces include not only hydrophobic $-CH_3$, $-CH_2-$, and -H but also hydrophilic -OH and Si-O-Si as found in the FT-IR analysis.

From the OES spectra, emission lines and bands from Ar, H, H_2, CO, C_2, and CH were detected. Figure 3.16 shows the optical emission intensity of the atomic H_α (656 nm) as well as the relative optical emission intensity of H_β/H_α in the Ar-TMMOS plasma. The emission intensity of H_α significantly decreased with the introduction of Ar gas (2 %). Generally, optical emission intensity indicates the degree of dissociation and the plasma/electron density. Therefore it can be said that the sharp decrease of the H_α intensity is caused by a decrease of electrons to dissociate the TMMOS molecules in plasma. The decrease of electrons is considered to be attributable to a lower ionization rate of Ar atoms compared with those of TMMOS molecules and their fragments, in contrast to a higher collision probability. Hence the degree of dissociation of the TMMOS molecules was reduced and the hydrophobic $–CH_3$ terminations increased to improve slightly the water contact angle at the Ar mixing ratio of 2 %. Meanwhile, with the increase in Ar mixing ratio, the physical Ar ion bombardment on the film surfaces must be remarkable. The physical bombardment effect of Ar ion has been

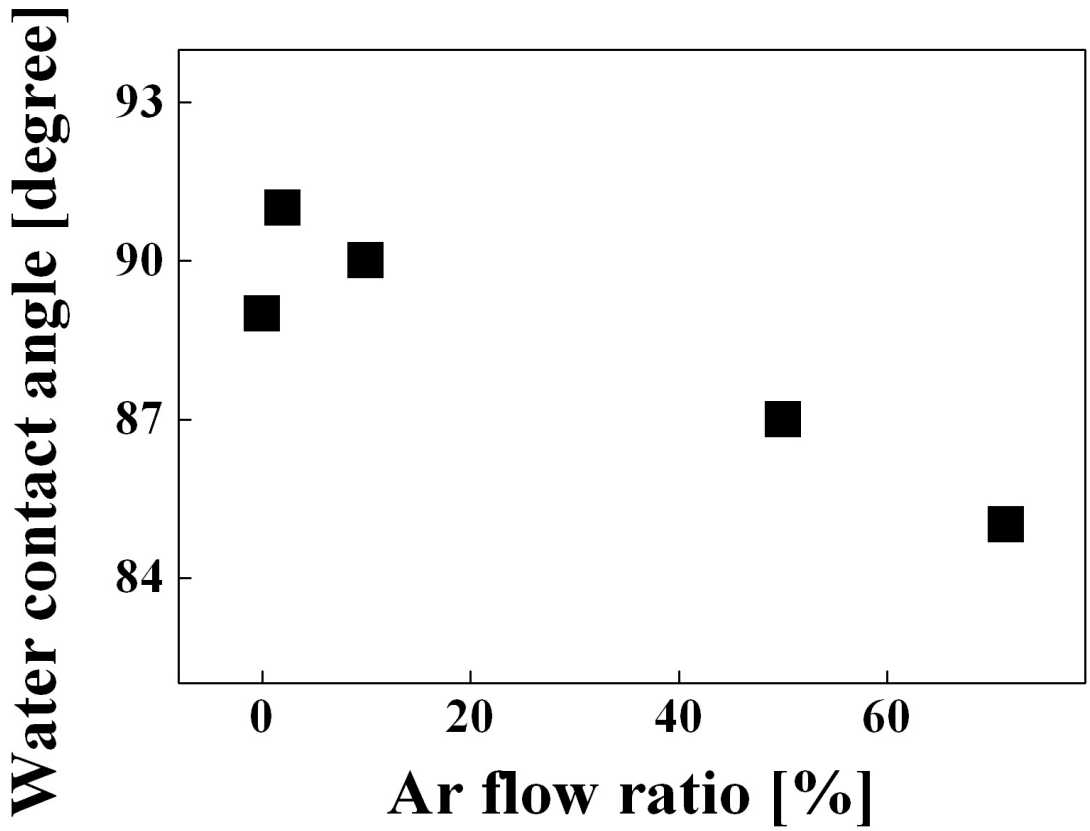

Figure 3.15. Water contact angle of the films deposited under various Ar gas flow ratio.

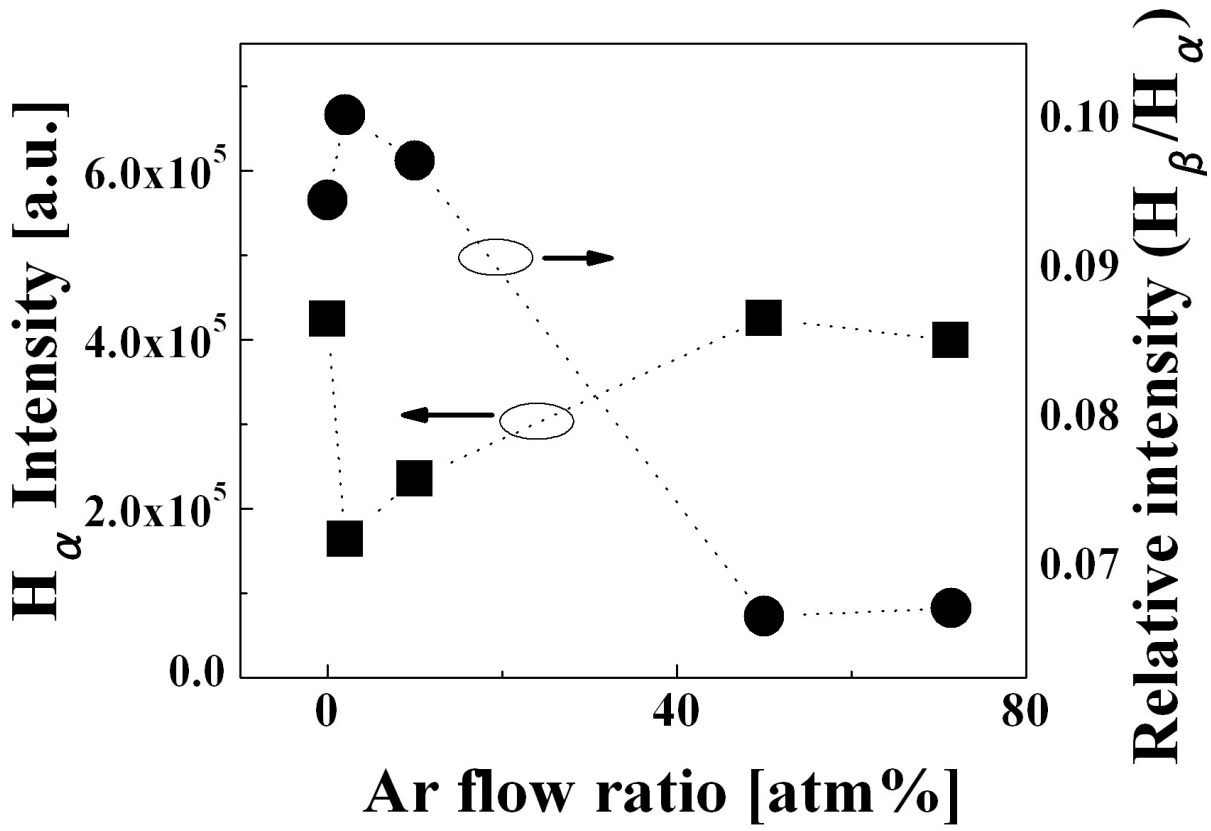

Figure 3.16. Optical emission intensity of H_α(■) and relative emission intensity of H_β/H_α (●) of the Ar-TMMOS plasma under various Ar gas flow ratio.

well-known to be much higher than the fragment species of TMMOS molecules. Also the film surfaces are negatively charged under floating potential during deposition, since the SiO:CH material has an electrical insulating property. Therefore the author supposes that the conversion of the hydrocarbon constituents from $–CH_3$ terminations into a-C:H-like networks is induced by the Ar ion bombardment effect, which has been reported in some papers, for example, Valentini, *et al*. described that increasing Ar ion bombardment causes more breaking of C-H bonds [10]. In this study, however, there is no experimental data for the energy analysis for the ion density as well as its energy impinging on the surface. Further precise studies focusing on the ion-surface interactions in PECVD of SiO:CH film deposition will make clear the origin of the change in the chemical bonding states.

3.2.4. Summary

From the consideration on the RF power dependence, the deposition mechanisms can be described as follows:

(1) in the reaction-controlled R-regime, the introduced RF power was used effectively to dissociate and recombine the TMMOS reactant, and led to increase the deposition rate,
(2) in the flow rate-controlled F-regime, the limited quantity of molecules in the plasma caused the saturation of dissociation and recombination reaction.

From the results of Ar gas flow rate dependence, deposition process and reactions in organosilicon plasma strongly depend on Ar gas flow rate. The ratio of mixing Ar gas affects to increase the amorphous carbon network, and dangling bonds or -OH terminations due to Ar ion bombardment. Moreover, Ar gas flow rate influence to decrease (2 % of Ar gas flow rate)

and increase the dissociation reaction in organosilicon plasma, and it led to change the chemical bonding states and the water contact angle.

References

[1] K. Teshima, H. Sugimura, Y. Inoue, O. Takai and A. Takano, Chem. Vapor Deposition 10 (2004) 295.

[2] Y. Yun, T. Yoshida, N. Shimazu, Y. Inoue, N. Saito and O. Takai, Solid State Phenom. 124-126 (2007) 347.

[3] G. Socrates, Infrared Characteristic Group Frequencies (Wiley, Chichester, U.K., 1994) 2nd ed., P. 188.

[4] A. Granier, M. Vervoloet, K. Aumaille and C. Vallee, Plasma Source Sci. Technol. 12 (2003) 89.

[5] Y. Inoue and O. Takai, Plasma Sources Sci. Technol. 5 (1996) 339.

[6] M. Shimozuma, J. Appl. Phys. 70 (1991) 645.

[7] A. Mizuike and H. Kawakuchi, Introduction to analytic chemistry (SangyoTosho, Tokyo, 2001) P. 143 [in Japanese].

[8] A. M. Almanza-Workman, S. Raghavan, S. Petrovic, and B. Gogoi, P. Deymier, D. J. Monk and R. Roop, Thin Sold Films 423 (2003) 77.

[9] J. D. Kim, K. H. Lee, K. Y. Kim, H. Sugimura, O. Takai, Y. Wu and Y. Inoue, Surf. Coat. Tech., 162 (2003) 135.

[10] L. Valentini, J. M. Kenny, G. Mariotto and P. Tosi, J. Mater. Sci., 36 (2001) 5295.

Chapter 4. Formation of SiO:CH UWR thin films by the inductively coupled RF PECVD

In the previous chapter, the deposition process of SiO:CH thin films was investigated by using inductively-coupled plasma (ICP) and capacitively-coupled plasma (CCP) systems, on the basis of the electron-impact dissociation phenomenon in organosilicon plasma and the recombination reaction on the substrate. From the results of FT-IR, it cannot be seen significant differences of chemical bonding states between the SiO:CH thin films by those two types of systems. However, the optical emission intensity of CH radical under the ICP was higher than one under the CCP. This result is caused by high electron density in the ICP, which is one of advantages compared with CCP. Therefore, in order to fabricate the UWR thin films which require severe recombination reactions, *i.e.* nano-clusters, ICP is more appropriate than CCP. Moreover, the remote-type configuration available in ICP does not damage the substrate directly. Hence ICP system is possible to deposit on many types of substrate, such as plastics, glass, semiconductors, metals, and paper. In this chapter, SiO:CH UWR thin films which consists of SiO:CH nano-clusters and binding films (described in Section 3.1) are fabricated by using ICP PECVD system. Moreover, the formation process of UWR thin films are investigated by surface morphology, water contact angle of the films, and laser scattering method.

4.1. Formation of SiO:CH UWR thin films

4.1.1. Introduction

As mentioned in Chapter 1, UWR thin films are attractive material in many industrial fields, such as prevention of adhesion of raindrops or snowflakes onto windows and antennas, traffic

indicators with self-cleaning surface, reduction of frictional drag on ship hulls, metal refining, stain-resistant textiles and cell motility [1-12]. By mimicking surface morphology of lotus leaves, Takai laboratory have succeeded in fabricating transparent and highly-durable UWR thin films at room temperature by microwave PECVD (MPECVD) using organosilicon molecules [1-2,13-18]. However, in the usage of microwave in the field, it has limitations due to a cost performance and its manageability. Therefore, it is necessary to change a plasma source from microwave to radio frequency, which can control easily.

In this section, I report my work on synthesis of the UWR thin films by RF PECVD instead of MPECVD. The relationships between the deposition conditions and of the film properties such as morphological and chemical properties of the films were discussed. Moreover, from the analysis of plasma diagnostics using OES, formation mechanism of ultra water-repellent thin films was discussed.

4.1.2. Experimental procedure

This work was carried out with the RF PECVD system, which is described in Section 3.1. The reactant used in this work was trimetylmethoxysilane [TMMOS; $(CH_3)_3SiOCH_3$]. A n-type Si (100) substrates were located at 200 mm below from the center of plasma to avoid direct thermal damage by plasma. In order to regulate the total gas flow rate, firstly Ar gas was introduced into the chamber with a constant flow rate of 10 sccm then its pressure was fixed at 80 Pa by controlling vacuuming rate. Secondly, the reactant TMMOS gas was introduced up to the total pressure of Ar and TMMOS of 500 Pa. The films were prepared under various RF power in the range of 50~200 W. Deposition time was fixed at 3 minutes. After deposition, water-droplet contact angle of the films was measured by a static water-contact-angle meter (Kyowa Interface Science, CA-D and Kuluss, DSA10-Mk2). The

surface morphologies were observed by a field-emission scanning electron microscope (FESEM, JEOL, JSM-6330F). The chemical bonding states were characterized by a Fourier-transform infrared spectrometer (FT-IR, Digilab, FTS-7000). Plasma diagnostics was performed by optical plasma emission spectroscopy (OES, Chromex, 500-IS). Details of this device were mentioned in Subsection 3.1.2.

4.1.3. Results and discussion

4.1.3.1. Deposition of UWR thin films

Figure 4.1 shows the relation between water-droplet contact angles of the films and RF power. The water-droplet contact angle of the deposited films increases with the RF power. In the deposition conditions at 150 and 200 W, the water-droplet contact angle exceeds 150°, called ultra-water repellency.

The surface morphologies of the films observed by FESEM are shown in Figures 4.2 and 4.3. Under 50 and 75 W of the RF power, the surface morphologies of the films are quite flat without any texture nor nano-clusters (Figures 4.2 and 4.3 (a), (b)). Under 100~200 W of the RF power, the nanoclusters which are in size of several tens of nm can be observed. From the spherical shape, these nano-clusters were supposed to be originated from a polymerization process in the gas phase and deposit on the substrate. The SEM images indicate that the morphology depends clearly on the RF power. Under the lower RF power (100 W), the surface morphology of the films is approximately flat with low density of the nanoclusters (Figures 4.2 and 4.3 (c)). Because of the smooth surface structure, the water-droplet contact angle of the film deposited at 100 W does not exhibit the ultra water-repellency. The films deposited at higher RF power, on the other hand, show micrometer-scaled roughness. For example at 200 W of the RF power as shown in Figures 4.2 and 4.3 (e), micro-size particles

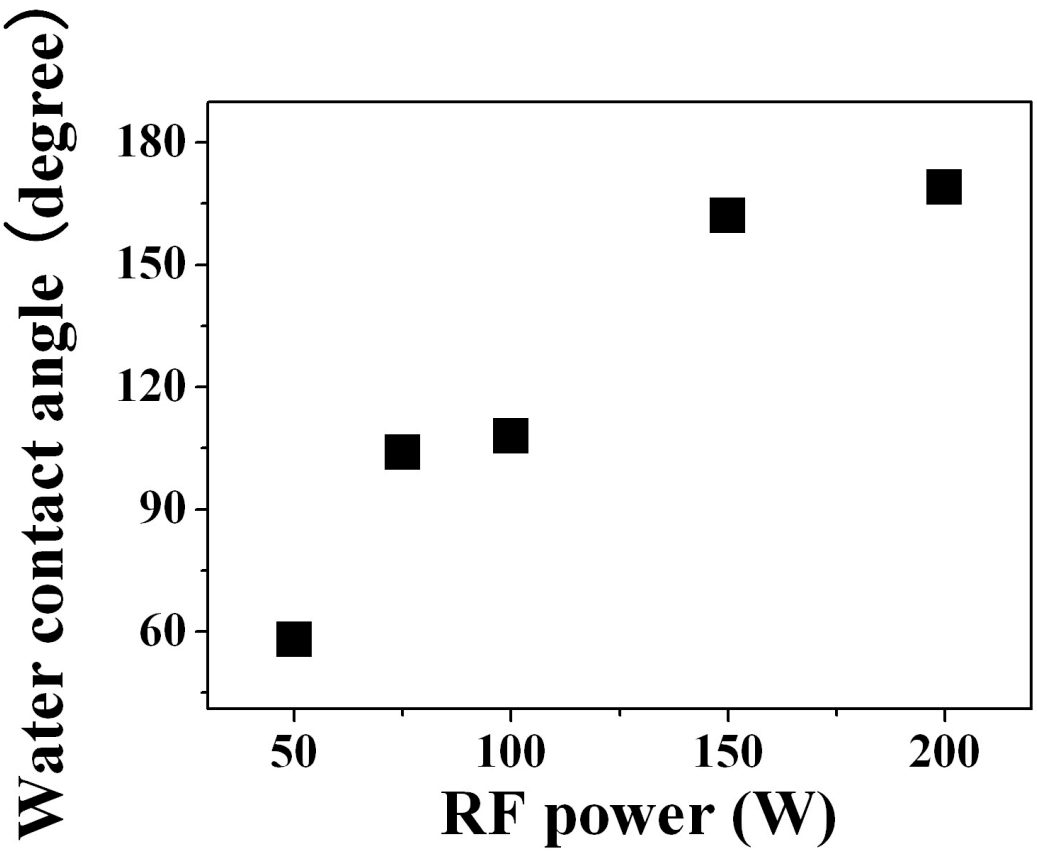

Figure 4.1. Effect of RF power on water contact angle of thin films prepared by PECVD on Si(100) substrate.

which consist of nano-clusters are observed. These films have particular nano-textures with nano-scale pores of a few hundreds nanometer in diameter among the cancellous web-like structure of the nano-cluster agglomerates (Figures 4.2 and 4.3 (d)) or the micro-particles (Figures 4.2 and 4.3 (e)). The rough surfaces of the films result in the water contact angles greater than 150°. The geometrical effect for these film surfaces is ascribable not only to the expansion of the nominal surface area (Wenzel-style effect [19]), but also to the air trapping between the water-droplet and agglomerated textures on the film surfaces which minimizes the contact area (Cassie-style effect [20], which has been utilized by other researchers [21-22]).

4.1.3.2. Chemical bonding states of UWR thin films

The FT-IR spectra of the films are shown in Figure 4.4. Each absorption band was identified as O-H stretching (A), C-H stretching (B), Si-H stretching (C), Si-CH_3 stretching (D), Si-CH_3 symmetric deformation (E), poly Si-X-Si asymmetric (F), Si-$(CH_3)_3$ rocking (G) and poly Si-O-Si deformation (H) [16,23-24] (note that the notations are different from those in Chapter 3). In the FT-IR spectrum for the film deposited at 50 W, there is no absorption band related to Si, instead, only two absorption bands, A (O-H) and B (C-H), were observed. This result indicates that SiO:CH film deposition does not occur in this condition, but the small amount of radicals impinge onto the substrate to modify the substrate surface. Then the surface is predominantly covered with -OH termination, which is known as hydrophilic functional group. Therefore, water-droplet contact angle of the surface at 50 W is markedly low comparing with the other samples. At the RF power of 75 ~ 200 W, SiO:CH deposition can be confirmed from the existence of the absorption band F in the FT-IR spectra, where no variation in the sorts of the detected band is observed. The absorption intensities of these

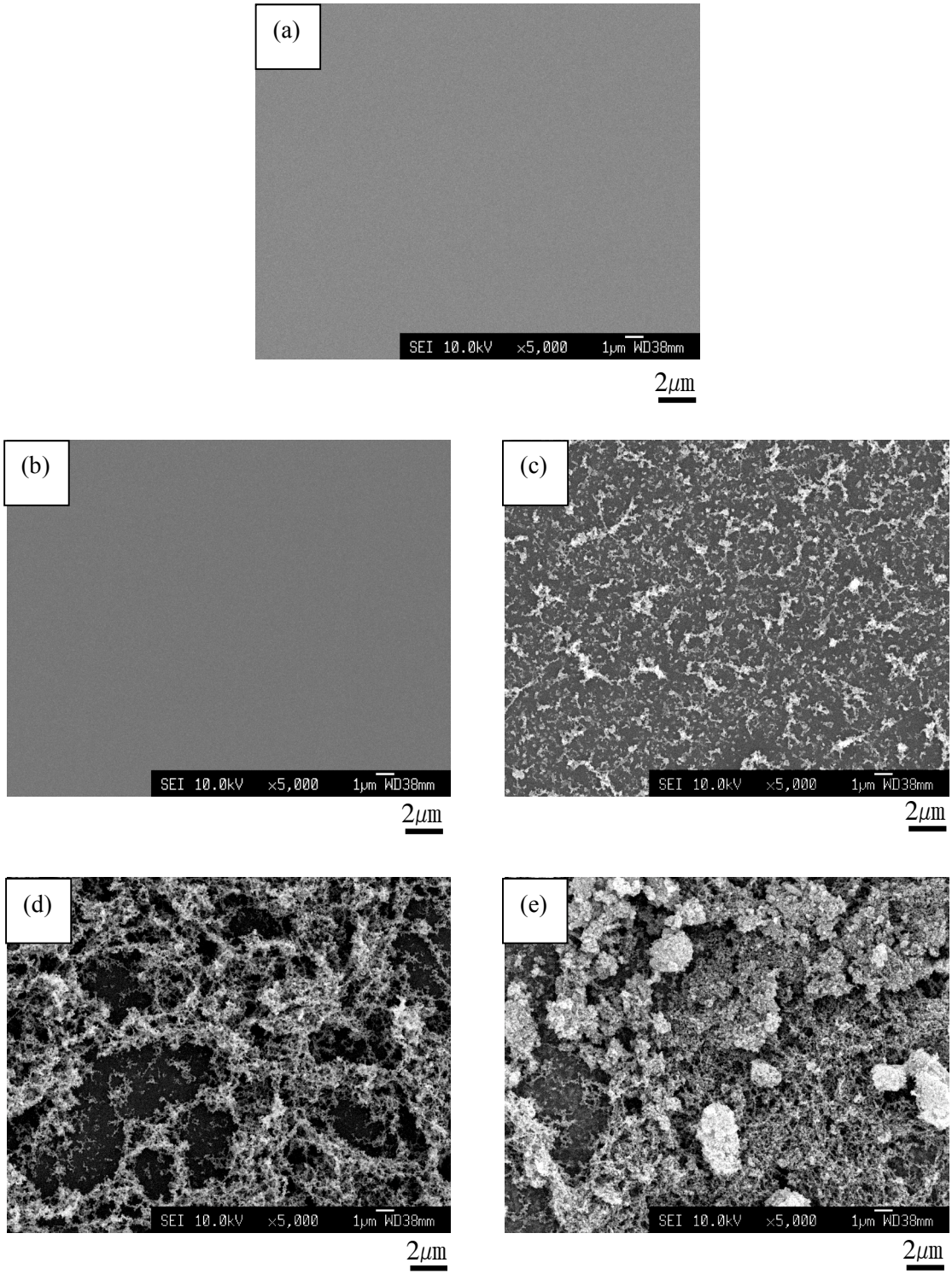

Figure 4.2. FESEM images of the films prepared at various RF power ((a): 50W, (b): 75W, (c): 100W, (d): 150W and (e): 200W).

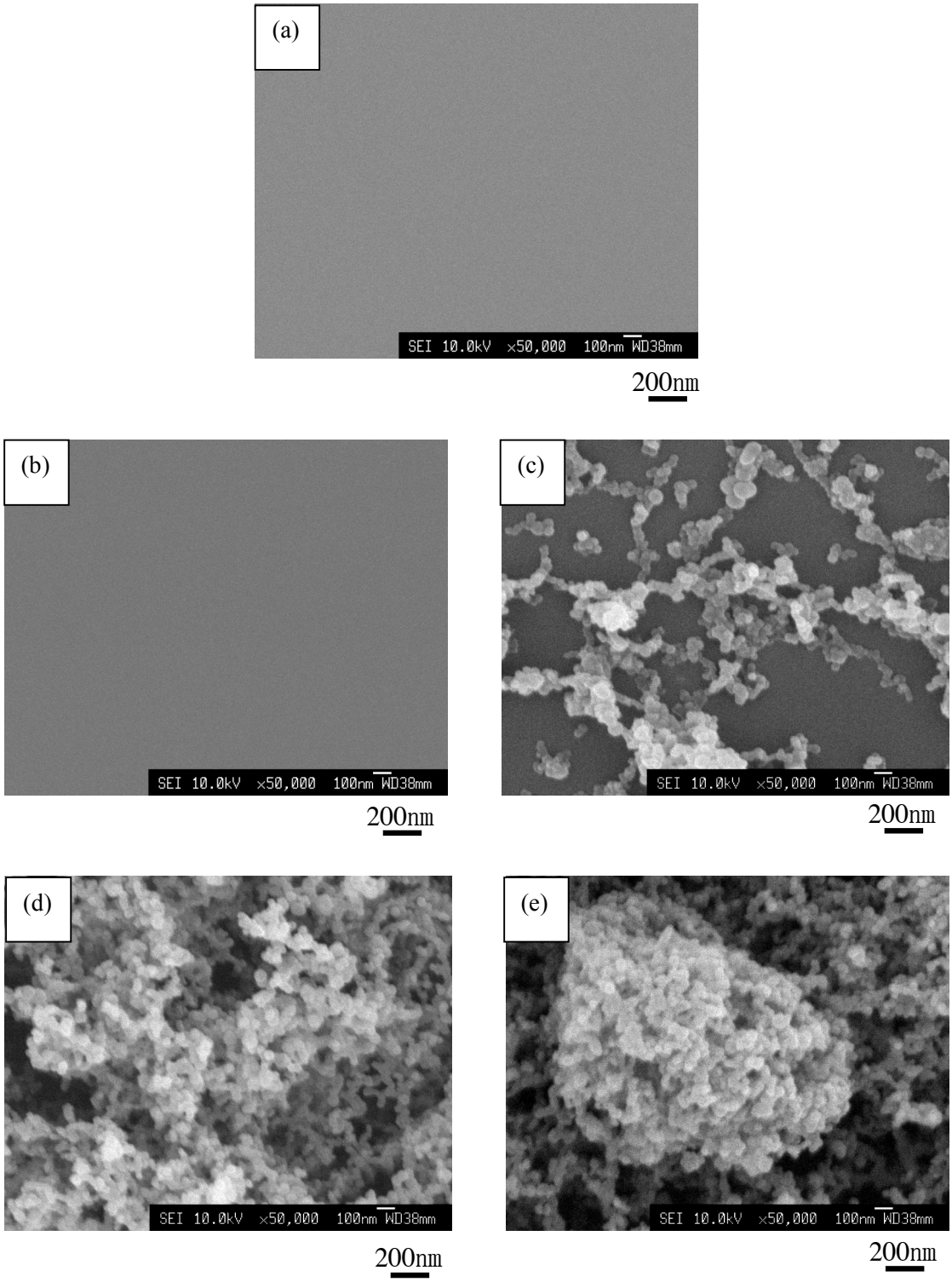

Figure 4.3. FESEM images of the films prepared at various RF power ((a): 50W, (b): 75W, (c): 100W, (d): 150W and (e): 200W).

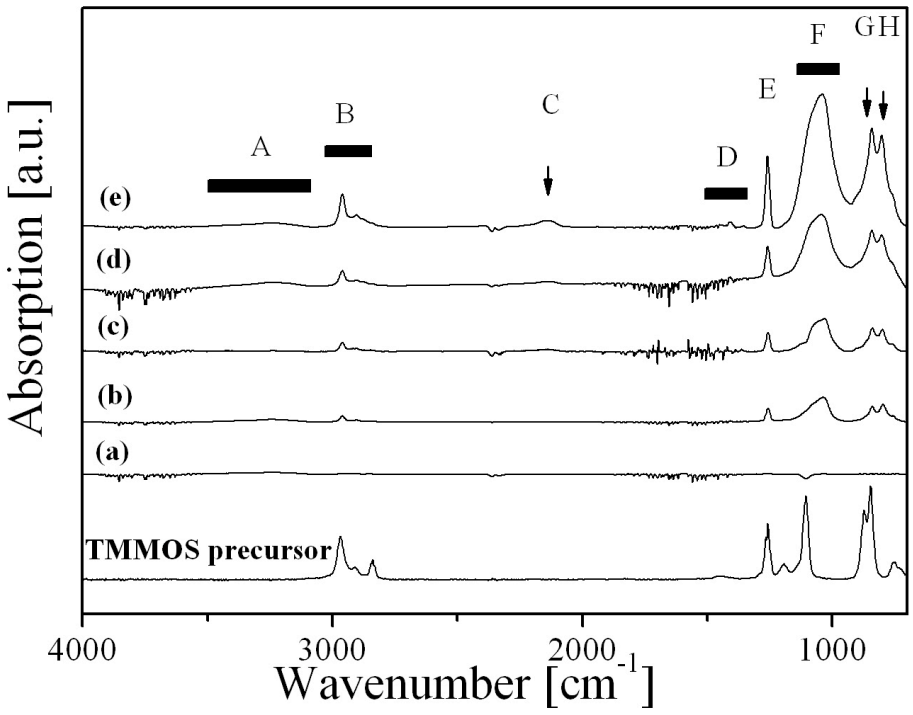

Figure 4.4. FT-IR absorption spectra for the TMMOS reactant and films ((a): 50W, (b): 75W, (c): 100W, (d): 150W and (e): 200W). The alphabet notations are defined in the text.

bands grow with an increase in the RF power except the band A (O-H), which shows maximum absorption intensity at the RF power of 100 W. The band B (C-H) becomes broader with an increase in the RF power, same tendency shown in the SiO:CH films deposited at lower pressure investigated in Chapter 3. The appearances of the absorption bands are fundamentally identical to those in the spectra for the SiO:CH films deposited at lower pressure investigated in Chapter 3. These results show that the film consists of Si-X-Si (X=O, CH_x) and/or -CH_2- networks with -OH, -CH_3 and -H terminations. The basic chemical bonding states of the terminations seem to be not far from that of the reactant molecule since the positions and the fundamental shapes of the absorption bands B, E and G are similar to the reactant except the broadening of these bands, which is due to the diverseness of the bonding states. Therefore, the films are supposed to be formed through plasma polymerization reaction of partly-dissociated reactant molecules and termination of the dangling bonds by the small fragments of the reactant molecules such as methyl radicals and hydrogen atoms.

The film surface is covered both with hydrophobic functional groups (-CH_3 and -H) and hydrophilic ones (-OH). Since the amount of the latter is much smaller than the former, the deposited film surfaces show strong hydrophobicity. The water contact angle of the -CH_3 terminated flat surface is reported as ~110° [25]. The film prepared in this study shows much higher value, greater than 150°. It is obvious that the ultra water repellency of the film surfaces is enhanced with the geometrical effect.

4.1.3.3. Plasma diagnostics in the formation of UWR thin films

Figures 4.5 and 4.6 show the optical emission spectra in visible range for the Ar-TMMOS plasma recorded during deposition of the WR (a) and the UWR (b) films. Emissions from Ar, H, CO and H_2 were detected mutually. At 150 W of RF power, however, emission bands from

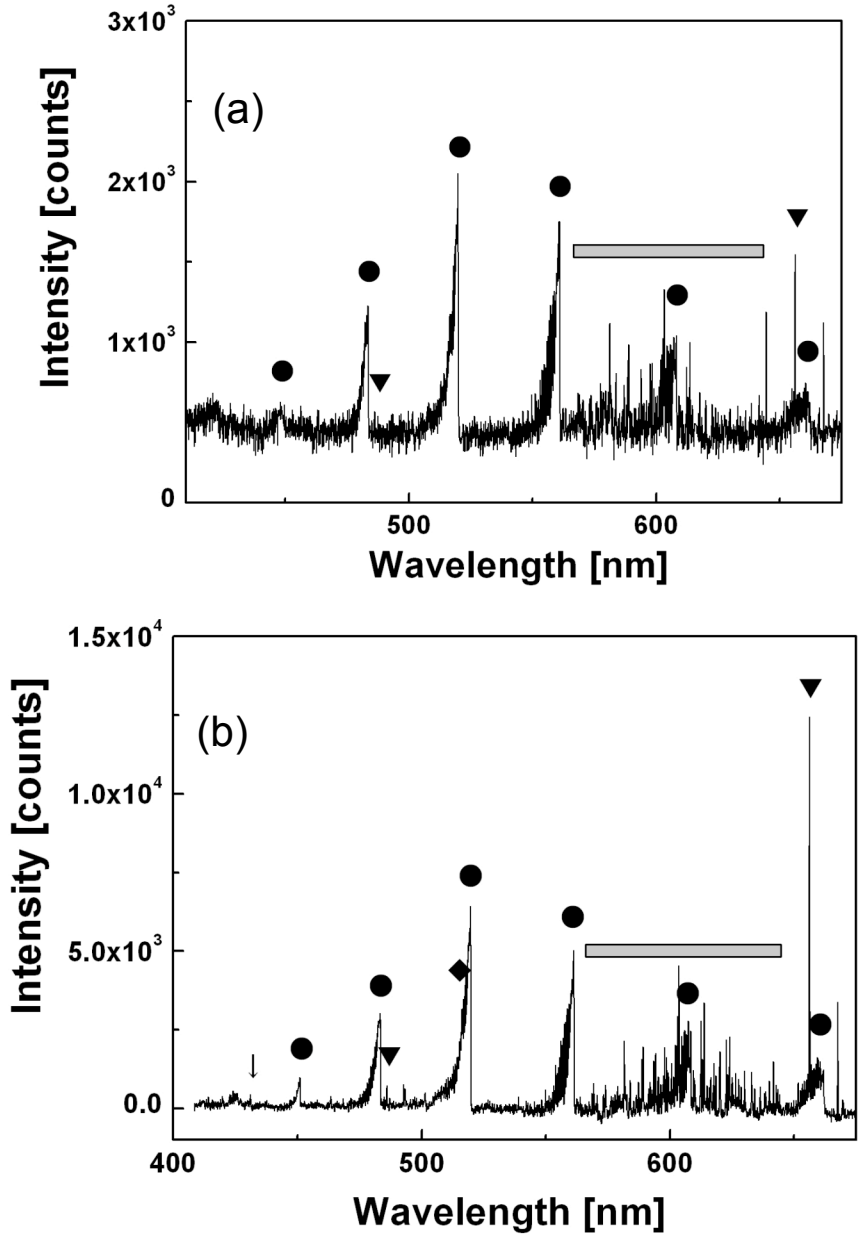

Figure 4.5. Optical emission spectra of inductively coupled plasma, during deposition of the UR and the UWR films at the RF power of (a) 100 W and (b) 150 W. Triangles(▼), circles(●), a diamond(◆) and an arrow(↓) indicate the lines from atomic H, CO Ångström emission bands, C_2 Swan system and CH band, respectively. A gray rectangle means the region where the H_2 lines are observed in a concentration. Other sharp line peaks are the emissions from Ar.

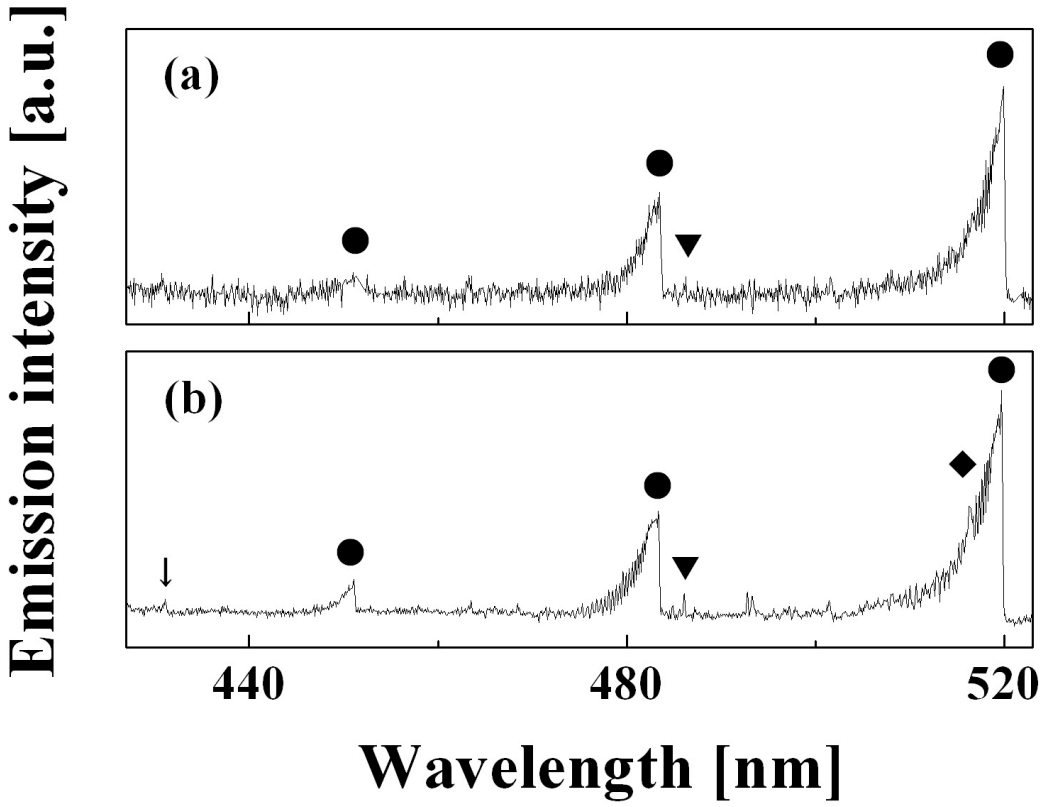

Figure 4.6. Optical emission spectra of inductively coupled plasma, during deposition of the UR and the UWR films at the RF power of (a) 100 W, (b) 150 W. A triangle(▼), circles(●), a diamond(◆) and an arrow(↓) indicate the lines from atomic H, CO Ångström emission bands, C_2 Swan system and CH band, respectively.

CH (4300 Å system, $A^2\Delta$-$X^2\Pi$) and C_2 (swan system, $A^3\Pi_g$-$X'^3\Pi_u$) were also detected at 431 and 516 nm, respectively. About the CO emission, the Ångström system band ($B^1\Sigma^-A^1\Pi$) were observed between 480 and 560 nm wavelengths. In the range of 560~690 nm, overlapped lines from H_2 can be seen. Origins of H, CO and H_2 in organosilicon plasma were mentioned in previous Section 3.1.3.1. One of the origins of the CH molecule is supposed to be the hydrogen abstraction reaction, which comes mainly from dissociation of the -CH_3 groups in the TMMOS.

$$-CH_2 + H \rightarrow H_2 + CH \text{ emission.} \quad (4.1)$$

Moreover, those can be emitted through

$$\text{TMMOS} + e \rightarrow CH \text{ emission,} \quad (4.2)$$

$$\text{TMMOS like radicals} \rightarrow CH \text{ emission,} \quad (4.3)$$

$$C_xH_m \text{ stable molecules} + e \rightarrow CH \text{ emission,} \quad (4.4)$$

$$C_xH_n \text{ radicals} + e \rightarrow CH \text{ emission.} \quad (4.5)$$

In the low power regime, Equation 4.2 should be predominant and hence all the emission intensities as well as the deposition rate are proportional to the RF power. In a RF power regime of 40-100 W the contribution of Equation 4.3 - 4.5 becomes appreciable, because the emission intensities increase with the RF power whereas the deposition rate is constant. Two methyl radicals (CH_x+CH_y) recombine into a hydrocarbon molecule (C_2H_{x+y}), which can be also striped by the hydrogen abstraction reaction resulting in the C_2 radical formation. Regarding the above reactions, the optical emissive species in the organosilicon plasma of relatively high pressure (500 Pa) show no major difference with those of low pressure in Section 3.1.3.1. That is, in the 500 Pa of relatively high pressure, similar plasma reactions happen in compared with those in low pressure. However, appearance of emissions of CH and C_2 radicals at the 500 Pa of pressure and 150 W of RF power, which is condition for the UWR

films, provide a clue of the recombination reaction as well as the clustering phenomenon, *i.e.* the clusters can be formed only in the condition of severe recombination reaction. The clustering phenomenon will be referred to in the following Section 4.2.

Table 4.1 shows the optical emission intensities of H_α and H_β during the deposition of the water-repellent thin films. From the optical emission intensities of atomic H_α (656 nm) and H_β (486 nm), the OES intensity increased approximately 10,000 and 500 counts with RF power, respectively. However, a relative intensity of H_β/H_α decreased with the RF power. From the relation between the optical emission intensity and the electron temperature, it is well known that H_β/H_α can indicate the electron temperature in plasma [26-28]. These results suggest that higher RF power increases the electron density, which is mainly due to the further activation of dissociative ionization reaction in the plasma, while the increased electron density influences a decrease of the electron temperature. Since the RF plasma of the Ar-TMMOS mixture gas is used in this study, the above- mentioned dissociation reactions (1) - (4) can be induced by the collision with metastable Ar* (11.55 or 11.72 eV), which has much higher energy than the bond dissociation energies of C-H (4.27 eV), H-H (4.52 eV) and C-O (3.64 eV) [29-30], i.e., the electrons can be replaced with Ar* in the reactions:

$$\text{TMMOS} + \text{Ar}^* \rightarrow \text{CH emission}, \tag{4.6}$$

$$C_xH_m \text{ stable molecules} + \text{Ar}^* \rightarrow \text{CH emission}, \tag{4.7}$$

$$C_xH_n \text{ radicals} + \text{Ar}^* \rightarrow \text{CH emission}. \tag{4.8}$$

From the above consideration on the plasma reactions, the deposition mechanisms can be described as follows;

(1) at low RF power, the dissociation of the reactant TMMOS is insufficient to be polymerized in the vapor phase, therefore the deposited films have the flat surface.

(2) at high RF power, on the contrary, polymerization of the partly-dissociated TMMOS

Table 4.1. Optical emission spectrum intensities of H_α and H_β at inductively coupled silane plasma with 420 Pa TMMOS and 80Pa Ar, during deposition of water-repellent thin films.

Deposition condition			H_α Intensity (counts)	H_β Intensity (counts)	H_β/H_α
Ar (Pa)	TMMOS (Pa)	RF Power (W)			
80	420	100	907	109	0.12
80	420	150	11377	665	0.06

becomes dominant in the vapor phase.

Figure 4.7 shows the relative intensities of each OES peaks calculated from the intensity at the RF power of 150 W divided by that at 100 W. The relative intensity of H_α is prominently higher compared with others. Hydrogen dissociation from the reactant molecules seems to be further activated at higher plasma power. This result supports the above consideration about the deposition scheme dependent on the RF power.

4.1.4. Summary

UWR thin films on Si (100) substrates were prepared by RF-PECVD. Contact angle of the deposited film was greater than 150°. This ultra water repellency was due to the combination effect of CH_3-terminated surfaces and the surface roughness which is self-assembled with nanoclusters and their agglomerates. From the result of the optical emission spectroscopy, existence of H, CO, CH, C_2, and H_2 were proved in organosilicon plasma for the fabrication of UWR thin films, which can describe the formation reaction of the ultra water repellent film in the plasma as polymerization of partly dissociated reactant molecules. Appearance of emissions of CH and C_2 at the deposition condition of UWR thin films, which is a proper deposition condition for the UWR films provide a clue of the recombination reaction as well as the clustering phenomenon, *i.e.* the clusters can be formed only in the condition of severe recombination reaction.

References

[1] Y. Wu, H. Sugimura, Y. Inoue and O. Takai, Thin Solid Films 435 (2003) 161.

[2] Y. Wu, Y. Inoue, H. Sugimura, O. Takai, H. Kato, S. Murai and H. Oda, Thin Solid Films 407 (2002) 45.

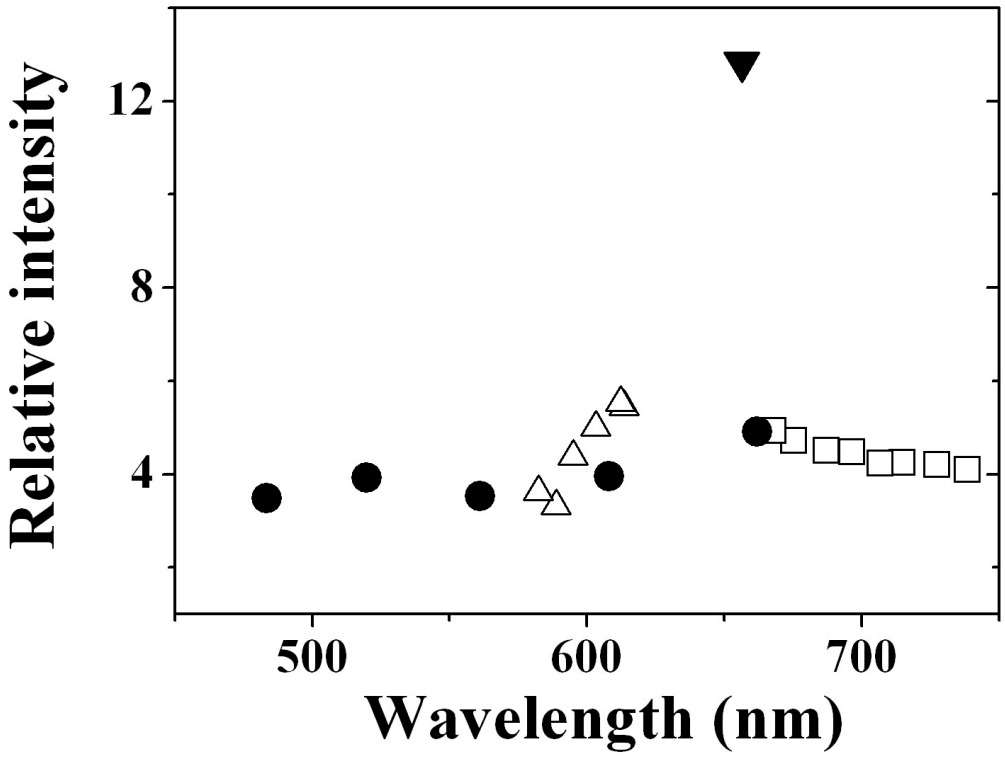

Figure 4.7. Relative intensity of the optical emission spectrum in the Ar-TMMOS plasma (□: Ar, ▼:H, △: H_2 and ●:CO).

[3] H.M. Shang, Y. Wang, S.J. Limmer, T.P. Chou, K. Takahashi and G.Z. Cao, Thin Solid Films 472 (2005) 37.

[4] X. Lu, C. Zhang and Y. Han, Macromol. Rapid Commun. 25 (2004) 1606.

[5] A. Hozumi, H. Sekoguchi, N. Kakinoki and O. Takai, J. Mater. Sci. 32 (1997) 4253.

[6] X. Feng and L. Jiang, Adv. Mater., 18 (2006) 3063.

[7] A. B. D. Cassie and S. Baxter, Trans. Faraday Soc., 40 (1944) 546.

[8] R. Blossey, Nat. Mater., 2 (2003) 301.

[9] A. Nakajima, K. Hashimoto and T. Watanabe, Monatsh. Chem., 132 (2001) 31.

[10] Y. Liu, L. Mu, B. H. Liu and J. L. Kong, Chem. Eur. J., 11 (2005) 2622.

[11] I. P. Parkin and R. G. Palgrave, J. Mater. Chem., 15 (2005) 1689.

[12] T. L. Sun, L. Feng, X. F. Gao and L. Jiang, Acc. Chem. Res., 38 (2005) 644.

[13] O. Takai, A. Hozumi and N. Sugimoto, J. Non-Cryst. Solids, 218 (1997) 280.

[14] A. Hozumi and O. Takai, Thin Solid Films, 334 (1998) 54.

[15] Y. Wu, M. Kuroda, H. Sugimura, Y. Inoue and O. Takai, Surf. Coat. Tech., 174-175 (2003) 867.

[16] Y. Yun, T. Yoshida, N. Shimazu, N. Nanba, Y. Inoue, N. Saito and O. Takai, J. Surf. Fin. Soc. Jpn, 58 (2007) 307 [in Japanese].

[17] A. Hozumi and O. Takai, Thin Solid Films, 303 (1997) 222.

[18] K. Teshima, H. Sugimura, Y. Inoue and O. Takai, A. Takano, Applied Surface Science, 244 (2005) 619.

[19] R. N. Wenzel, Ind. Eng. Chem., 28 (1936) 988.

[20] A. B. D. Cassie and S. Baxter, Trans. Faraday Soc., 40 (1944) 546.

[21] Takashi Nishino, Masashi Meguro, Katsuhiko Nakamae, Motonori Matsushita and Yasukiyo Ueda, , Langmuir, 15 (1999) 4321.

[22] Carsten Benndorf, Pierre Joeris and Roland Kröger, Pure Appl. Chem., 66 (1994) 1195.

[23] K. Teshima, H. Sugimura, Y. Inoue, O. Takai and A. Takano, Chemical Vapor Deposition, 10 (2004) 295.

[24] G.Socrates, Infrared Characteristic Group Frequencies 2nd ed., Wiley, Chichester, UK (1994) 188.

[25] A.M. Almanza-Workman, S. Raghavan, S. Petrovic, B. Gogoi, P. Deymier, D.J. Monk and R. Roop, Thin Sold Films 423 (2003) 77.

[26] Y. Inoue and O. Takai, Plasma Sources Sci. Technol. 5 (1996) 339.

[27] M. Shimozuma, J. Appl. Phys. 70 (1991) 645.

[28] A. Mizuike and H. Kawakuchi, Introduction to analytic chemistry (SangyoTosho, Tokyo, 2001) P. 143 [in Japanese].

[29] A. A. Radzig and B. M. Smirnov, Reference data on atoms molecules and ions, Spinger-Vgrlag, 197.

[30] P. W. Atkins, Physical chemistry 6th ed., Oxford University Press, (2001) A37.

4.2. Formation process of UWR thin films

4.2.1. Introduction

In the pervious section, I described the formation of UWR thin films. The UWR thin films could be formed by the combination effect of CH_3-terminated surfaces and surface roughness. From the OES, the existence of CH and C_2 radicals was proved in organosilicon plasma, which is a clue of the recombination reaction as well as the clustering phenomenon, *i.e.* the clusters can be formed only in the condition of severe recombination reaction. For step toward the practical use of these UWR thin films, it is necessary to improve the film properties, such as the hardness, adhesion, chemical durability and optical characteristic. In order to realize these improvements, it is indispensable to clarify the formation mechanism of the UWR thin films. In particular, it must be investigated the clustering process in organosilicon plasma, which is most important process in the formation of UWR thin films.

In this study, I investigated the clustering process by using surface morphology, water contact angle of the films, and in-situ laser scattering observation in Ar-TMMOS plasma.

4.2.2. Experimental procedure

This work was carried out with the ICP RF PECVD system. Details of this system were stated in Subsections 3.1.2 and 4.1.2. The reactant used in this work was trimethylmethoxysilane [TMMOS; $(CH_3)_3SiOCH_3$]. A n-type Si (100) substrate was located at 200 mm below from the center of the plasma to avoid direct thermal damage by the plasma. The total pressure of chamber was fixed at 500 Pa (80 Pa of Ar gas and 420 Pa of the TMMOS). After the deposition, water repellency of the films was measured by a static water-contact-angle meter (Kuluss, DSA10-Mk2). The surface morphology was observed by a field-emission scanning electron microscope (FESEM, JEOL, JSM-6330F). As shown in

Figure 4.8, clusters in Ar-TMMOS plasma were observed using laser scattering method. A diode-pumped solid-state (DPSS) continuous-wave (CW) laser (Edmund optics), which wavelength is 532 nm was used as light source. Scattered light was detected by the optical equipment used for plasma emission spectroscopy in the previous chapter. Scattered laser light was monitored through a quartz-glass window positioned around the substrate area. A fiber optic cable transmitted collected light to a monochromator (Chromex, 500-IS) attached with a CCD detector (Princeton Instrument, CCD-1100PF/UV). Wavelength resolution of this system was 0.15 nm.

4.2.3. Results and discussion

4.2.3.1. Clustering phenomenon in formation of UWR thin films

The UWR films can be fabricated by controls of chemical functional groups on the surface and surface roughness. The functional groups on the surface can be easily controlled by a lot of surface modification processes including thermal CVD, PECVD, chemical grafting. Concerning to the surface roughness, on the other hand, it is difficult to control the surface roughness, or the three-dimensional shape in more precise expression, by plasma deposition method. In Section 4.1, I reported the fabrication of the films with rough surfaces for the UWR function by enhancement of clustering phenomena in TMMOS plasma. In order to fabricate the clusters in plasma, it is important following two conditions. One is an introduced energy to promote dissociation and recombination reactions. The other is a mean residence time of precursors to generate the cluster in the plasma. That is, it is necessary the specific mean residence time to transfer the RF energy for dissociation and recombination reaction in plasma phase. The UWR films could be fabricated reproducibly at the pressure condition of 500 Pa. That is, approximately 1.15 s of mean residence time of precursors in the chamber,

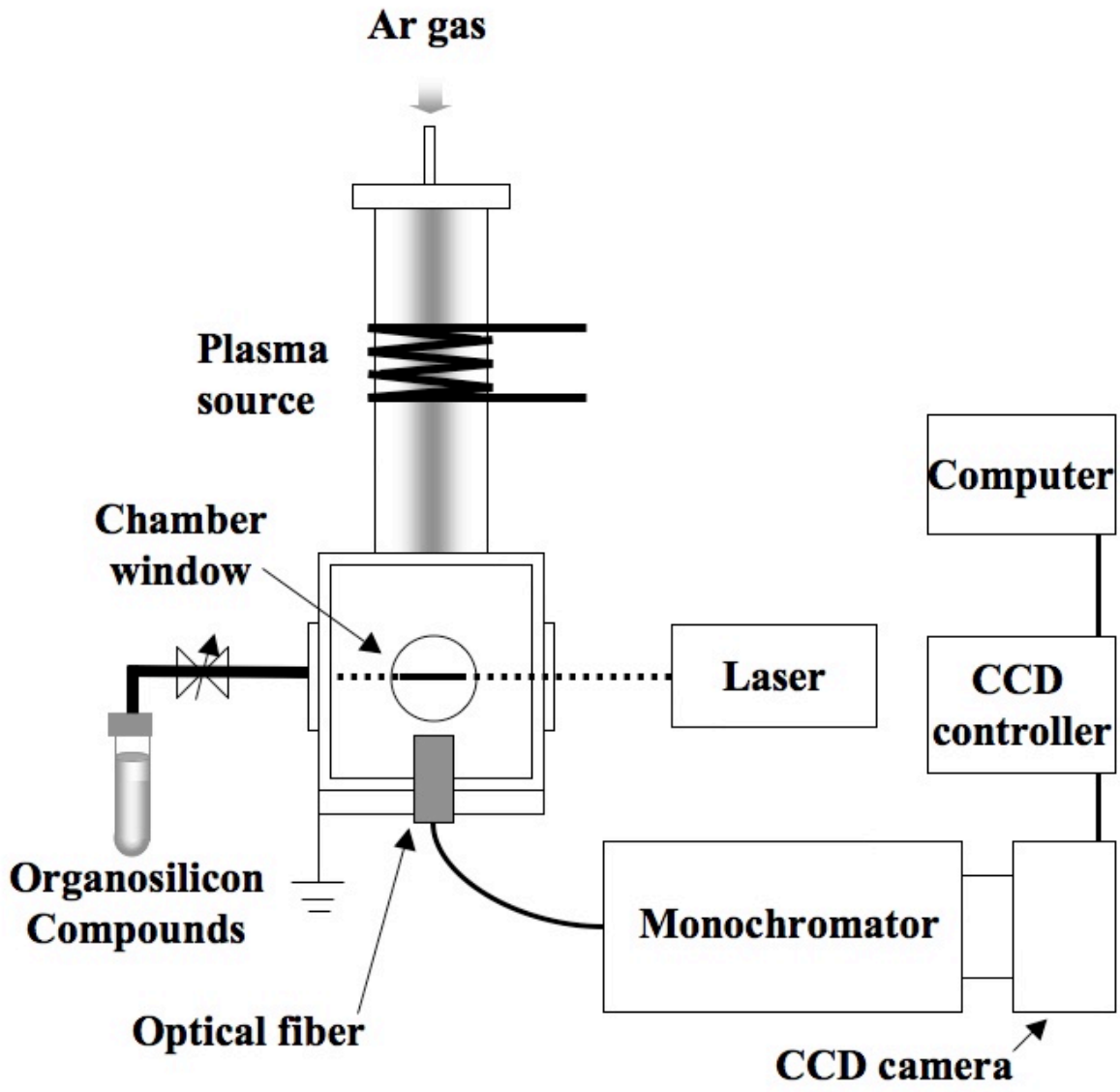

Figure 4.8. Schematic diagram of PECVD reactor equipped with detection system of laser scattering for measurement of clusters in Ar-TMMOS plasma.

calculated from the volume of chamber / the exhaust velocity, is necessary to form the sufficient surface roughness for UWR films. It should be noticed that this mean residence time was simply estimated from the performance data of exhaust speed for the rotary pump used in this study (Figure 4.9). It can be said, at least, that more than 1.15 s of actual mean residence time of precursors is necessary to form the clusters in organosilicon plasma, since the conductance of the vacuum line in the system is not considered in the above estimation.

From the RF power dependence in the formation of UWR films, the water contact angle was increased with RF power, and the UWR surfaces could be fabricated at above 150 W of the RF power in the previous section. Under 100 W, the surface morphology of thin films was close to flat even though the clusters existed, which led to just a WR property. Under 150 ~ 200 W, the film had micrometer-size pores in the self-assembled cancellous microstructure, which consists of the globular nano-clusters, resulted in the UWR property. Figures 4.10 and 4.11 show SEM images of the WR and UWR films as well as their size distribution of the nano-clusters, respectively. The size distribution was obtained from 80 pieces of the nanoclusters observed in the SEM image. The average sizes of nanoclusters were 63.4±22.6 nm (100 W), 58.3±10.1 nm (150 W) and 62.5±11.8 nm (200 W). On the whole, the size distribution was not altered under different RF power. This result suggests following two things.

(1) RF power relates to only an essential condition where the formation of the nano-clusters occurs or not, *i.e.* clustering of the fragments in the plasma phase takes place when the introduced RF power exceeds a certain threshold value, since the transferred RF energy achieves a sufficient level of dissociation and recombination of the TMMOS.

(2) The important factors determining the distribution of the nano-cluster size lie in other deposition conditions than the RF power. It may be the mean residence time of the TMMOS,

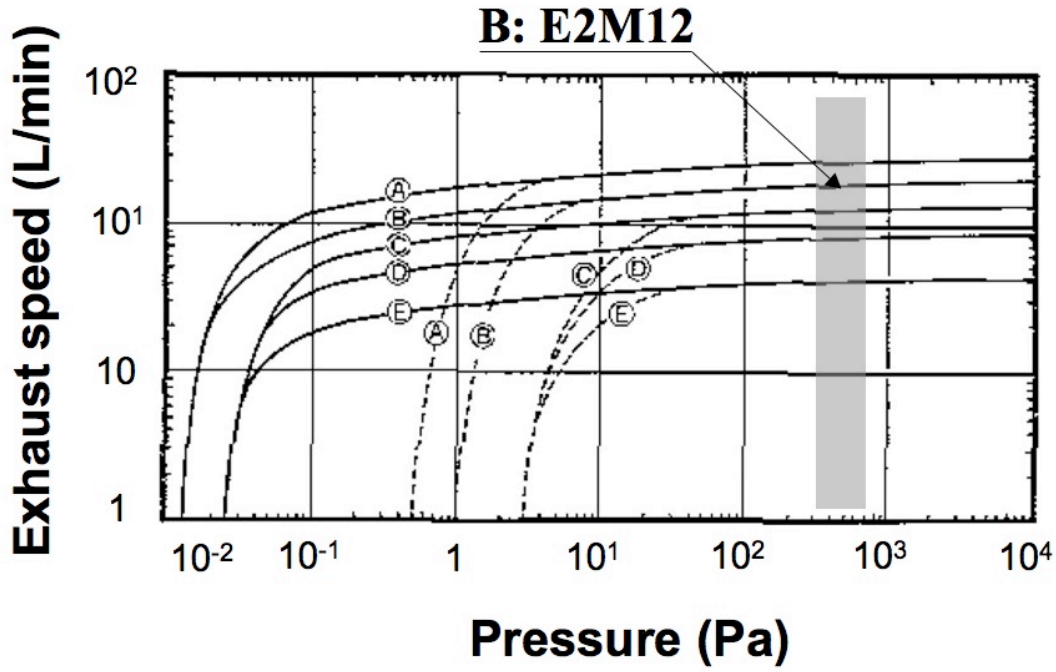

Figure 4.9. Exhaust speed of rotary pump (Edwards E2M12). Continuous line and dotted line corresponds to an open state and closed state of ballast valve, respectively. Gray area in the figure come under 500 Pa of pressure.

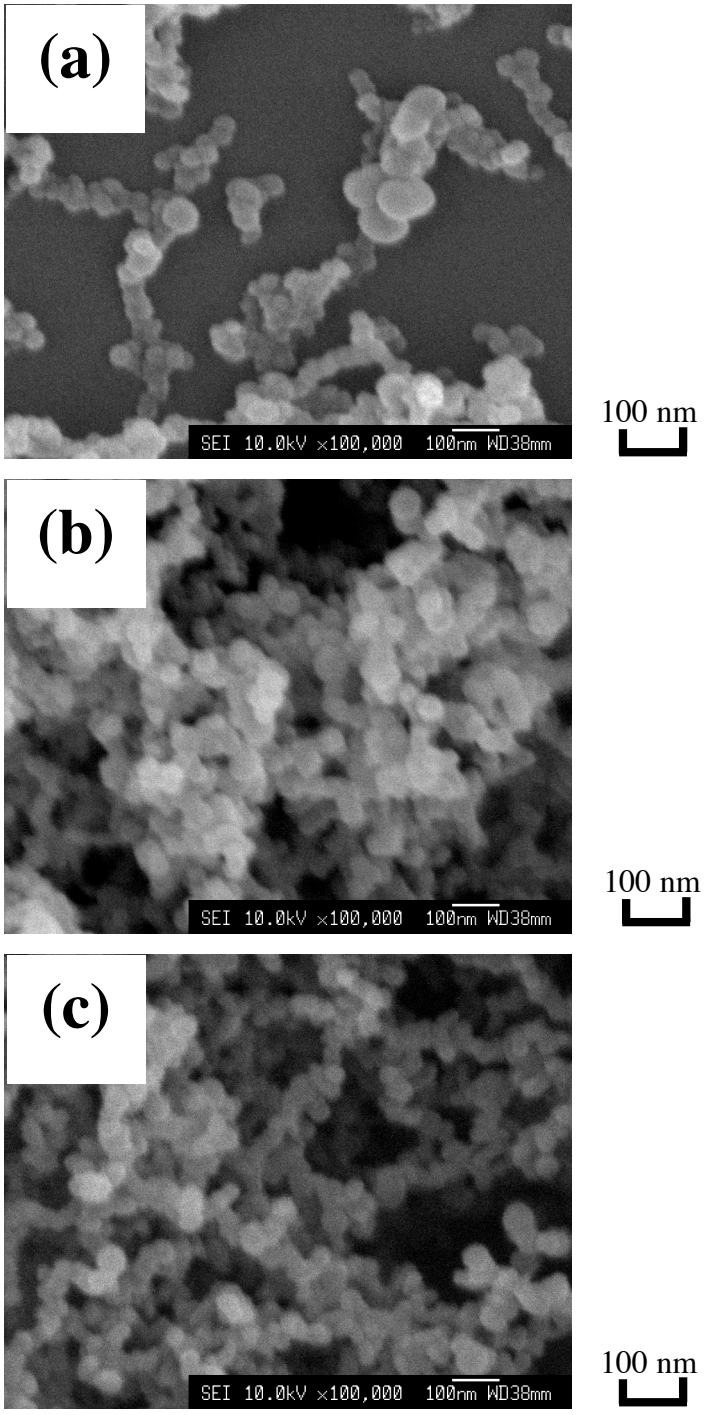

Figure 4.10. FESEM image of the films prepared at 100 W (a), 150 W (b) and 200 W (c) of RF power.

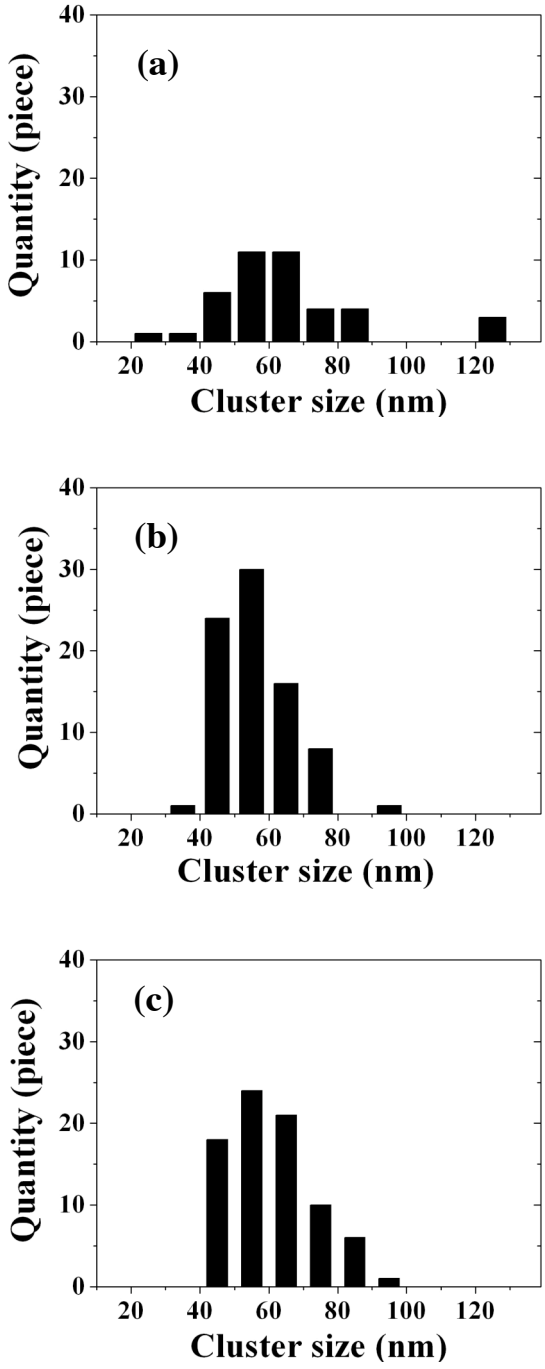

Figure 4.11. Cluster size distribution of the films prepared at 100 W (a), 150 W (b) and 200 W (c) of RF power. Cluster size was obtained from SEM image.

the spatial configuration of the deposition system, or the self bias of the nano-clusters which are negatively charged in plasma phase. It should be considered, at least, that there is a self-stopping mechanism against the growth of the nano-clusters in the plasma phase. In either case, further investigations will be mandatory in order to clarify this mechanism.

For the clustering phenomenon or polymerization-like reactions in gas phase, it is important to investigate the dissociation reaction, *i.e.* a formation reaction of monomer-like gas species in plasma. In the previous Subsection 4.1.3.3, in the deposition conditions for the WR (100 W) and the UWR (150 W) films, emissions from Ar, H, CO and H_2 were commonly detected. At 150 W of the RF power, emission bands from CH and C_2 were also detected at 431 and 516 nm, respectively. The appearance of the emissions of CH and C_2 provide a clue of the recombination reaction as well as the clustering phenomenon, *i.e.* the clusters can be formed only in the condition of severe recombination reaction. The detection of these clusters will be discussed in Subsection 4.2.3.4.

4.2.3.2. Time dependence of the deposition of UWR thin films

To investigate the growth process of the clusters, the growth of ultra water repellent thin films was observed by using FESEM. Figures 4.12 and 4.13 shows the deposition-time dependence of the surface microstructure of the UWR thin films fabricated under 500 Pa of pressure, 150 W of RF power and ~ 10 - 180 s of deposition time. At the first stage of the growth (Figures 4.12 and 4.13 (a)), nano-clusters or agglomerates which is consists of several nano-clusters can be observed on the film surface. It can be said that these clusters originate from a recombination process in the gas phase and deposit randomly on the substrate. When the film was deposited for 30 or 60 s (Figures 4.12 and 4.13 (b, c)), the nano-clusters show a tendency to form chains rather than islands. Because the substrate in the chamber is kept

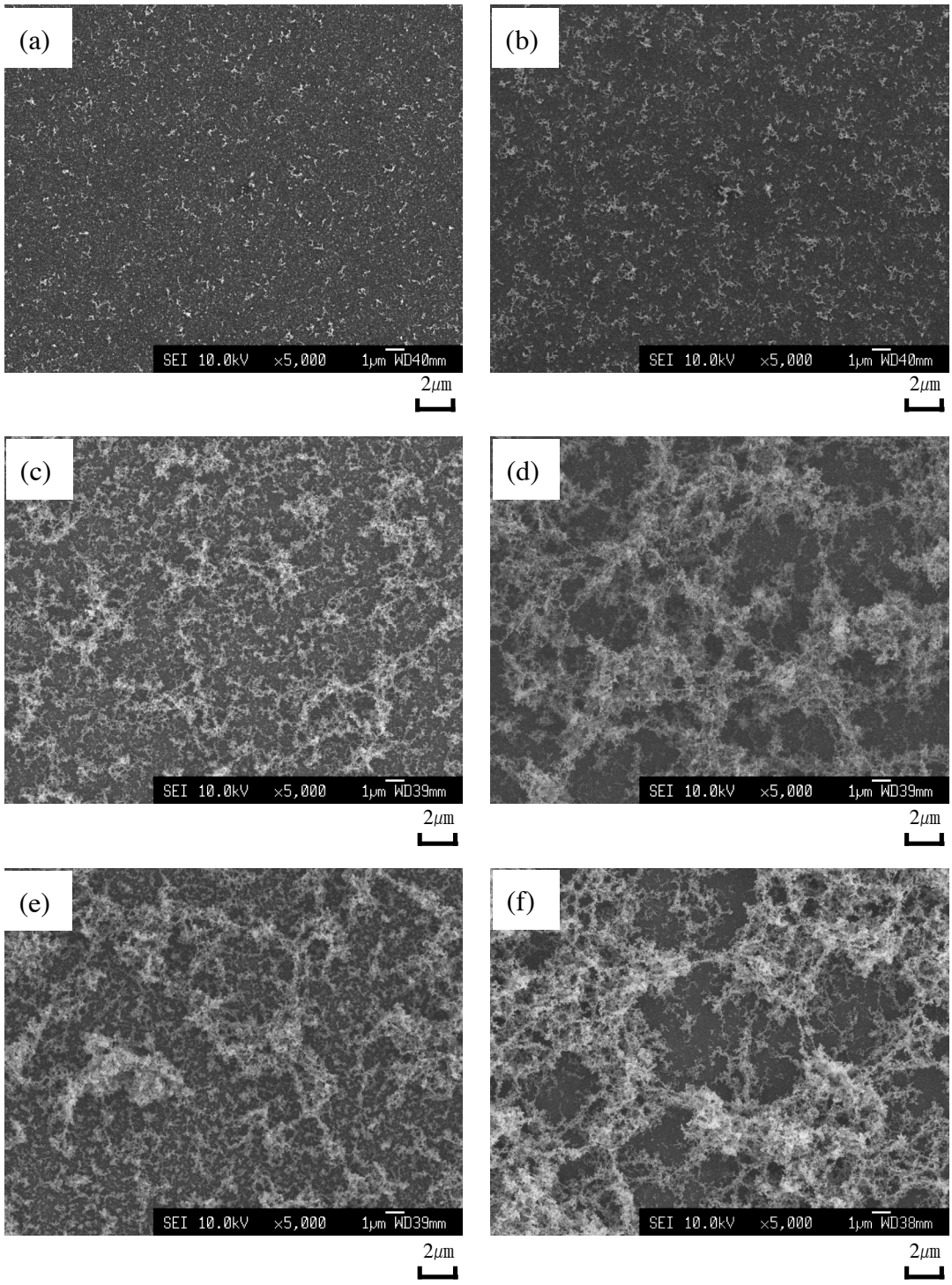

Figure 4.12. FESEM images of the films prepared for each deposition time ((a): 10, (b): 30, (c): 60, (d): 90, (e): 120 and (f): 180 s).

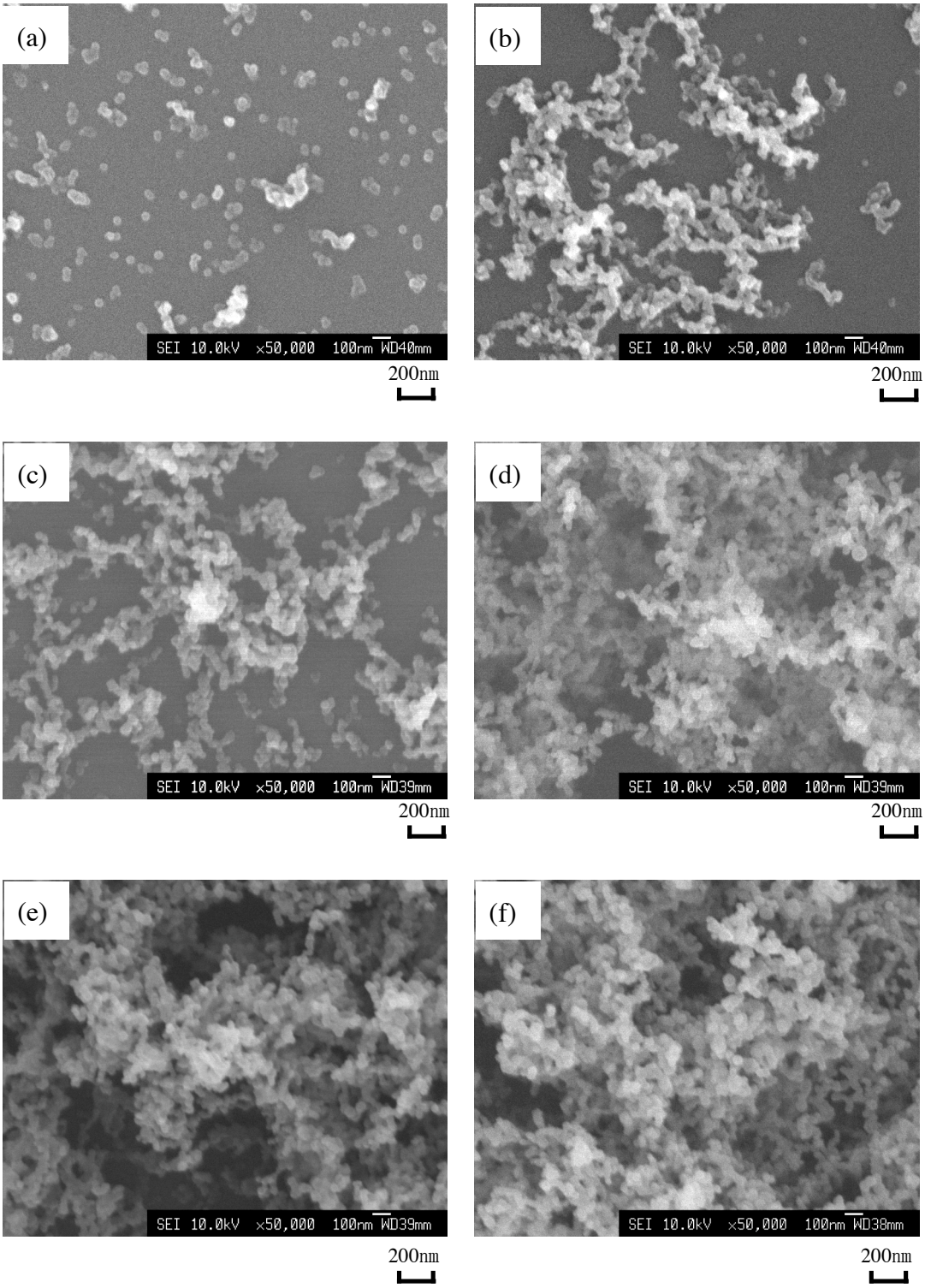

Figure 4.13. FESEM images of the films prepared for each deposition time ((a): 10, (b): 30, (c): 60, (d): 90, (e): 120 and (f): 180 s).

around near room temperature, nano-clusters cannot migrate on the surface of the films. Therefore, the presence of these agglomerates indicates that the clusters must have a spatial preference, *i.e*. clusters do not agglomerate randomly with three-dimensional direction. At the 90 s (Figure 4.12 and 4.13 (c)), the nano-clusters and agglomerates increased markedly whereas surface coverage was low until 60 s. These results can be arisen from following three mechanisms:

(1) nano-clusters are formed markedly during ~ 60 - 90 s, and agglomerates in organosilicon plasma,
(2) in order to agglomerate among the nano-clusters, it takes ~ 60 - 90 s,
(3) due to the distance from the location of nano-clusters formation to substrate, it is necessary ~ 60 - 90 s to transport the nano-clusters and agglomerates.

However, due to constant deposition conditions of reactant supply and RF power in the discharge, it is difficult to conclude that the dissociation and recombination reaction in organosilane plasma activated with the deposition time. Therefore, the contribution of (2) and (3) becomes appropriately. Concerning this deposition process, it will be discussed in the following Section 4.2.3.3 again. After 120 s, an increased geometric progression of the clusters can be observed. These films have particular nano-textures with nano-scale pores of a few hundreds nanometer in size among the cancellous web-like structure of the nano-cluster agglomerates

Figure 4.14 shows the cluster size distribution with deposition time. The size of clusters was estimated from processing the SEM images. Each size of clusters was calculated 80 pieces. On the whole, the size distribution was not altered under different deposition time, *i.e*.

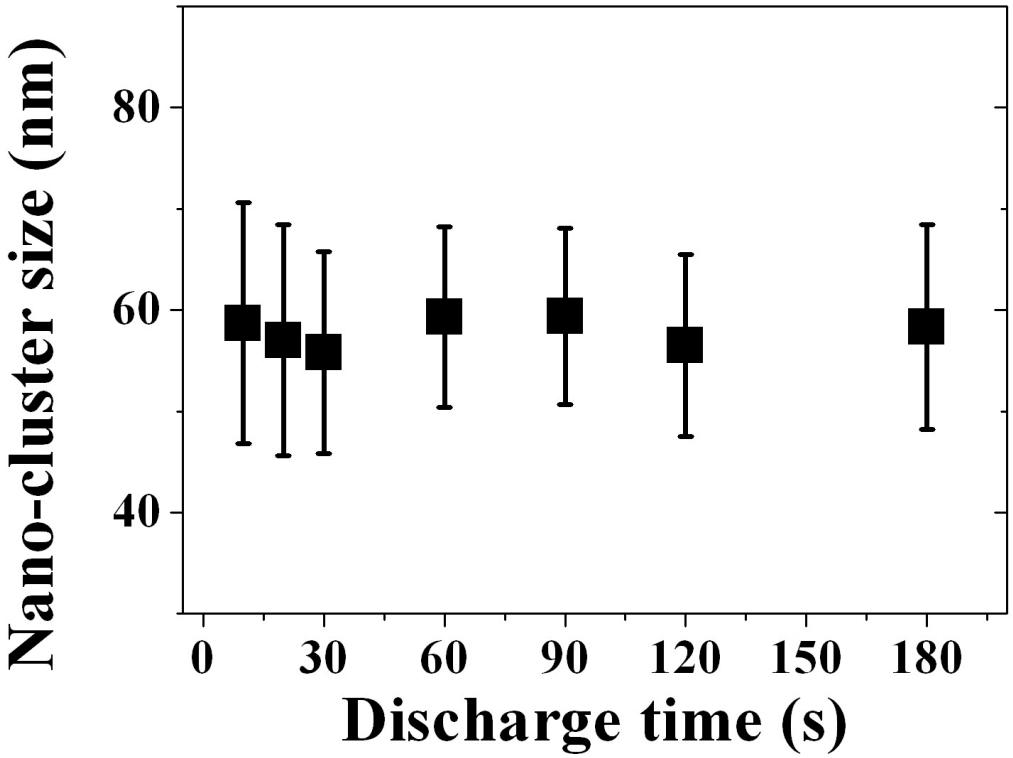

Figure 4.14. Cluster size distribution with the deposition time at 500 Pa of pressure and 150 W of RF power. Cluster size was obtained from SEM image.

all the sizes of nano-clusters were obtained approximately 60 nm in diameter. This result suggests that the nano-clusters are possible to grow up the specific space and time in the chamber independent of deposition time.

Figure 4.15 indicates the water contact angle of the films deposited at different deposition time of ~ 10 - 180 s. The water contact angle was increased with deposition time. In 10 s of deposition time, the water contact angle of the films was approximately 115 degree, caused by the relatively smooth surface terminated by CH_3- hydrophobic functional group from TMMOS reactant. In 20 ~ 30 s of deposition time, the water contact angle was elevated than that of 10 s due to an enhancement of surface roughness by the nano-clusters. The geometrical effect for these surfaces is ascribable to the expansion of the nominal surface area (Wenzel-style effect). In 60 s, the rough surface of the film results in over 150 degree of the water contact angle. The water contact angle of the films was increased slightly until 162 degree for 180 s. In this regime, the geometrical effect of the air trapping between a water-droplet and textures on the film surface, which minimizes the contact area, can be caused (Cassie-style effect) [1-2].

4.2.3.3. Time zone dependence of the deposition of UWR thin films

As the previous discussion about the deposition time dependence, it can be thought that the nano-clusters and the agglomerates are not deposited constantly on the surface of the substrates. Therefore, I prepared six samples, which were fabricated with six time segments in one deposition batch. Details of this experiment are as follows:

(1) six substrates were attached on a hexagonal sample holder,

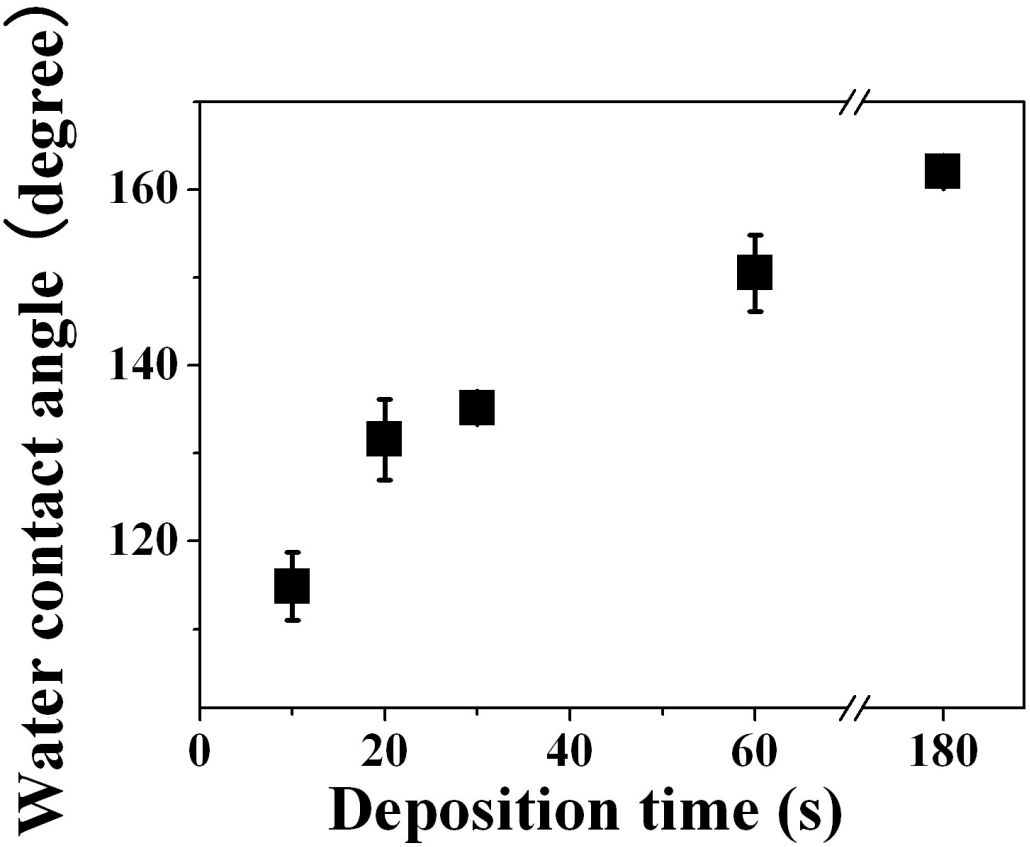

Figure 4.15. Water contact angle of the films deposited with various deposition times at 150 W of RF power.

(2) the hexagonal sample holder which is in laterally fixed to the plasma source was set up in the lower side of chamber,

(3) in order to expose only the substrate in the top of a hexagonal sample holder, the sample holder was covered excepting the top side,

(4) six samples were prepared through rotating the sample holder every 30 s.

Figure 4.16 shows SEM images of films prepared at each deposition time region (under 500 Pa of pressure, 150 W of RF power). At 0 ~ 30 s (Figure 4.16 (a)), both single nano-clusters and small agglomerates which is consists of the nano-clusters were observed randomly. At 30 ~ 60 s (Figure 4.16 (b)), density of agglomerates increased slightly compared with the time zone of 0 ~ 30 s. At 60 ~ 90 s (Figure 4.16 (c)), it can be confirmed that the agglomerates increased markedly than those of 0 ~ 60 s. These results correspond to the previous results of surface morphology with deposition time. Meanwhile, it can be observed the growth of films until ~ 150 s, and it seems to saturates at 150 ~ 180 s. This results indicates that the agglomeration phenomenon in the organosilicon plasma develops until ~ 150 s, and saturates at the time zone of 150 ~ 180 s.

4.2.3.4. In-situ observation of nano-clusters in plasma using laser scattering method

4.2.3.4.1. Scattering phenomenon [3-11]

Scattering is a general physical process whereby some forms of radiation, such as light, sound or moving clusters. In this work, however, the scattering phenomenon was restricted to the light scattering. Scattering phenomenon is distinguished between two broad types, elastic and inelastic. Elastic scattering involves no (or a very small) loss or gain of energy by the

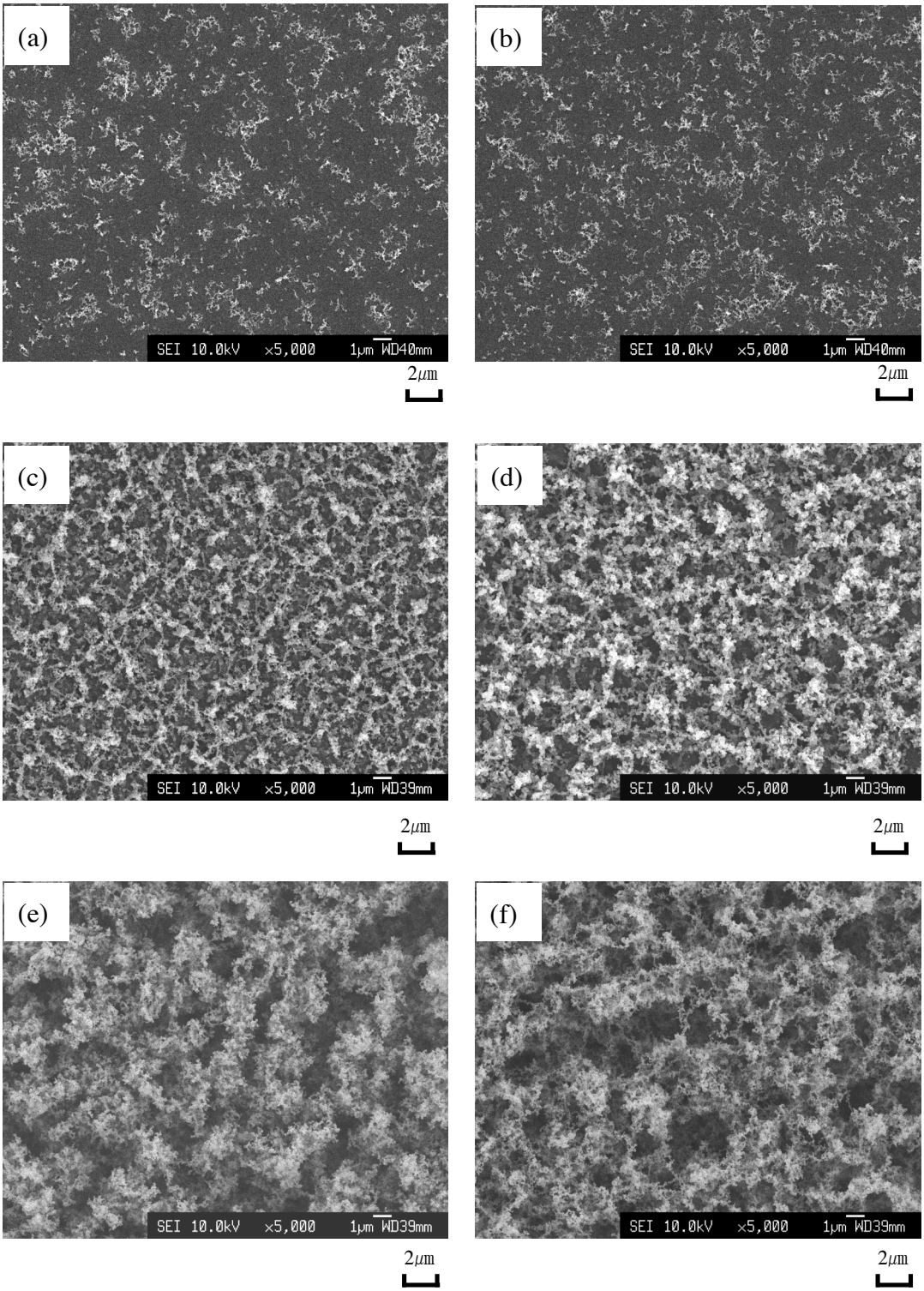

Figure 4.16. FESEM images of the films prepared at each deposition time region ((a): 0~30, (b): 30~60, (c): 60~90, (d): 90~120, (e): 120~150 and (f): 150~180 s).

radiation, whereas inelastic scattering does involve some change in the energy of the radiation. Major forms of elastic scattering (involving negligible energy transfer) are Rayleigh and Mie scattering. Inelastic scattering effects include Brillouin scattering, Raman scattering, inelastic X-ray scattering and Compton scattering. Concerning the scattered light to want to detect in this work, it is closely related to Rayleigh scattering more than Mie scattering in the elastic scattering due to the cluster size, hence Rayleigh scattering phenomenon will be discussed in this section.

Rayleigh scattering (named after Lord Rayleigh) is a process in which electromagnetic radiation (including light) is scattered by a small spherical volume of variant refractive index, such as a cluster, bubble, droplet, or even a density fluctuation. The intensity I of light scattered by a single small particle from a beam of unpolarized light of wavelength λ and intensity I_0 is given by:

$$I = I_0 \frac{1+\cos^2\theta}{2R^2}\left(\frac{2\pi}{\lambda}\right)^4\left(\frac{n^2-1}{n^2+1}\right)^2\left(\frac{d}{2}\right)^6, \qquad (4.1)$$

where R is the distance to the particle, θ is the scattering angle, n is the refractive index of the cluster, and d is the diameter of the cluster. In order for Rayleigh's model to apply, the sphere must be much smaller in diameter than the wavelength (λ) of the scattered wave; typically the upper limit is taken to be about 1/10 the wavelength. In this size regime, the exact shape of the scattering center (or scatterer) is usually not very significant and can often be treated as a sphere of equivalent volume. Because a scattered light shapes point-symmetrically as the basis for scatter center (Figure 4.17 (a)), scattered intensity depend on only size of clusters. Moreover, due to the uniformity of scattered light, scattered intensity is usable to analyze the

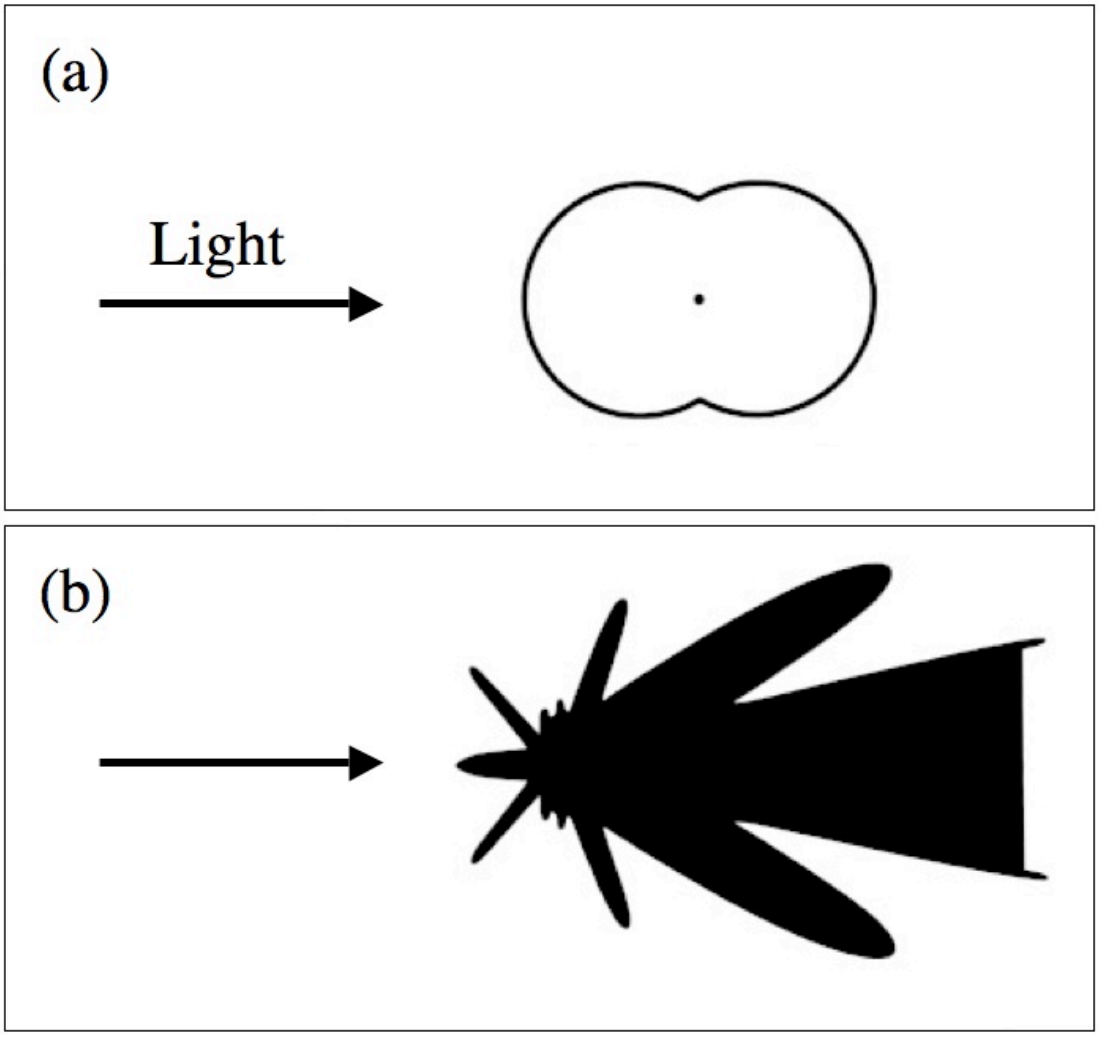

Figure 4.17. Scattering patterns of Rayleigh (a) and Mie scattering (b).

cluster size in dusty plasma [5-11]. The inherent scattering that radiation undergoes passing through a pure gas is due to microscopic density fluctuations as the gas molecules move around, which are normally small enough in scale for Rayleigh's model to apply. This scattering mechanism is the primary cause of the blue color of the Earth's sky on a clear day, as the shorter blue wavelengths of sunlight passing overhead are more strongly scattered than the longer red wavelengths according to the relation of above Rayleigh's equation 4.1 (scattered intensity is proportion to $1/\lambda^4$).

Meanwhile, scattering by spheres larger than the Rayleigh range is usually known as Mie scattering (named after Gustav Mie). In the Mie regime, the shape of the scattering center becomes much more significant, and complicated patterns of scattered light were revealed due to forward-scattered light with an increase of cluster size (Figure 4.17 (b)). The intensity of scattered light depends on the angle of scattered light, and it is proportion to cluster diameter squared (d^2). At values of the ratio of particle diameter to wavelength more than about 10, the laws of geometric optics are mostly sufficient to describe the interaction of light with the cluster, and at this point the interaction is not usually described as scattering.

4.2.3.4.2. Nano-clusters detection in plasma during the formation of UWR thin films

As the previous discussion about the growth process in the UWR thin films, the film was fabricated with several different stages by deposition time. This result was attributed by the flux of nano-clusters near the substrate, *i.e.* a quantitative change of nano-clusters influence to the deposition process. Hence, it can be clarified the deposition process through an investigation of nano-clusters near the substrate. In order to observe the nano-clusters, laser scattering system was prepared as Figure 4.8. 532 nm DPSS laser introduced to a chamber window, and scattered laser was detected by the same system for OES. Intensity of scattered

laser was obtained for 3 s later from plasma turned off.

Figure 4.18 shows the images of scattered laser by clusters formed in organosilicon plasma. Under the 500 Pa of pressure and 150 W of RF power, which is the deposition condition for the UWR films, scattered light was observed at turning off plasma. These results signify the existence of nano-clusters in organosilicon plasma, supporting that the UWR films were deposited with nano-clusters formed in plasma. From a relation between the average size of nano-clusters (58.3±10.1 nm, deposition condition of 500 Pa, 150 W) and the wavelength of DPSS laser was 532 nm, it can be said that scattered light by the single nano-clusters originated by Rayleigh scattering phenomenon. In the case of agglomerates, those of sizes were over 500 nm, *i.e.* scattering phenomenon is possible to transfer from Rayleigh to Mie scattering. In the Mie scattering regime, I described that complicated patterns of scattered light revealed due to forward-scattered light by large cluster size. In this work, however, dependence of scattered angle cannot be expected due to a random distribution of low dense and non-spherical agglomerates in the plasma.

Figure 4.19 shows the time dependence on intensity of scattered laser by clusters formed in organosilicon plasma. Scattered laser intensity increased linearly with the deposition time. The intensity of scattered laser consists of an ingredient of Rayleigh scattered light by single nano-clusters and one of Mie scattered light by agglomerates. Regarding the Rayleigh scattered light, it can be said that the scattered intensity of 10 s is originated only by Rayleigh scattering phenomenon of single nano-clusters, and one of other discharge time condition includes a similar or less amount of Rayleigh scattered light. Concerning the increase of scattered light, this is included the meaning of an increase of amount of nano-clusters or agglomerates, and an enlargement of agglomerates. Despite a quantitative analysis about

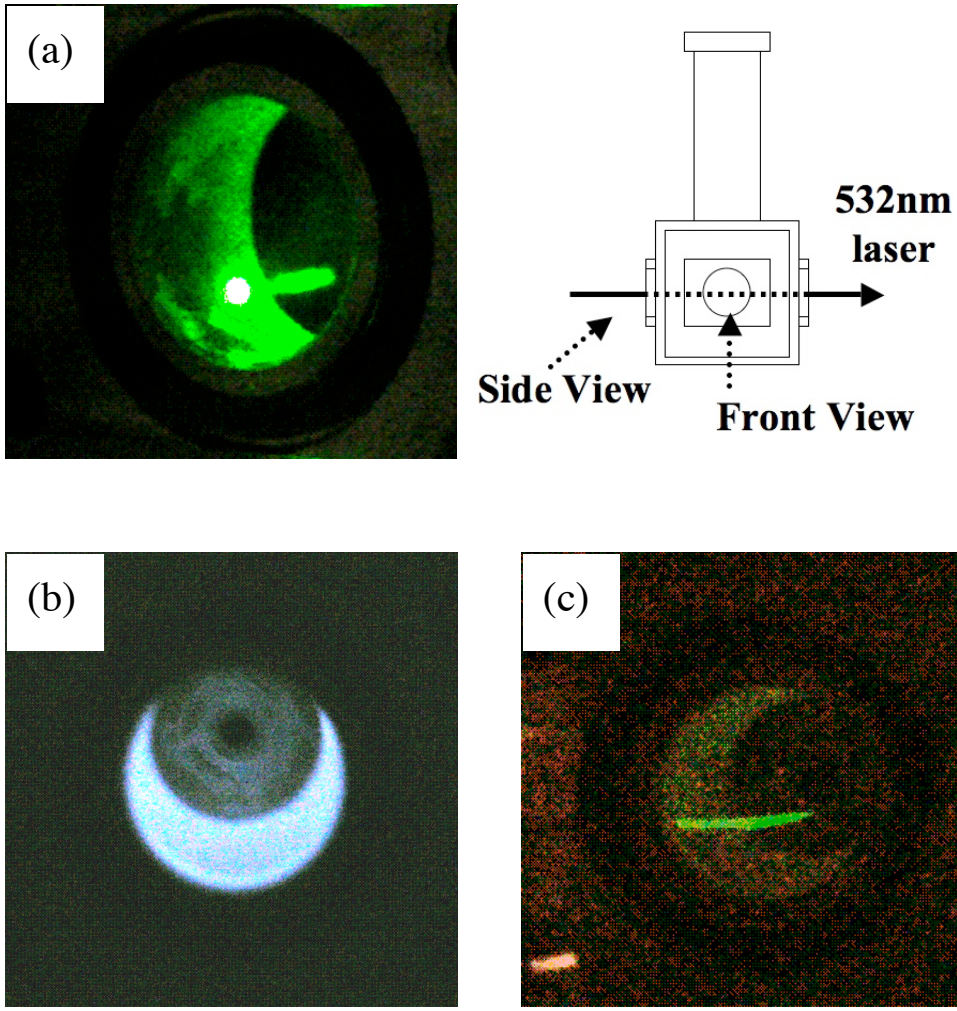

Figure 4.18. Images of scattered laser by clusters formed in organosilicon plasma ((a): side view, (b): front view, plasma on and (c): front view, plasma off).

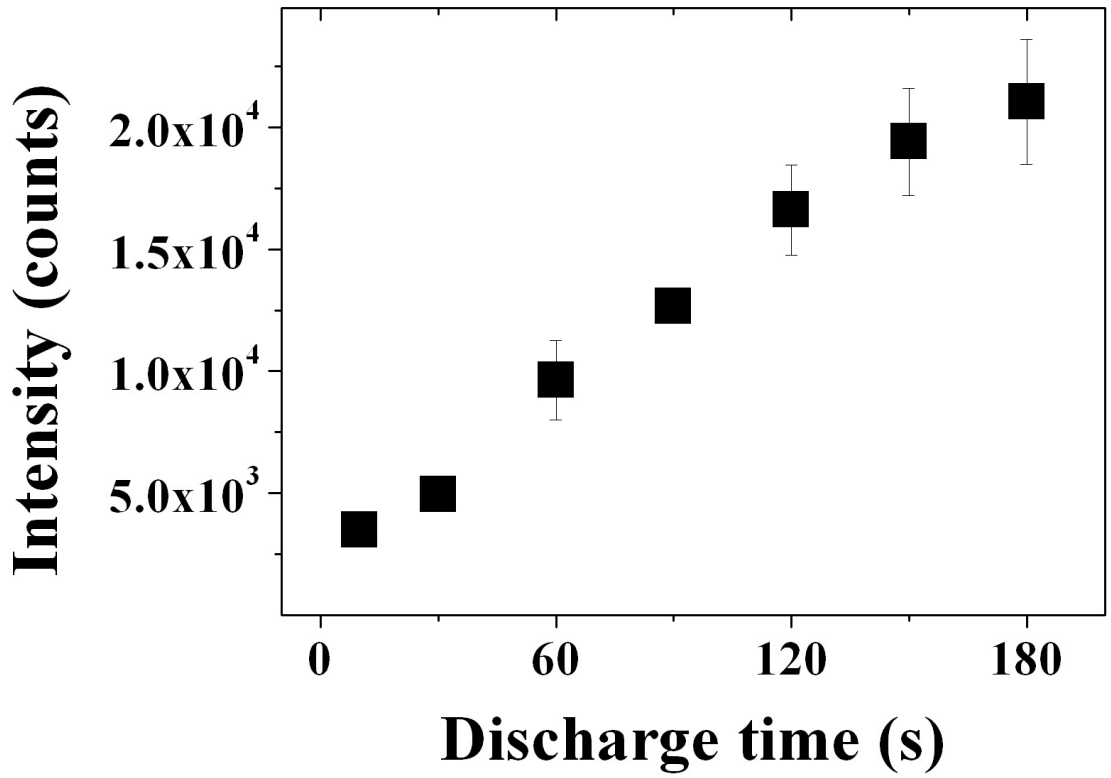

Figure 4.19. Time dependence on intensity of scattered laser by clusters formed in organosilicon plasma. 532 nm DPSS laser introduced to a chamber, and scattered laser was detected by OES. Optical emission spectra of scattered laser were obtained for 1 s and 3 s later from plasma turned off.

above ingredients cannot approach by this scattered intensity, it is clear that clustering and agglomerating phenomena, and those of transportation to the substrate were accelerated with discharge time. However, as I mentioned in Subsection 4.2.3.2, it is difficult to conclude that the dissociation and recombination reaction activated with discharge time due to constant deposition conditions. Hence the activation of agglomerate and transportation process becomes appropriately.

Regarding the scattered laser intensity, several analyses were performed by some assumptions. Firstly, Figure 4.20 shows the time dependence on amounts of nano-clusters calculated from the intensity of scattered laser (Figure 4.19) and SEM image (Figure 4.13). This graph was plotted from the following procedure: from the quantity of nano-clusters, 83 pieces, in Figure 4.13 ((a), 10 s), it assumed that scattered laser intensity at 10 s is equivalent to 83 pieces of the nano-clusters reached on the substrate from the plasma. This calculation was performed by a hypothetical condition of Rayleigh scattering agglomerates, *i.e*. because of unique shapes of low dense agglomerates, each single clusters in the agglomerates are possible to scatter individually as Rayleigh scattering model. With this model, it is convenient to analyze the aspect of clustering process in the organosilicon plasma, because a size of agglomerates can be included in a quantity of nano-clusters. However, it is necessary to confirm the scattering phenomenon of complicated shape of scattering centers. From the result of calculation, quantity of nano-clusters increased with deposition time, and increase of nano-clusters seem to be saturated slightly at approximately 500 pieces. It is considered that this aspect caused by a decrease of dissociation and recombination reaction in plasma due to a loss of electrons by electron attachment to the clusters. It could be confirmed by the fact that plasma could not maintained after 180 s.

In order to indicate a size of agglomerates in the organosilicon plasma, the square root of

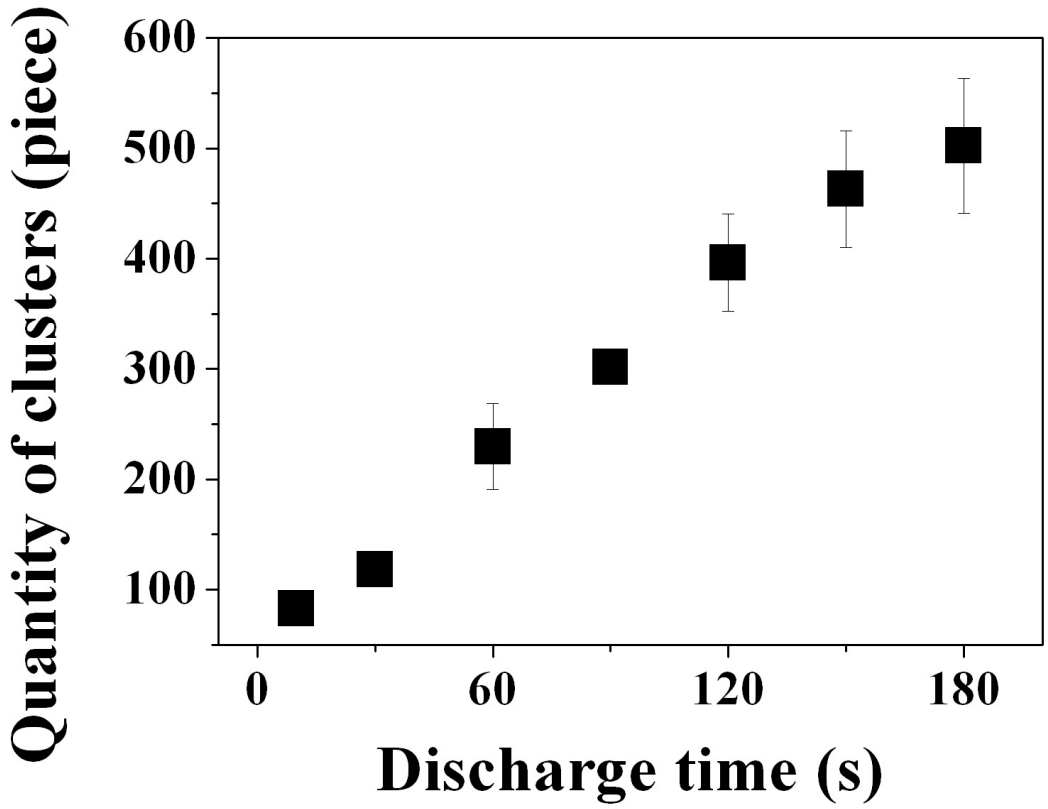

Figure 4.20. Time dependence on the quantity of nano-clusters calculated from the intensity of scattered laser (Figure 4.12) and SEM image (Figure 4.6).

scattered laser intensity (I_C) was plotted in Figure 4.21. This calculation was based on a hypothetical condition of Mie scattering agglomerates, *i.e.* from the proportional relation between scattered laser intensity and diameter squared, I_C can be useful for the determination of agglomerates in the plasma. However, due to the model to disregard an increase of agglomerates quantity, and the low dense non-spherical shape of agglomerates, it is difficult to analyze quantitatively by this model. In spite of this too simple model, it can be an excellent reference data to clarify the deposition process. That is, I_C increased with deposition time, and saturated slightly near 150 s. Moreover, in 60 s, increment of I_C accelerated comparing with one of below 60 s.

4.2.4. Summary

From considerations of formation process and laser scattering, formation process of the UWR films were confirmed. The UWR films were deposited with nano-clusters and those of agglomerates, which formed in organosilicon plasma, and formation of agglomerates were depended on the deposition time. Moreover, using laser scattering method, the relative change of quantity of nano-clusters or size of agglomerates could be confirmed. However, for the precise detection, it is necessary further investigations, such as definition of agglomerate size and scattering phenomenon of complicated shape of clusters, etc.

References

[1] A. Nakazima, A. Fuzishima, K. Hashimoto and T. Watanabe, Adv. Mater. 111 (1999) 365.

[2] Y. Wu, M. Kuroda, H. Sugimura, Y. Inoue and O. Takai, Surf. Coating Tech. 174-175 (2003) 867.

[3] J. Tsubaki and A. Hayakawa, Cluster Measurement Technology, Nikkan, Tokyo (2001) P.

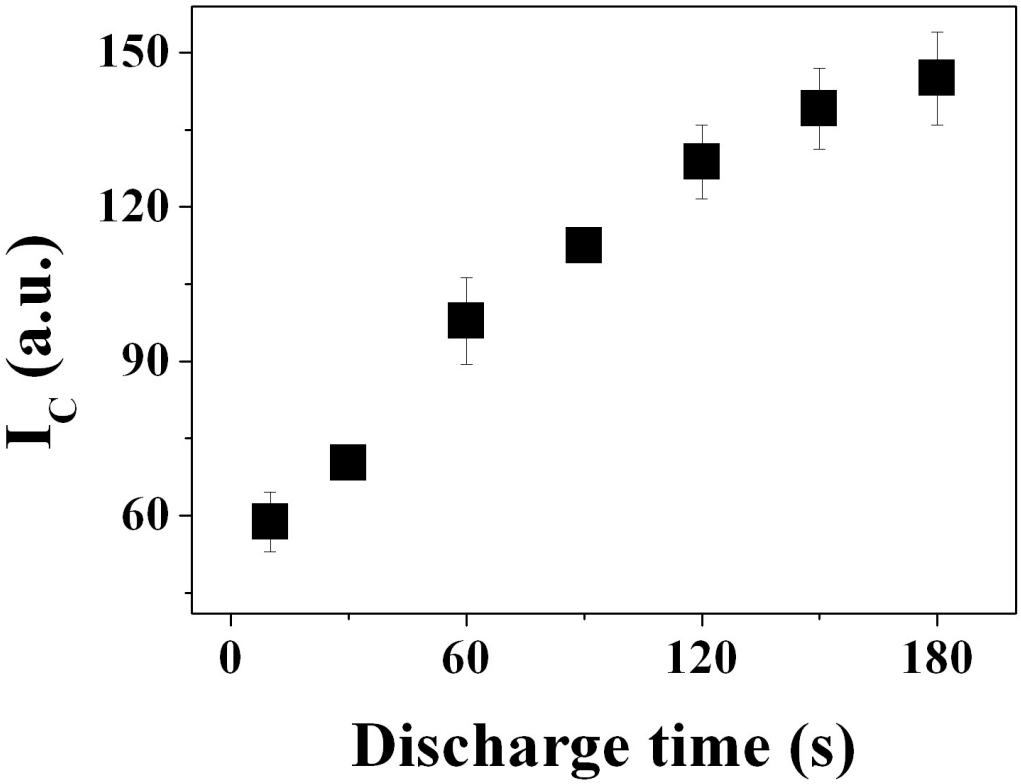

Figure 4.21. Time dependence on the square root of intensity of scattered laser (I_C).

65 [in Japanese].

[4] K. Muraoka and M. Maeda, Laser Application Measurement, Kogyo Tosho, Tokyo (1995) P. 27.

[5] The Japan Society of Plasma Science and Nuclear Fusion Research, Principles and Applications of Plasma Diagnostics, Korona, Tokyo (2006) P. 274.

[6] K. Koga, Y. Matsuoka, K. Tanaka and M. Shiratani, Appl. Phy. Lett., 77 (2000) 196.

[7] H. Kawasaki, J. Kida, K. Sakamoto, T. Fukuzawa, M. Shiratani and Y. Watanabe, J. Appl. Phys., 83 (1998) 5665.

[8] Y. Watanabe, M. Shiratani and M. Yamashita, Appl. Phy. Lett., 61 (1992) 1510.

[9] M. Shiratani, H. Kawasaki, T. Fukuzawa, H. Tsuruoka, T. Yoshioka and Y. Watanabe, Appl. Phy. Lett., 65 (1994) 1900.

[10] Y. Watanabe, M. Shiratani, Y. Kudo, I. Ogawa and S. Ogi, Appl. Phy. Lett., 53 (1988) 1263.

[11] H. Kawasaki, Y. Ueda, T. Yoshioka, T. Fukuzawa, M. Shiratani and Y. Watanabe, Appl. Phy. Lett., 67 (1995) 3880.

5. Conclusions

In the present dissertation, the fabrication of UWR thin films by RF PECVD and the consideration of the formation process were described. This thesis was organized into 5 chapters.

Chapter 1 was introduced for describing the general information of SiO:CH films, water repellency, various types of UWR films and their applications. This dissertation aimed to fabricate the functional SiO:CH thin films, including UWR thin films, and clarify the formation process.

In Chapter 2, electron impact dissociation behavior of organosilicon molecules was investigated by using a QMS and the simple molecular orbital calculation (MOPAC-PM3). From the fragment patterns of the reactants, it could be known that the HMDSO was hard to dissociate comparing with the TMMOS due to the strong Si-O bonding force, and it affected the dissociation in plasma. Dissociation reactions by electron impact could be partly identified.

In Chapter 3, the SiO:CH thin films were fabricated by RF PECVD. Moreover, the RF power and Ar gas dependence in the film formation was investigated by FT-IR, XPS, water contact angle and OES. From the RF power dependence in the ICP process, the existence of atomic H, CO, CH radicals and H_2 molecules were proved in TMMOS plasma, which describes that the oxygen atoms of methoxy groups in TMMOS molecules can be dissociated easily in the plasma and behave as a kind of oxidizing agent. In HMDSO plasma, atomic H, CH radicals and H_2 molecules were observed, which indicates that siloxane bondings in HMDSO hardly expel oxygen atoms. From the consideration on the RF power and Ar gas flow rate dependence in the CCP process, the correlations between RF power and Ar gas as

well as TMMOS flow rate were confirmed. In the RF power dependence, it could be classified by two regimes, the reaction-controlled (R-) regime and the flow rate-controlled (F-) regime. In the R-regime, the introduced RF power was used effectively to dissociate and recombine the TMMOS reactant, and led to increase the deposition rate. In the F-regime, the limited quantity of molecules in the plasma caused the saturation of dissociation and recombination reaction. From the results of Ar gas flow rate dependence, the ratio of mixing Ar gas affects to increase the amorphous carbon network and dangling bonds or -OH terminations due to Ar ion bombardment.

In Chapter 4, UWR thin films were fabricated by the inductively-coupled RF PECVD method, and formation process of the films was observed with SEM and laser scattering method. Contact angles of the films deposited at 150 ~ 200 W of RF power and 500 Pa of chamber pressure were greater than 150°. These ultra water-repellencies were due to the combination effect of CH_3-terminated surface and film roughness. From the result of the OES, the existence of atomic H, CO, CH, C_2 radicals and H_2 molecules were proved in organosilicon plasma. In particular, for the fabrication of UWR thin films, it has to be accompanied with emissions of CH and C_2 radicals, which is a clue of the severe recombination reaction as well as the nano-clustering phenomenon. From the results of observation in the UWR film formation, formation process of the UWR films was confirmed, *i.e.* the UWR films were deposited with nano-clusters and those of agglomerates, which is formed in organosilicon plasma, and formation of agglomerates were depended on the deposition time. Moreover, using laser scattering method, the relative change of nano-clusters quantity or agglomerates size could be obtained.

From this dissertation, deposition process of functional SiO:CH thin films was considered through investigations from electron impact dissociation behavior of organosilicon molecules

to formation of those films. Precursors, which are mainly dissociated from reactant by electron and metastable Ar impact in organosilicon plasma, recombine with each other in plasma and on the substrate. The acceleration of recombination reactions proceeds to form the nano-clusters and those of agglomerates in organosilicon plasma, and it leads to the formation of UWR thin films. Lastly, I intensively discussed the clustering phenomenon in organosilicon plasma, which is most important process in the formation of UWR thin films. The author believes that this dissertation provides the crucial information on understanding of the UWR films and their formation process.

Publications list

Scientific journals:

[1] Y.S. Yun, T. Yoshida, N. Shimazu, Y. Inoue, N. Saito and O. Takai, Behavior of various organosilicon molecules in PECVD processes for hydrocarbon-doped silicon oxide films, Solid State Phenomena, 124-126 (2007) 347-350.

[2] Y.S. Yun, T. Yoshida, N. Shimazu, N. Nanba, Y. Inoue, N. Saito and O. Takai, Fabrication of ultra water-repellent thin films by PECVD method and observation of deposition process, Journal of The Surface Finishing Society of Japan 58 (2007) 307-311

[3] Y.S. Yun, T. Yoshida, N. Shimazu, N. Nanba, Y. Inoue, N. Saito and O. Takai, Radio frequency power dependence in formation of SiO:CH thin films by plasma-enhanced chemical vapor deposition, Japanese Journal of Applied Physics, in press.

[4] Y.S. Yun, N. Shimazu, N. Nanba, Y. Inoue, N. Saito and O. Takai, Clustering process in formation of ultra water-repellent thin films by PECVD, Vacuum, Submitted.

[5] Y.S. Yun, T. Yoshida, N. Shimazu, N. Nanba, Y. Inoue, N. Saito and O. Takai, Influence of Ar gas flow rate in organosilicon plasma for the fabrication of SiO:CH thin films by PECVD method, Surface and coatings technology, Submitted.

Publications in proceedings of international conferences:

[1] Y.S. Yun, N. Saito, Y. Inoue, O. Takai, Corrosion resistance of amorphous Mo-Ni-B thin films prepared by shielded arc ion plating method, Plasma Science Symposium 2005, Nagoya, Japan, 2005. 1. 28.

[2] Y.S. Yun, N. Saito, Y. Inoue, O. Takai, Corrosion resistance of amorphous Mo-Ni-B thin films prepared by shielded arc ion plating method, Korea-Japan Workshop on Advanced Plasma Processing and Diagnostics, Busan, Korea, 2005. 4. 22.

[3] Y.S. Yun, N. Shimazu, E. Oriyama, T. Yoshida, Y. Inoue, N. Saito, O. Takai, Plasma diagnosis in formation of ultra water repellent thin films by PECVD method, The 27th International Symposium on Dry Process, Jeju, Korea, 2005. 11. 28, P. 101-102.

[4] E. Oriyama, Y.S. Yun, T. Yoshida, N. Shimazu, N. Saito, Y. Inoue, O. Takai, Characterization of ultra water-repellent thin films by PECVD method, The 27th International Symposium on Dry Process, Jeju, Korea, 2005. 11. 29, P. 315-316.

[5] Y.S. Yun, N. Shimazu, E. Oriyama, T. Yoshida, Y. Inoue, N. Saito, O. Takai, Ultra water-repellent characteristics of plasma polymerized nano-cluster films prepared by PECVD method, Sixth International Symposium on Biomimetic Materials Processing, Nagoya, Japan, 2006. 1. 26, P. 34.

[6] Y.S. Yun, N. Shimazu, E. Oriyama, T. Yoshida, Y. Inoue, N. Saito and O. Takai, Diagnosis of organosilane plasma for fabrication of ultra water-repellent thin films, The 3rd international workshop on advanced plasma processing and diagnostics, Seoul, Korea, 2006. 4. 15, P. 29.

[7] Y.S. Yun, T. Yoshida, N. Shimazu, Y. Inoue, N. Saito, O. Takai, Diagnosis of organosilane plasma in formation of ultra water repellent thin films by PECVD method, 8th Asia – pacific conference on plasma science and technology, Cairns, Australia, 2006. 7. 4, Available online.

[8] Y.S. Yun, N. Shimazu, T. Yoshida, Y. Inoue, N. Saito and O. Takai, FESEM observation in formation of the ultra water repellent thin films prepared by PECVD, The 16th international microscopy congress, Sapporo, Japan, 2006. 9. 7, P. 1191.

[9] T. Yoshida, Y.S. Yun, N. Shimazu, Y. Inoue, N. Saito and O. Takai, Behavior of Various Organosilicon Molecules in PECVD Processes, IUMRS-ICA-2006, Jeju, Korea, 2006. 9. 11, Available online.

[10] T. Yoshida, Y. S. Yun, N. Shimazu, N. Saito, Y. Inoue, O. Takai, Behavior of Intramolecular Bondings of Organosilicon Reactants in PECVD Processes for SiO:CH Films, The 6th Korea-Japan Symposium on Plasma and Thin Film Technolog, Busan, Korea, 2006. 10. 20, P. 42.

[11] N. Shimazu, Y.S. Yun, T. Yoshida, Y. Inoue, N. Saito and O. Takai, Deposition process of ultra water repellent thin films by PECVD method, The 6th Korea-Japan Symposium on Plasma and Thin Film Technology, Busan, Korea, 2006. 10. 20, P. 44.

[12] Y.S. Yun, T. Yoshida, N. Shimazu, Y. Inoue, N. Saito and O. Takai, Formation of ultra water-repellent thin films in organosilane plasma by PECVD method, AVS 53th international symposium & exhibition, San fransisco, USA 2006. 11. 14, Available online.

[13] T. Yoshida, Y.S, Yun, N. Shimazu, Y. Inoue, N. Saito and O. Takai, Behavior Analysis of Various Organosilicon Moleculesin PECVD Processes, AVS 53th international symposium & exhibition, San fransisco, USA, 2006. 11. 14, Available online.

[14] Y.S. Yun, T. Yoshida, N. Shimazu, N. Nanba, Y. Inoue, N. Saito, O. Takai, Behavior analysis of organosilane molecules in plasmas for fabrication of SiOCH thin films, The 27th International Symposium on Dry Process, Nagoya, Japan, 2006. 11. 29, P. 93-94.

[15] Y.S. Yun, N. Shimazu, N. Nanba, Y. Inoue, N. Saito and O. Takai, Consideration for clustering process in formation of ultra water-repellent thin films by PECVD method, The 9th International Symposium on Sputtering & Plasma Processes, Kanazawa, Japan, 2007. 6. 8, P. 473.

[16] Y.S. Yun, T. Yoshida, N. Shimazu, N. Nanba, Y. Inoue, N. Saito and O. Takai, RF power dependence in formation of SiO:CH thin films by PECVD method, The 20th Symposium on Plasma Science for Materials, Nagoya, Japan, 2007. 6. 22, P. 105.

[17] N. Shimazu, Y.S. Yun, N. Nanba, Y. Inoue, N. Saito and O. Takai, Fabrication of ultra water-repellent surface by parallel-plate plasma CVD, The 20th Symposium on Plasma Science for Materials, Nagoya, Japan, 2007. 6. 22, P. 119.

[18] N. Nanba, Y.S. Yun, N. Shimazu, Y. Inoue, N. Saito and O. Takai, Analysis of electron impact dissociation of organosilicon molecules, The 20th Symposium on Plasma Science for Materials, Nagoya, Japan, 2007. 6. 22, P. 142.

Acknowledgments

I would like to express my sincere appreciation to Professor Osamu TAKAI (EcoTopia Science Institute, Nagoya University) who gave me a great chance to be in an excellent research environment, and provided his invaluable guidance, sincere encouragement and support during the doctoral course at Nagoya University. I would like to express my sincere gratitude to Professor Hirotaka TOYOTA and Professor Hidefumi ASANO (Graduate School of Engineering, Nagoya University) for reviewing this thesis, and his valuable comments. I would deeply like to thank Professor Myeong-Hoon LEE (Department of Marine System Engineering, Korea Maritime University) who conferred an opportunity to study Material Engineering upon a student of Maritime Police (me), and has greatly encouraged me during last 12 years, from the undergraduate to the doctoral course.

I would like to give my deep appreciation to Associate Professor Yasushi INOUE (EcoTopia Science Institute, Nagoya University) for his in-depth interest in my research, invaluable comments and continuous encouragements in the completion of this thesis, and to Associate Professor Nagahiro SAITO (Graduate School of Engineering, Nagoya University) for his in-depth discussions and kind comments on this study. I would also like to thank to Associate Professor Naoto OHTAKE and Assistant Professor Takahiro ISHIZAKI (Graduate School of Engineering, Nagoya University) for their kind advices on the study in the doctoral course.

I would like to express my thanks to Professor Masaharu SHIRATANI and Assistant Professor Kazunori KOGA (Graduate School of Information Science and Electrical Engineering, Kyushu University) for their professional advices and comments regarding the laser scattering system.

Also, I would like to express my heartfelt appreciation and thanks to all members of TAKAI

Labo. including graduate students and researchers. In particular, I would like to express my thanks to all members of INOUE Labo. including CVD group members (Enju ORIYAMA, Takanori YOSHIDA, Norifumi SHIMAZU, Naoki NANBA). I would like to express my thanks to Dr. Kyounghwang LEE (RIST), Dr. Hanjin RYU (POSCO), and Mr. Sangkweon KIM (TAKAI Labo., Nagoya University) for their advices on the research as well as the life in Korea and Japan. Special thanks must go to my friends Dr. Riichiro OHTA (NASA Ames Research Center), Dr. Pavel BAROCH (Department of Physics, University of West Bohemia), Dr. Hajime SATO (Canon Inc.), Dr. Koji MITAMURA (TAKAI Labo., Nagoya University), Mr. Pilwon HEO (Graduate School of Engineering, Nagoya university), Mr. Sunhyung LEE and Miss Kyounghee LEE (TAKAI Labo., Nagoya University) for their encouragements and advices during doctoral course.

I would like to express my sincere gratitude to my guarantor in Japan Mr. Masaji KANBE (FURUENG CO., LTD.) for his kindness and encouragements.

Lastly, my heartfelt thanks must go to my girl friend for her constant encouragements and supports during last 11 years. I give my sincere gratitude and this thesis to my brother, and parents who always work from dawn till dusk for their own son.

October 2007

Yongsup Yun